BONDING IN POLYHEDRAL BORANES - QUALITATIVE ELECTRON COUNTING RULES AND QUANTITATIVE ELECTRONIC STRUCTURE STUDIES

A Thesis

Submitted for the Degree of

DOCTOR OF PHILOSOPHY

By

Pattath D. Pancharatna

School of Chemistry

University of Hyderabad

Hyderabad 500 046

INDIA

June 2003

This thesis is dedicated to

My Achan, the beacon of my life

And BaLu, the beacon of my research

and eventually of my life

CONTENTS

CHAPTER 5: Bonding in Extended Systems

STATEMENT

I do hereby declare **that the** work embodied in this thesis is the result of investigations carried out by me in the **School of Chemistry, University of Hyderabad, Hyderabad, India,** under the supervision of **Prof. Eluvathingal D. Jemmis.**

In keeping with the general practice of reporting scientific observations, due acknowledgements have been made whenever the work described is based on the findings of other investigators.

Pattath I). Pancharatna

CERIFICATE

Certified that the work embodied in the thesis entitled **Bonding in Polyhedral Boranes - Qualitative Electron Counting Rules and Quantitative Electronic Structure Studies** has been carried out by **Ms. Pattath D. Pancharatna** under my supervision and the same has not been submitted elsewhere for any degree.

Eluvathingal D. Jemmis

Thesis Supervisor

DEAN
School of Chemistry
University of Hyd.
Hyderabad-46.

Dean

School of Chemistry

ACKNOWLEDGEMENTS

I feel very fortunate to have worked with my supervisor, Prof. E. D. Jemmis. I had very good exposure to different aspects of applied theoretical chemistry and the freedom to choose topics of my interest. I extend my heartfelt gratitude for his valuable guidance and constant encouragement in both academic and personal avenues. I also take this opportunity to thank his family.

I thank all faculty members of the School of Chemistry with special thanks to Prof. M. Durga Prasad and Prof. T. P. Radhakrishnan. I greatly acknowledge Prof. Roald Hoffmann for his effective collaboration on the project, tubular boranes, of Chapter 4. Computational facilities of the Computer Centre, University of Hyderabad and financial assistance from the Council of Scientific and Industrial Research (CSIR), New Delhi are greatly acknowledged.

1 thank the non-teaching staff, University of Hyderabad for their patience and cooperation in dealing with official matters. I express my sincere thanks to all my labmates, both past and present, my seniors (Balu, Kiran, Pankaz, Ashwini, Saradha) who taught me how to do research in various ways, my juniors (Anoop, Param, Bishu, Prasad) who gave me new insights with long discussions and debates and my friends who were always there for me to share my sweet successes, to encourage me when I am down, to correct me when 1 am wrong. My best friend (Sru) was omnipresent and she was there for me taking up all possible roles. She was the one on whom I can lean at all circumstances and will remain my greatest supporter for the years to come. I also thank all my other friends and well-wishers at the University of Hyderabad. I acknowledge all my teachers, both past and present, who have played a major role in molding my life.

My family members were always very encouraging and supportive. I am here because of them and will try to achieve greater heights for them. I express my deepest love to all of them.

My prayers to the Lord Almighty for all His Blessings.

Pancharatna

ABSTRACT

The thesis begins with an introduction to the evolution of various theories of chemical bonding with its application to polyhedral bonding. The quantitative tools used to study the various systems discussed in the thesis and the qualitative ideas of electron counting rules are discussed in Chapter 1.

Polyhedral boranes have always been a fascination for chemists despite the complexity of the structural patterns they exhibit. A great advancement in the development of polyhedral boranes began with the formulation of Wade's rule. The n+1 skeletal electron pair rule by Wade could account for the bonding in many existing monopolyhedral boranes. Some condensed polyhedral boranes known at that time required additional parameters to be incorporated into Wade's rule. With an enormous number of such condensed systems emerging, an extension of Wade's rule became essential. The n+m rule invented by Balakrishnarajan and Jemmis could throw light in many of these systems where sharing of more than one atom is involved. Single vertex bridged complexes needed an additional refinement of the n+m rule which resulted in a generalized *mno* rule. This rule helped to bring many diverse systems together. Chapter 2 discusses the rule in detail illustrating it using known examples. Justification of the rule based on molecular orbital theory is provided. Application of the *mno* rule in solving an error in an edge shared macropolyhedral borane is also given.

The condensation of two polyhedral boranes can occur by the sharing of one or more atoms. A survey of the experimental structures suggested the interactions between the non-bonded atoms on adjacent polyhedra as one of the factors affecting the stability of a macropolyhedral borane. The nature of such interactions are looked at in detail, first

with all-boron systems and then with heavy **atom** substitution, both main group **and** transition metals, to understand the effect of hetero atoms on them **and** forms Chapter 3 of the thesis.

The bonding in tubular boranes starting from the very common dianions $B_nH_n^{4-}$ (n=6, 7, 10, 12) are explored which also helped in examining the explanations given by Wade for the n+1 rule. As the analysis on the nature of bonding between the rings showed that five membered stacking are more preferred, mini-nanotubes like $B_{17}H_{17}^{2-}$, $B_{22}H_{22}^{2-}$, $B27H27^{2-}$ and an infinite extension of B_5H_5 rings in a staggered form are studied. These give a generalized picture and forms the subject matter of Chapter 4.

The application of *mno* rule in an extended system based on polyhedra is examined in Chapter 5 by designing an edge shared system with simple pentagonal pyramid units. The resulting 3-D boride network require metal ions to attenuate their charge requirements and density functional theory based computations using plane wave basis arc employed for the detailed study of the system. The studies show that the *mno* rule has many more promising potentials to be put into use in extended systems involving any polyhedral borane as the repeating unit.

CHAPTER 1

THEORETICAL TOOLS IN CHEMICAL BONDING

1.0. INTRODUCTION

The nature of bonding in non-classical structures, observed abundantly in several molecular systems and solids where the traditional ball and stick model fails, is always an intriguing area of research. Typical examples of such systems are polyhedral boranes which exhibit fascinating cluster patterns and have characteristic electronic requirements. These special features are attributed to the electron deficiency of boron hydrides. This thesis involves the investigation of such molecular structures and their extended systems by employing both qualitative and quantitative tools of electronic structure theory. The present chapter discusses briefly the evolution of the concept of bonding using quantitative and qualitative ideas with special emphasis to polyhedral bonding.

The concept of chemical bonding evolved as a result of the quest towards the nature of interactions between atoms to form molecules.[1] During the early nineteenth century the bond was depicted by lines drawn between two atoms represented by their atomic symbol.[1] It was after the discovery of electrons that attempts started to provide an electronic meaning to a bond. In 1916 Lewis developed the Octet theory where only the valence electrons were considered on the basis of the stable electronic configuration of inert gases.[1] This enabled the understanding of bonding in many main group elements where the bond consists of two electrons. Based on this, different types of bonds - ionic bond, covalent bond, coordinate bond - emerged.

Simple Lewis structures failed to predict the geometry of a given molecule. Quantum mechanics was emerging at the early twentieth century in the attempts to explain the motion of microscopic particles. The quantum mechanical treatment by Heitler and London in 1927 paved way to a general theory of bonding, the Valence Bond

1

Theory (VBT). The VBT considers the valence electrons to be involved in binding two atoms by forming a two centre - two electron (2c-2e) bond between them. An extensive application of VBT into chemical bonding was possible with the assistance of the resonance and Valence Shell Electron Pair Repulsion (VSEPR) theories which marked their entry by successfully explaining and predicting the geometries of large number of molecules; both organic and inorganic.[2] Quantum mechanics assisted in finding out the different resonating forms with their percentages contributing to a given molecule though the calculations were tedious. Resonance theory was introduced by Pauling in the 1930s and VSEPR theory by Sidgwick and Powell in 1940 which was later extended by Gillespie. Attempts were also made to apply these localized theories to account for the bonding in electron deficient compounds such as the deltahedral clusters formed by boron and by metals. Though Pauling tried to explain the bonding in polyhedral boranes using resonating one electron bonds, many of the geometrical predictions including diborane (B_2H_6) came out to be wrong.

A theoretical understanding of the bonding in polyhedral boranes became a great challenge for chemists. Encouraged by the experimental isolation and structural determination of compounds such as B_4H_{10}, B_5H_9 and B_5H_{11}, Lipscomb in 1954 formulated a valence based rule using three centre-two electron (3c-2e) bonds with the goal of an improved understanding of the bonding in these systems.[3] Lipscomb's approach is often termed *styx* rules because of the four parameters which has to be determined from the molecular formula of the boron hydride, B_pH_{p+q}. According to this treatment, a polyhedron can be approximated to a sphere with two concentric ones. The inner sphere consists of p boron atoms and q bridging or *endo* hydrogens. The p terminal

hydrogens on the p boron atoms, which radiate out, form the outer sphere. The four different types of bonds present in such a polyhedron are s BHB and t BBB 3c-2e bonds and y BB and x BH 2c-2e bonds. Each boron atom is assumed to use all its four valence orbitals out of which one will be involved in the *exo* BH bond. The remaining three orbitals and two electrons on each boron atom will be involved in the skeletal bonding. This follows that the total number of 3c-2e bonds (s + t) must be equal to the number of boron atoms (p). Now the q hydrogen atoms maybe either involved in 2c-2e BH bonds or 3c-2e BHB bonds so that s + x must be equal to q. Moreover the number of skeletal electron pairs (2p + q)/2 should be equal to the number of skeletal bonds (s + t + y + x). Thus, s = p - t, x = q - s and 2y = s - x. With three equations and four unknowns one cannot expect a unique solution for the equation, but can deduce what kind of bond networks is capable of holding the skeletal atoms together. The different solutions correspond to different isomers of the same molecule.

The 3c-2e bond formalism used by Lipscomb to explain the bonding in polyhedral boranes is an outcome of Molecular Orbital Theory (MOT). But applications of MOT in clusters started even before the work of Lipscomb with the calculations of Longuet-Higgins and M. de V. Roberts on octahedral and icosahedral boranes.[4] MOT treats electrons as delocalized over the entire nuclei involved in bonding. Such a concept helped in perceiving the skeletal patterns and comprehending the bonding of polyhedral boranes in a better way. The nature of MOT to suite general quantitative or semi-quantitative calculations and the revelation of orbital symmetry principles in governing chemical bonding made it widely acceptable over the years.[5] The first section of this chapter gives a summary of the underlying theories[6] based on quantum mechanics for the

computations of the molecular structures and energies. Reliability of the calculations depends on the approximations employed in the theoretical formulations. The different methods involved in the calculations reported in the thesis are also discussed. In the second section, an overview of the development of chemical bonding using various qualitative ideas is given.

1.1. QUANTITATIVE METHODS

Classical mechanics which governs the motion of macroscopic bodies fails to describe atoms and molecules. A series of observations such as the black-body radiation, photoelectric effect etc. during the beginning of the last century led to the advent of quantum mechanics.[7] The Schrödinger equation (eqn) in its time independent form used in the thesis can be expressed in the most succinct form as eqn (1.1).

$$\{T + V\}\,\Psi = E\,\Psi \text{ ----------------- (1.1)}$$

where, T and V are the linear operator for kinetic and potential energy respectively and E is the total energy of the system. Sum of the kinetic and potential energy operators form the Hamiltonian operator, H and the Schrödinger equation is commonly written by the form

$$H\,\Psi = E\,\Psi \text{ ---------------- (1.2)}$$

The different methods to arrive at the solutions of eqn (1.2) are covered in the following sections. As the thesis does not include any time dependent effects, our discussions are restricted to the time independent Schrödinger eqn.

1.1.1 Theoretical Background based on Quantum Mechanics[¹¹]

i. The Born-Oppenheimer Approximation

For a molecule consisting of N nuclei and n electrons, the Hamiltonian of the Schrödinger equation is given by eqn (1.3), which is the sum of kinetic and potential energy operators.

$$H = -\frac{h^2}{8\pi^2}\sum_A^N M_A^{-1}\Delta_A^2 + \sum_{A<B} e^2 Z_A Z_B r_{AB}^{-1} - \frac{h^2}{8\pi^2 m^2}\sum_p^n \Delta_p^2 + \sum_{p<q} e^2 r_{pq}^{-1} - \sum_A \sum_p e^2 Z_A r_{Ap}^{-1} \quad \text{-------- (1.3)}$$

Here M_A is the mass of nucleus A; m and e are the electronic mass and charge, respectively; $Z_A e$ and $Z_B e$ are the charges on nuclei A and B respectively; and r_{ij} is the distance between particles i and j. Summations involving indices A and B are over atomic nuclei and those involving p and q are over electrons. The first and third terms of equation (1.3) are the nuclear and electronic kinetic energy operators respectively. The rest three terms in (1.3) can be dissected into nucleus-nucleus, electron-electron and nucleus-electron potential energies respectively. The first two terms are characteristic of the nucleus, next two terms of electrons and the last one involves combinations of the two.

The Hamiltonian can be simplified based on the Born-Oppenheimer approximation. According to this approximation, the motion of the nuclei is negligible as they are several thousand times larger than the masses of electrons. It helps in considering the motion of the electrons in the field of stationary nuclei which results in separate, purely electronic problem for each set of nuclear positions. In more quantitative terms, Born-Oppenheimer approximation amounts to separating off the nuclear kinetic energy and nuclear-nuclear repulsion terms from the Hamiltonian and considering only

the part which depends on the positions but not the momenta of the nuclei. The resulting electronic Hamiltonian operator, H^{el} is given by

$$H^{el} = -\frac{h^2}{8\pi^2 m^2} \sum_p \Delta_p{}^2 - \sum_A \sum_p e^2 Z_A r_{Ap}{}^{-1} + \sum_{p<q} e^2 r_{pq}{}^{-1} \text{ ------------------------- (1.4)}$$

The modified electronic Schrödinger eqn can be written in a simplified form as

$$H^{el} \Psi^{el} = E^{el} \Psi^{el} \text{ ---------------- (1.5)}$$

The solutions of eqn (1.5) are purely electronic wave functions, describing the motion of the electrons in the field of the fixed nuclei. The total energy E of the system of a given internuclear distance is then given as

$$E = E^{el} + \sum_{A<B} e^2 Z_A Z_B r_{AB}{}^{-1} \text{ ----------------------- (1.6)}$$

The second term is the electrostatic internuclear repulsion energy.

ii. Representation of electronic wave functions

As eqn. (1.5) can be exactly solved only for one electron systems (like hydrogen atom), further approximations are necessary while considering many electron systems. In MOT, the full wave function of a molecule is approximated based on one electron functions or orbitals which have the nature of hydrogen atom orbitals. Molecular orbitals (MO) are usually expressed as a Linear Combination of the Atomic Orbitals (LCAO). A basis set is a mathematical representation of the MOs within a system used to perform the theoretical calculation. Basis sets assign a group of basis functions to each atom within a molecule to approximate its orbitals.

The atomic orbitals (AO) are always represented in a best way by Slater Type functions and have exponential radial parts. Thus a Slater Type Orbital (STO) with principal quantum number n is written as;

6

$$\chi(r, \theta, \phi) \ \alpha \ r^{n-1} \exp(-\zeta r) . Y(\theta, \phi) \ \text{---------------------- (1.7)}$$

where ζ is the orbital exponent. $Y(0, \phi)$ contains all the angular information needed to describe the wavefunction. STOs can be used as basis functions for more accurate solutions for atoms and small, especially linear molecules. The many-centre two-electron integrals involving STOs are rather difficult, require numerical integration techniques and are very time consuming. This problem has been overcome to some extent by the introduction of Gaussian type functions to the MO computations by Boys. They have the important advantage that all integrals in the computation can be evaluated explicitly without recourse to numerical integration and has proved extremely useful in *ab initio* calculations of polyatomic molecules. The cartesian Gaussian Type Orbital (GTO) is of the form;

$$\chi(x, y, z) \ \alpha \ x^l y^m z^n \exp(-\alpha r^2) \ \text{------------------------ (1.8)}$$

where 1, m and n are positive integers or zero. Here a is the orbital exponent. The main disadvantage of the Gaussian function is that it does not resemble very closely the form of real AO wave functions. In particular, the Gaussian function lacks a cusp at the nucleus and hence the region near the nucleus is described rather poorly. In practice, the functional behavior of an STO is simulated by the number of GTOs with different orbital exponents. These GTOs are then referred as primitives and the resulting STO as the contracted Gaussians. If the basis functions are $\phi_1, \phi_2, \ldots, \phi_N$, **then** an individual molecular orbital ψ_i can be written as;

$$\psi_i = \sum_{\mu=1}^{N} c_{\mu i} \ \phi_\mu \ \text{---------------------- (1.9)}$$

where $c_{\mu i}$ are the molecular orbital expansion coefficients.

7

MOs can be obtained to essentially any accuracy desired by appropriate adjustment of the number of basis functions employed in the LCAO expansion. There are different types of basis sets commonly employed. *Minimal basis set* comprises of those AOs up to and including the orbitals of the valence shell of each atom of the system. Inner and outer part of each AO can be described better by doubling the basis functions and the resulting basis set is termed *Double Zeta* (DZ). Since only valence orbitals are involved in chemical bonding, the efficiency can be enhanced without excessive computing time by doubling only the valence orbitals. This results in *split valence basis*. In a similar way, Triple Zeta (TZ), Quadruple Zeta (QZ) etc. basis sets are also available. Adding polarization functions to the DZ split valence basis results in *Double Zeta plus Polarization* (DZP). It involves addition of higher angular momentum functions like p-functions for hydrogen and d-functions for heavy atoms. The same is applicable to higher split valence basis. *Valence basis sets* comprise of just those orbitals of the valence shell of each atom of the system and are not commonly used.

The simplest type of wave function appropriate for the description of an n-electron system would be in the form of a product of spin orbitals. To ensure antisymmetry based on Pauli's exclusion principle, the spin orbitals are arranged in a determinantal form and the determinant is called the slater determinant. Spin orbitals are the product of a MO and a spin function. Thus the slater determinant of the closed-shell ground state of a molecule with n electrons occupying n/2 orbitals is written as,

$$\Psi = (n!)^{-1/2} \begin{vmatrix} \psi_1(1)\,\alpha(1) & \psi_1(1)\,\beta(1) & \psi_2(1)\,\alpha(1) & \cdots\cdots & \psi_{n/2}(1)\,\beta(1) \\ \psi_1(2)\,\alpha(2) & \psi_1(2)\,\beta(2) & \psi_2(2)\,\alpha(2) & \cdots\cdots & \psi_{n/2}(2)\,\beta(2) \\ & & & \vdots & \\ \psi_1(n)\,\alpha(n) & \psi_1(n)\,\beta(n) & \psi_2(n)\,\alpha(n) & \cdots\cdots & \psi_{n/2}(n)\,\beta(n) \end{vmatrix} \quad \cdots\cdots\cdots (1.10)$$

iii. Variational Principle

The set of MO expansion coefficients, $c_{\mu i}$ can be solved using the principles of varialional theorem. If Ψ is any antisymmetric normalized function representing the total wave function, then the expectation value of the energy (E') obtained by the postulates of quantum mechanics is greater than or equal to the ground state energy of the system E which is represented by the exact wave function;

$$E' = \frac{\int \Psi^* \hat{H} \Psi \, d\tau}{\int \Psi^* \Psi \, d\tau} \geq E \quad \text{------------} (1.11)$$

Substitution for Ψ from the relation (1.9) and introducing the overlap integral $(S_{\mu\nu})$ and resonance integral $(H_{\mu\nu})$ gives

$$\sum_{\mu=1}^{N} c_\mu \sum_{\nu=1}^{N} c_\nu \, S_{\mu\nu} \; E' = \sum_{\mu=1}^{N} c_\mu \sum_{\nu=1}^{N} c_\nu \, H_{\mu\nu} \quad \text{------------------------} (1.12)$$

where, $S_{\mu\nu} = \int \phi_\mu \phi_\nu$ and $H\mu\nu = \int \phi_\mu \hat{H} \phi_\nu$

Thus if the only flexibility allowed in a particular type of calculation is the variation of the orbital coefficients, an optimum can be determined by minimizing E' with respect to the coefficients $c_{\mu i}$;

$$\frac{\delta E'}{\delta c_{\mu i}} = \frac{\delta E'}{\delta c_1} \delta c_1 + \frac{\delta E'}{\delta c_2} \delta c_2 + \text{------------} + \frac{\delta E'}{\delta c_N} \delta c_N = 0 \quad \text{------------------------} (1.13)$$

Differentiating eqn (1.12) with respect to the coefficients leads to N simultaneous, linear, and homogenous equations which can be written in a **determinantal** form and is called the secular determinant (eqn. 1.14)

$$\left| H - E\,S \right| = 0 \quad \text{--------------------- (1.14)}$$

Solving eqn (1.14) gives the energies of the N states of the system. Once the determinant is known, the coefficients can be calculated.

1.1.2. Electronic Structure Methods[6,7]

Electronic structure studies generally consist of *Ab initio* and semi empirical methods. *Ab initio* methods do not use any parameters in their computations. The only values used are the fundamental constants, mass and charges of electron and nuclei, the Planck's constant and the speed of light. Semi-empirical methods on the other hand simplify the computation either by approximating the different integrals in the Hamiltonian using parameters derived from the experimental data on atoms and prototype molecular systems or by neglecting some of them. All the computations in this thesis are based on the laws of quantum mechanics.

i. Ab initio Methods

Though *ab initio* methods are computationally more expensive than the semi empirical methods, with modern computers one can handle reasonably big molecular systems efficiently. The accuracy of the results is also higher than semi-empirical methods which make it better in high quality quantitative predictions. Any of the different basis sets explained earlier can be employed depending on the system chosen for the study. Normally extended basis sets along with diffused functions or polarized functions are found to give good results. Presently both Wave Function (WF) and

Density Function (DF) based techniques are widely in use.   The Hartree-Fock approximation plays a key role in the former **to** arrive at the molecular Schrödinger equation whereas the Hohnberg-Kohn theorems have led to the development of DFT to be applied on to molecular problems.

A. Hartree Fock - Self Consistent Field (HF-SCF) Method

The electron interactions are introduced in the Hartree-Fock model by defining an effective one-electron potential of the form

$$V_i^{eff} = \sum_{j \neq i}^{N} \int \frac{\phi_j^*(j)\,\phi_j(j)}{r_{ij}}\, dv_j$$

$$= \sum_{j \neq i}^{N} \left\langle \phi_j(j) \left| \frac{1}{r_{ij}} \right| \phi_j(j) \right\rangle \quad \text{-------------------- (1.15)}$$

Eqn. (1.15) gives an average potential provided by N-1 electrons in an N electron system in which an electron moves.   The Schrödinger equation in terms of individual electron coordinates is then given by

$$(H_i^{(0)} + V_i^{eff})\,\phi_i(i) = E_i\,\phi_i(i) \quad \text{--------------------- (1.16)}$$

where, $H_i^{(0)} = -\frac{1}{2}\nabla_i^2 - \frac{Z}{r_i}$ in atomic units.

The total Hamiltonian in eqn (1.16) is called the Fock operator $\hat{F}_i$. V_i^{eff} can be written in terms of coulomb operator J_j and exchange operator K_j and the resulting Fock operator is given as

$$\hat{F}_i = -\frac{1}{2}\nabla_i^2 - \frac{Z}{r_i} + \sum_{j=i}^{n} (2\hat{J}_j - \hat{K}_j) \quad \text{------------------- (1.17)}$$

Application of the Fock operator on $\phi_j(i)$ leads to integrals such as

$$\langle \phi i | \hat{J_j} | \phi i \rangle = \langle \phi i(1)\phi j(2) | 1/r_{12} | \phi i(1)\phi j(2) \rangle = J_{ij} \quad \text{------------------- (1.18)}$$

$$\langle \phi i | \hat{K_j} | \phi i \rangle = \langle \phi i(1)\phi j(2) | 1/r_{12} | \phi i(2)\phi j(1) \rangle = K_{ij} \quad \text{------------------- (1.19)}$$

The effective potential V_i^{eff}, is calculated from the initially assumed basis set. The N eqns of the electronic Schrödinger eqn (1.16) are solved to obtain the first improved set of orbitals. The first-improved orbitals are now used to define the first-improved Fock operator. The process is repeated until some set of Fock operators leads to the same set of Hamiltonian:

$$H_i^{(n)} \sim H_i^{(n+1)} = H^{SCF}$$

$$\phi_i^{(n)}(i) \sim \phi_i^{(n+1)}(i) = \phi_i(i)$$

Since the molecular orbitals are derived from their own effective potential, this method is known as the Self Consistent Field (SCF) method.

B. Post **Hartree** Fock Methods

Though HF methods account for 99% of the total energy of the system, a significant amount which is important in explaining the chemical behavior is still left out. The difference in energy between the HF and the lowest possible energy is called the electron correlation. Post Hartree-Fock methods[7] bring in electron correlations in many ways. Multi-configuration SCF, for example, uses a linear combination of determinants corresponding to different configurations to represent a wave function.

$$\Psi = a_0 \Phi_{HF} + \sum_{i=1} a_i \Phi_i \quad \text{-------------- (1.20)}$$

This is distinct from the improvements in the basis set, though small basis sets within post HF methods may not always provide better results than with HF using more polarized and diffused basis sets. Limited Configuration Interaction (CI), Møller-Plesset

(MP) and Coupled Cluster (CC) methods are commonly used approaches to include electron correlation. All these methods are computationally time consuming while dealing with larger systems.

C. Density Functional Theory (DFT)

Methods based on DFT are gaining popularity, being more advantageous with higher effects of electron correlation and lower computation time. DFT has evolved on the basic idea that energy can be expressed in terms of electron density which is the first Hohnberg - Kohn Theorem. Since integration of the electron density gives the total number of electrons, it determines the Hamiltonian and thereby all properties defined by the Hamiltonian.

$$\rho\,(r) \leftrightarrow \nu\,(r) \leftrightarrow \Psi$$

Here $\nu\,(r)$ is the external potential and the total Hamiltonian is given as

$$H = -\frac{1}{2} \sum_j \Delta_j^2 + \sum_j \nu\,(r) + \frac{1}{2} \sum_{i \neq j} \frac{1}{\left| r_i - r_j \right|} \quad \text{------------------- (1.21)}$$

Eqn (1.21) can be written in a simplified way as

$$H = T + V + U \quad \text{------------------- (1.22)}$$

The total energy expression now becomes

$$E_\nu(\rho) = \left\langle \left| \psi[\rho] \right| T + V + U \left| \psi[\rho] \right| \right\rangle \quad \text{------------------- (1.23)}$$

This theorem is known as the second Hohnberg – Kohn Theorem. Eqn. (1.23) can be rewritten as

$$E_{\nu(r)}[\rho(r)] = \int \nu\,(r)\,\rho\,(r)\,dr + F[\rho(r)] \quad \text{------------------- (1.24)}$$

$$F[\rho(r)] = T_s[\rho(r)] + \frac{\rho(r)\rho(r)}{\left| r - r \right|}\,drdr + E_{xc}[\rho(r)] \quad \text{------------------- (1.25)}$$

where $T_s[\rho(r)]$ is the kinetic energy of a non-interacting system with density p (r); the next term is the expression of interaction energy in the appropriate v(r) and the last term is the exchange correlation energy. Good approximations of $E_{xc}[\rho(r)]$ are necessary for any practical applications of DFT.

Several hybrid functionals (HF-DFT) are also known which define the exchange functional as a linear combination of HF, local and gradient-corrected exchange terms. This exchange functional is then combined with a local or a gradient-corrected correlational functional. Different levels of theory are available based on the approximations to the exchange and correlation functional.

Polyhedral boranes, which are the major focus of the thesis, are found to give reliable results at B3LYP level which consists of Becke's exchange functional and Lee, Yang and Parr's correlation functional. The basis sets normally used in the calculations are 6-31g* for molecules having only main group elements and LANL2DZ for transition metal contained molecules. A 6-31g basis set is a split valence type. Here the inner shell consists of 6 primitive gaussians and the valence basis functions are split into two; each consisting of three primitive Gaussians (the inner function) and one primitive Gaussian (the outer function). The asterisk (*) designates addition of a polarization function to the 6-31g basis set. This basis set adds d functions to heavy atoms and helps to change the shape of the orbital in addition to the size which is achieved by the split valence nature. For transition metals, electrons of the inner levels are treated in an approximate way, via Effective Core Potentials (ECP). LANL2DZ consists of a double zeta ECP potential due to Hay and Wadt.

ii. Semi Empirical Methods[7]

Semi empirical methods can be classified into two categories; those using a Hamiltonian which is the sum of all one electron terms (no SCF equations) and those which use both one electron and two electron terms in the Hamiltonian. While Hückel and Extended Hiickel (EH) are of the first type, methods like AM1, MNDO, PM3 etc. belong to the second category and consists of different parameters. Semi-empirical calculations are relatively inexpensive and provide reasonable qualitative descriptions about molecular systems. All methods which include two electron integrals is centered around HF approximations whereas those involving one electron integrals forms a different type and is discussed below.

A. Extended Hiickel Method[9]

The method considers only the valence electrons and the Hamiltonian is the sum of the one-electron effective Hamiltonians. Nuclei are ignored, so are electron-electron interactions. The basis set used is the STO AOs themselves and MOs are expressed as linear combinations of the AOs. Thus EH forms the simplest approximate LCAO-MO method. The major difference of EH from Hiickel theory is that all valence orbitals are included in the former. In addition all the overlaps between atoms are calculated in EH. The secular determinant is obtained after applying the variational principle from which the MO coefficients are determined. The total energy is taken as the sum of the one electron energies.

EH calculations help in having an excellent qualitative understanding about the chemical bonding in molecules. The MOs generated are more close to the chemical intuition and can be perceived easily. They are also computationally inexpensive as only

overlap integrals are calculated. Fragment Molecular Orbital (FMO) analysis as a part of the EH calculations is widely used in this thesis. The theory behind the FMO analysis is given in the next section. EH is also beneficial while dealing with Walsh diagrams. EH does not consider electron-electron interactions and should be used only to obtain the qualitative ideas of bonding. Quantitative conclusions based only on EH are not reliable.

1.1.3 FMO Theory

Theories of intermolecular perturbation are employed in an FMO analysis.[10] The Wolfsberg-Helmholtz formula is used here which is given by;

$$H_{\mu\nu} = K \, (H_{\mu\mu} + H_{\nu\nu}) \, S_{\mu\nu} \quad \text{----------------} \quad (1.26)$$

The diagonal elements of H refers to the effective potential of an electron in the corresponding AO χ. The off-diagonal elements of H are called the interaction or resonance integral. $S_{\mu\nu}$ is the overlap integral between two orbitals χ_μ and χ_ν. K is a proportionality constant. Since the effective potentials are negative quantities, $H_{\mu\nu} \propto - S_{\mu\nu}$.

The modification of the orbitals of one fragment due to another fragment is studied using the perturbation theory. Consider the perturbation of the orbital, ψ^0_{iA} on fragment A due to the fragment orbitals on B, ψ^0_{jB} and also the remaining orbitals on A, ψ^0_{kA}, the $\delta H_{\mu\nu}$ and $\delta S_{\mu\nu}$ values will be the $H_{\mu\nu}$ and $S_{\mu\nu}$ of the composite system AB. The various terms of the mixing coefficients are given by;

$$t_{ji}^0 = t_{ji}^{(2)} = 0$$

$$t_{ji}^{(1)} = \frac{H_{ij} - e_{iA}^0 S_{ij}}{e_{iA}^0 - e_{jB}^0} \propto \frac{-S_{ij}}{e_{iA}^0 - e_{jB}^0} \quad \text{.................} \quad (1.27)$$

$$t_{ki}^0 = t_{ki}^{(1)} = 0$$

$$t_{ki}^{(2)} = \sum_{j \in B} \frac{(H_{ij} - e_{iA}^0 S_{ij})(H_{jk} - e_{iA}^0 S_{jk})}{(e_{iA}^0 - e_{kA}^0)(e_{iA}^0 - e_{jB}^0)} \propto \sum_{j \in B} \frac{S_{ij} S_{jk}}{(e_{iA}^0 - e_{kA}^0)(e_{iA}^0 - e_{jB}^0)} \quad\text{.................... (1.28)}$$

$$t_{ii}^0 = 1; \; t_{ii}^{(1)} = 0$$

$$t_{ii}^{(2)} = -\sum_{j \in B} [S_{ij} t_{ji}^{(1)} + \frac{1}{2}(t_{ji}^{(1)})^2] \quad\text{................. (1.29)}$$

The set of perturbed orbitals, ψ_i with energy E_i, can be written as a linear combination of the unperturbed orbitals;

$$\Psi_i = t_{ii} \psi_i^0 + \sum_{j \neq i} t_{ji} \psi_j^0 \quad\text{---------------- (1.30)}$$

Replacing the mixing coefficients, equation (1.30) becomes

$$\Psi_i = (1 + t_{ii}^{(2)}) \psi_{iA}^0 + \sum_{j \in B} t_{ji}^{(1)} \psi_{jB}^0 + \sum_{\substack{k \in A \\ k \neq i}} t_{ki}^{(2)} \psi_{kA}^0 \quad\text{.................... (1.31)}$$

Based on the equations (1.27), (1.28) and (1.31), one can arrive at the nature of the resultant wave function, depending on the relative ordering of ψ_{iA}^0, ψ_{kA}^0 and ψ_{jB}^0 with respect to their energies.

1.1.4 Population Analysis[7]

The probability of finding an electron in a small volume element dr is given by $\rho(r)dr$ where $\rho(r)$ is the electron density function. Integral over the space r, gives the total number of electrons, n. The electron density function is given by;

$$\rho(r) = \sum_{\mu}^{N}\sum_{\upsilon}^{N} P_{\mu\upsilon} \phi_\mu \phi_\upsilon \quad\text{-------------- (1.32)}$$

where $P_{\mu\upsilon}$ are the elements of the density matrix. Integration of (1.32) leads to

$$\int \rho(r)\, dr = \sum_{\mu}^{N}\sum_{\upsilon}^{N} P_{\mu\upsilon} S_{\mu\upsilon} \quad\text{------------ (1.33)}$$

17

where $S_{\mu\nu}$ is the overlap matrix over basis functions. Since the basis functions are normalized, $S_{\mu\mu} = 1$ and the diagonal elements are just $P_{\mu\mu}$. Each of these diagonal components then represents the number of electrons directly associated with a particular basis function ϕ_μ. The off-diagonal elements that occur in pairs of equal magnitude, $P_{\mu\nu} S_{\mu\nu}$ and $P_{\nu\mu} S_{\nu\mu}$, are summed to give the overlap population between the two basis functions, ϕ_μ and ϕ_ν. It is given by;

$$Q_{\mu\nu} = 2 P_{\mu\nu} S_{\mu\nu} \text{----------------} (1.34)$$

A more convenient way of analyzing the electron distribution is by partitioning the total charge among only the individual basis functions. It is done by dividing overlap population, $Q_{\mu\nu}$, equally between the basis functions, ϕ_μ and ϕ_ν. This type of partitioning is termed as Mulliken's Population Analysis. The partitioning gives a gross population for ϕ_μ as

$$q_\mu = P_{\mu\mu} + \sum_{\nu \ne \mu} P_{\mu\nu} S_{\mu\nu} \text{----------------} (1.35)$$

Summation of q_μ for all basis functions on a particular atom gives the gross atomic population. Similarly total overlap population q_{AB}, between two atoms A and B is defined as

$$q_{AB} = \sum_{\mu}^{A} \sum_{\nu}^{B} Q_{\mu\nu} \text{----------------} (1.36)$$

A large positive value for q_{AB} indicates bonding interactions between the two atoms and a large negative value indicates antibonding interactions. Hence it provides qualitative information about the bonding. It strongly depends on the nature of the basis set and also should be used with caution as the above partitioning is arbitrary.

1.1.5 Quantum Mechanical Calculations in Extended Systems

i. Extended Hückel Method[10]

Application of simple Hückel theory on a finite cyclic system with N atoms having N π orbitals gives the energy of the jth orbital as;

$$e_j = \alpha + 2\beta \cos \frac{2\pi j}{N} \quad \text{.............} \quad (1.37)$$

Applying the cyclic boundary condition on a chain of N atoms where N is very large, the extended system can be taken as a segment of a large ring. Since N is a large number, equation (1.37) can be modified introducing a new index, k, which makes it easier to handle. k is related to j and N through the length of the unit cell, a; $k = 2\pi j/Na$. Equation (1.37) then becomes;

$$e_j = \alpha + 2\beta \cos ka \quad \text{............} \quad (1.38)$$

As j varies from 0 to $\pm(N-1)/2$, k runs from 0 through $\pm\pi/a$. One important difference between the finite and infinite cases is that whereas j increases in discrete steps, k increases continuously. In both the cases when $|j| > (N-1)/2$ and $|k| > \pi/a$ leads to redundant information. In the crystal the region of k values between π/a and $-\pi/a$ is called the First Brillouin Zone. The wavefunctions with different energies e_j have characteristics similar to Hückel MOs. Thus the number of nodes increases as the energy is raised – the lowest lever nodeless and the highest having the maximum number of nodes. This LCAO approach in extended systems is called the tight-binding method. Here the wave functions are given by the Bloch function

$$\psi_k \sim \sum_{r=0}^{N-1} e^{ikra} \phi_r \quad \text{............} \quad (1.39)$$

ϕ_r is the basis set of the rth unit cell in a system containing N of them.

ii. Density Functional Theory[11]

The electronic wave functions at each k point are expanded in terms of discrete plane-wave basis set. The plane-wave basis is possible because of the special pseudo potential experienced by the pseudo valence electrons from the pseudo ion cores, which is the same as the original electrons outside the core region and weaker inside the core region. When plane-waves are used as a basis set for the electronic wave functions, the resulting Kohn-Sham equation, after substituting for the Bloch function and integration gives the secular equation;

$$\sum_{G'} \left[\frac{h^2}{2m} \left| k + G \right|^2 \delta_{GG'} + V_{ion}(G - G') + V_H(G - G') + V_{XC}(G - G') \right] c_{i, k+G'} = \varepsilon_i \, c_{i, k+G}$$

where G is the reciprocal lattice vectors, V_{ion} is the total electron-ion potential, V_H is the Hartree potential and Vxc is the exchange-correlational potential. Since the coefficients $c_{i, k}$ + G for the plane waves with small kinetic energy $\frac{h^2}{2m} \left| k + G \right|^2$ is more important than those with large kinetic energies, the plane-wave basis set is truncated to include only the plane waves that have kinetic energies below a cut-off value. Also the electronic wave functions at k points that are very close will be almost identical. Hence it is possible to represent the wave functions over a region of k space by the wave functions at a single k point.

The minimization techniques using conventional matrix diagonalization requires an initial guess for the electronic charge density, from which V_H and V_{XC} is calculated. The Hamiltonian matrices are constructed at each k point and diagonalized to obtain the Kohn-Sham eigen states. Using these eigen states a different charge density is constructed and the process is repeated until the solutions are self-consistent. The total

energy should be converged both as a function of the number of k points and as a function of the cut off energy for the plane-wave basis set.

Conventional matrix diagonalization methods are very expensive computationally and alternative methods allowing calculations on larger and more complex systems are available. In the molecular dynamics method developed by Car and Parrinello, a single function is minimized through simulated annealing. Conjugate-gradients method replaces simulated annealing with a direct, completely self-consistent second-order search for the minimum.

The self-consistent field theory is usually implemented within the local-spin density approximation (LSD) for the exchange correlation energy.

$$E_{xc}[n_\uparrow, n_\downarrow] = \int d^3r \; n_\sigma \, \varepsilon(r_s, \zeta)$$

Where $n(r) = n_\uparrow + n_\downarrow$ and n_σ is the density of electrons with spin a. Here $r_s = (\tfrac{3}{4}\pi n)^{1/3}$ is the local seitz radius, $\zeta = (n_\uparrow - n_\downarrow)/n$, is the local polarization and $\varepsilon(r_s, \zeta)$ is the exchange-correlation energy per particle for a uniform electron gas. The LSD approximation is valid in principle for slowly varying densities. It has met with impressive practical success but it underbinds the core electrons in an atom and overbinds the atoms in a molecule or solid.

An alternative form known as conjugated gradient approximations (CGA) uses the additional information about the electron gas of slowly varying electron density

$$E_{xc}[n_\uparrow, n_\downarrow] = \int d^3r \; f(n_\uparrow, n_\downarrow, \Delta n_\uparrow, \Delta n_\downarrow)$$

These "semilocal" functionals have demonstrated to be very much improved over LSD in applications to molecules as well as solids and is employed in our calculations on extended structures.

1.2. QUALITATIVE IDEAS

In the history of chemical bonding, qualitative tools have always advanced ahead of the quantitative measurements. While qualitative ideas provide a simple, but comprehensible way of perceiving a problem, quantitative tools are necessary to verify such predictions, to clarify where ambiguities exist and to obtain theoretical data where experiments are difficult. The lack of sufficient computational power often limited extensive quantitative predictions. The important electron counting rules that emerged as a part of comprehending chemical bonding and structure are briefed below.

1.2.1. Electron Counting Rules

Electron counting rules lead to a systematic expansion of knowledge concerning a set of molecules of interest, by permitting the incorporation of experimental and theoretical findings within a logically consistent and reasonably simple framework. It's most significant aspect is to reduce the complexity of the full problem of large number of experimental observations, by presenting the relevant generalizations. The most prevalent conviction about electron counting rules is to consider them as facts and molecules that are not following these rules are termed as disobedient. On the contrary, an electron-counting rule is merely an unsubstantiated hypothesis or a speculation concerning the reality, which will become useful only when appropriate confirmatory data have been obtained. Though exceptions occur in significant amounts for all these

rules, they still represent a considerable step forward in chemical reasoning and often these exceptions lead to further research and improved understanding. The counting rules described in this section played a crucial role in the development of borane chemistry, even though most of these rules cannot be extended to the condensed polyhedral boranes.

i. Atomic Electron Counting Rules

Lewis' octet rule[1] was developed in the early twenties of the last century as the offspring of Mosley's modern periodic table. It is based on the assumption that most atoms utilize only their s and p orbitals. Therefore, each atom has a maximum of eight electrons in the valence shell, which is the sum of shared pairs and lone pairs. The octet rule enjoyed major success in explaining the valences exhibited by atoms and in accounting for the nature of chemical bonds. The octet rule also indirectly indicates the nature of interactions by classifying them as covalent (or coordinate) or ionic depending on the number of electrons shared, given up or accepted in reaching the octet. While $LiCl$ or NaF on the ionic side and CH4 on the covalent side were the prototypical examples of the eight-electron rule, the diborane, B_2H_6 was one among the several exceptions. The tendency of boron to form non-ionic multi-centered bonds is impossible to comprehend using the classical valence bond description of a 2c-2e bond. This multi-centered bonding picture proposed for diborane (B_2H_6) was debated for a long time and acquired universal acceptance only after a decisive experimental verification.[12, 13] The difficulty of boron to have four 2c-2e covalent bonds in a neutral hydride led to the concept of electron deficiency of atoms. Polyhedral bonding is exhibited by boron to reduce electron deficiency, by sharing electrons between many centers. This inherent tendency

of boron to form non-classical structures is also exhibited by other elements when they are placed in an electron deficient environment.

The eighteen-electron rule is the transition metal version of the octet rule formulated by Sidgwick[14] to evaluate the electronic requirements of complexes, as the basic assumption of the octet rule limits its applicability to main group elements. Also referred as the EAN (Effective Atomic Number) rule, this predicts that the sum of the electrons on the metals plus the electrons donated by the ligands should be equal to the atomic number of the nearest noble gas. As transition metals form large number of complexes with main group elements, this rule is extremely powerful in traditional transition metal chemistry. The availability of the d orbitals with their varied symmetry, the larger size of the transition metal atom and a variety of ligands all lead to many exceptions. In many polyhedral borane-transition metal complexes, the estimation of the number of electrons donated from the borane to the transition metal is not straightforward, except for the dicarbollide ligands. The dicarbollides are found to mimic hydrocarbyl ligands and stabilize transition metal complexes.[15, 16] This is especially true if the borane ligand is a macropolyhedral system.[17] It is increasingly felt that cluster electron counting rules and isolobal relationships are much more reliable in assessing the electronic requirements.[16]

ii. Molecular Electron Counting Rules for Monomers

Just as attaining the noble gas configuration is the prime criterion for the above electron counting rules, attaining aromatic character is the basic premise upon which the molecular electron counting rules are formulated. The dimensional attribute of aromaticity arises from the nature of delocalization, i.e., cyclic systems exhibit two-dimensional aromaticity and spherical systems involve three-dimensional aromaticity.[18]

Almost all of these counting rules are derived using MOT and can be understood by analyzing the nature of interactions between the orbitals of the concerned fragments or groups.

A. Annulenes

Hiickel's (4n+2) rule governs the two-dimensional aromaticity of planar monocyclic systems. This rule is derived from the simple Hückel's Molecular Orbital (HMO) theory,[19-21] where the σ-framework is completely neglected. In this π-electron method, both the HOMO and LUMO are always doubly degenerate for cyclic systems except in a very few cases. Removal of an electron pair leaves the aromatic system with unpaired spins and makes it unstable (4n systems - anti-aromatic). The set of molecular orbitals obtained by the HMO analysis show that a closed shell system is obtained only when there are 4n+2 π electrons,

$$N = 4n+2 \qquad \qquad \qquad (2.1)$$

Where N is the total number of π-electrons and n = 0, 1,2, etc.

This rule is applicable if the molecular system under consideration has cyclic delocalization of π-electrons arising from the unhybridized p orbitals that are perpendicular to the σ-framework. It is important to note that the only variable 'n' in eqn.(2.1) can be any positive integer and is completely independent of any system-specific attributes. Hence, any system with unhybridized perpendicular p orbitals within overlapping distance can be aromatic provided the right number of electrons is available. This unrestricted nature of the rule made it applicable to a variety of structures, leading to different classes of aromaticity. The prototypical example is benzene, and its many variations have been dealt extensively in the past.

B. Polyhedral Boranes

A systematic MO theoretical investigation on polyhedral boranes of higher symmetry ($B_{12}H_{12}{}^{2-}(I_h)$, $B_6H_6{}^{2-}(O_h)$) was made in the early fifties, much before the experimental characterization of these boranes.[4] This revealed that these high-symmetry structures require two electrons in addition to what is available in the neutral skeleton and also that the $B_{10}H_{14}$ polyhedral skeleton can be viewed as an icosahedron with some missing vertices. Recognition of the different bonding patterns[22, 23] exhibited by boranes synthesized in sixties and seventies[3] led Wade to formulate a generalized electron counting rule for all simple polyhedral boranes.[24"28] Generally referred as Wade's rule[23"-28] (or William/Wade formalism[28]) it elegantly explains the structural motifs of various polyhedral boranes. Based on this revolutionary electron counting rule, all of the available polyhedral boranes can be classified into discrete classes like *closo*, *nido*, *arachno* etc. Though exceptions to this rule are also found,[-'--] it is impossible to understand the several distinct patterns exhibited by polyhedral boranes without this rule.

According to Wade's rule, the number of skeletal bonding molecular orbitals of a polyhedral borane that is homeomorphic to a sphere (eg. *closo*-borane) is just one more than the number of boron atoms in the cluster. The second important attribute is that this requirement of $n+1$ electron pairs is not altered even if the *closo*-borane has defects by losing some vertices to form *nido* or *arachno* structures or by having additional capping vertices.[26, 29-30] Hence, the total number of skeletal electron pairs required for *closo* and open *{nido* or *arachno)* structures are given by eqns. (2.2) and (2.3) respectively.

$$N = n + 1 \quad\text{————————(2.2)}$$

$$N = n + 1 + p \quad\text{------(2.3)}$$

Where,

n → number of vertices in the polyhedral skeleton

p → number of vertices that are absent.

This implies that the number of electron pairs required is n+1 for *closo*-borane, n+2 for a *nido*-borane and n+3 for an *arachno*-borane. Among these, *closo* boranes exist as charged species with high stability. Other forms generally have bridging hydrogen atoms on the surface of the open face, each of which will donate their electron to the cluster bonding and such clusters are relatively more reactive. Thus $B_{12}H_{12}^{2-}$ has an electron pair count of n+1 whereas $B_{11}H_{14}^{1-}$ has n+p+1 (p=1) electron pairs (Figure 1). A cap when present over the polyhedron has to be subtracted from the total number of vertices, which includes the capping vertices as well, to arrive at the total number of skeletal electron pairs for such a system.

$$N = n + p - q + 1 \quad\text{————————}\quad (2.4)$$

q → number of capping vertices

$B_{13}H_{13}$ (Figure 1) is a hypothetical example in which an extra electron pair is obtained from a capped BH vertex on an icosahedron (q=1) so that it is neutral rather than charged.[31]

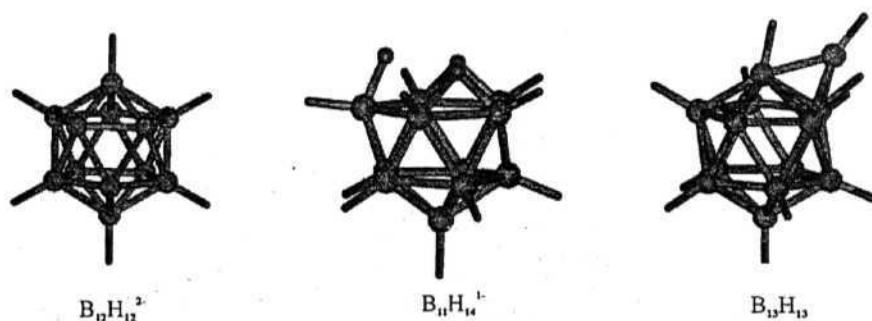$B_{12}H_{12}^{2-}$ $B_{11}H_{14}^{1-}$ $B_{13}H_{13}$

Figure 1

The *nido* and the capped system originating from a *closo* B_{12} skeleton

Unlike the Hückel's 4n+2 rule, Wade's rule is a function of two variables, the number of total vertices of the polyhedra and the number of missing vertices with respect to its *closo* form. Both of them are exclusively system specific. In several occasions, the value of q is ambiguous, which can be attributed primarily due to the lack of clear distinctive features in the open structures.[28] Perception of the number of missing vertices in the parent *closo*-borane skeleton, by visual inspection of the open structure allows room for arbitrary conclusions. When B-H vertices are replaced by transition metal fragments, isolobal analogy[9f] is used to reduce the problem to a familiar ground. This has allowed the use of Wade's rule to connect seemingly different branches of chemistry *viz.*, boranes, transition metal clusters and even zintl type clusters.[32] Metallaboranes furthered these implications by representing a hybrid between boranes and transition metal clusters.[33] However these rules pertain to a single polyhedral system.

C. Transition Metal Clusters

In polyhedral boranes, the electronic requirement is given by the Skeletal Electron Count (SEC),[24] which is the number of electrons required to fill the Bonding Molecular Orbitals (BMO) involved in the skeletal bonding. In the case of transition metal clusters, it is expressed in terms of Polyhedral Electron Count[26, 34] (PEC) which is the sum of the number of electrons required for skeletal bonding and the number of electrons involved in *exo*-2c-2e bond along with the number of non bonding pairs.[35] A comparison of the calculated MO energies of the bare octahedral clusters of cobalt and boron[34] showed greater resemblance in the antibonding region. In addition to the MOs originating from s and p orbitals, the cobalt cluster has a narrow band of MOs derived from the d orbitals[34, 35] which render it difficult to have a sharp boundary for skeletal MOs. It can also result in a partial involvement of the metal 'non-bonding' orbitals in the skeletal bonding. This

necessitates the use of polyhedral electron count rather than skeletal electron count as a criterion for the determination of electronic requirements. Termed as Polyhedral Skeletal Electron Pair Theory (PSEPT), it successfully explains the charges exhibited by several transition metal carbonyl clusters. Using this methodology, the electrons required for a *closo*-borane is 4n+2 (n = number of vertices), which includes the electrons involved in the *exo*-2c-2e bonds. In the case of transition metal carbonyls, this expression becomes 14n+2, which includes the additional contribution of five d orbitals of the transition metals. $[Os_5(CO)_{15}]^{2-}$ has a trigonal bipyramidal structure and has a PEC of 72 (n=5). The osmium atoms and the carbonyl groups provide 70 electrons. This explains a charge of -2 for the compound. The straightforward extension of Wade's rule through isolobal analogy is also used in naked metal clusters with or without *exo* 2c-2e bonds.

D. The Relation between Two and Three-dimensional Aromaticity

The electron counting rules of aromaticity formulated for cyclic systems like annulenes and spherical systems like polyhedral boranes, though nurtured individually, are intimately related to each other. This can be easily visualized using the six-interstitial-electron rule,[36] which is devised primarily to explain the isomeric stability of carboranes. This approach involves the conceptual division of three-dimensional aromatic *closo* boranes such as $B_6H_6^{2-}$, $B7H7^{2"}$ into two-dimensional rings and caps. If we consider all the boron atoms in the ring to be of sp^2 hybridized, one of the sp^2-hybridized orbitals will be used in the *exo* B-H bond. The two remaining sp^2-hybrid orbitals form the σ-framework of the ring, which is equivalent to the σ-framework in annulenes. However, unlike annulenes, the unhybridized p orbital of each boron atom that is perpendicular to the plane of the ring is empty. Three of these vacant MOs of the ring

fragment are stabilized by the interaction with the orbitals of the two capping B-H groups on both sides of the ring, resulting in a complete spherical framework. Since each B-H cap has one electron pair that has to be delocalized, the total number of electrons involved is four. In order to fill the three stabilized MOs two more electrons are required which justifies the dianionic nature of these *closo* boranes.

This can also be illustrated by the successive removal of the capping vertices from the borane followed by the substitution of carbon atoms in the ring. Scheme I and II illustrate the effect of removing the capping atoms successively. Three-dimensional aromatic systems like *closo* $B_6H_6^{2-}$ and $B7H7^{2*}$, upon transformation, will be reduced to two-dimensional aromatic systems with proper charges. Here the electronic requirement specified by Wade's rule smoothly converges to Hückel's rule when a polyhedral borane is reduced to a cyclic aromatic hydrocarbon.[37]
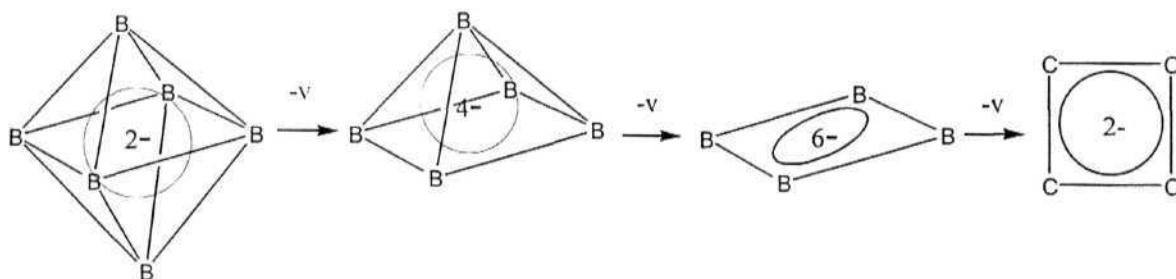
SCHEME I
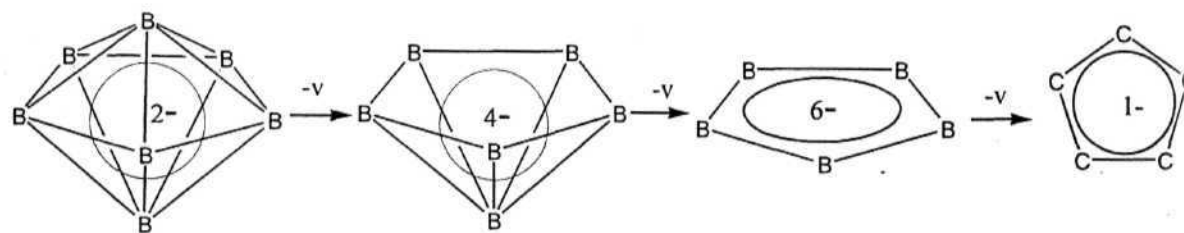
SCHEME II

Thus far, electron counting rules that govern the stability of an isolated aromatic unit were focused. In the next section, the behavior of condensed systems where two or more aromatic units interact together to form macro-aromatic systems will be considered.

iii. Electron Counting Rules for Macroaromatic Systems

Macro-aromatic systems in general can be defined as molecules that possess two or more mutually interacting aromatic fragments, which enables delocalization to be extended to span the individual fragments. Three different topological modes of interaction are possible between two aromatic units.[38]   i) A Condensed mode of interaction, in which the individual aromatic units share one or more edges. This pattern is ubiquitously found in both two-dimensional and three-dimensional aromatic compounds. Naphthalene is an example in the case of hydrocarbons and $B_{20}H_{16}$ (Figure 2) with a four-atom fusion is an example of condensed polyhedron. ii) A stacked mode of interaction, in which the individual aromatic units share a single vertex. This type of sharing is predominantly found among polydecker sandwiches where the shared vertex is preferentially occupied by bigger heteroatoms, though some transition metal clusters do exhibit this pattern. Ferrocene and other metal-carborane sandwich complexes belong to this class of compounds. iii) A linked mode of interaction, in which the two aromatic units are interconnected by 2c-2e / 3c-2e bonds. Biphenyl forms a model of C-C linkage in two-dimensional aromatic systems. In three-dimensional structures, examples are known where two $B_{10}(D_{4d})$ units are joined by a 2c-2e bond between two boron atoms. Here, the electronic requirement is found to be additive, i.e., the total electron requirement is the sum of the electronic requirements of the individual aromatic units. Electron counting rules that govern aromatic stability of different molecular systems were reported and they all share some common characteristics as discussed below.

A. Polycyclic Aromatic Hydrocarbons

The high and innate catenation tendency of carbon leads to huge number of polycyclic aromatic hydrocarbons. All of them exhibit either a condensed mode sharing an edge or a linked mode of interaction. The stacked mode of interaction is completely absent owing to its "electron sufficient" nature. Most of the compounds contain hexagonal units as the dominant repeating unit. Such hexagons are found even in the polymorphs of carbon, such as graphite and fullerenes.

Hückel's 4n+2 rule itself can be applied to the many polycyclic systems like linear and catacondensed hydrocarbons where all the carbon atoms lie on the perimeter of the molecule. Unlike boranes, many of the polycyclic aromatic hydrocarbons are stable neutral species. Hence, the presence or absence of Kekulé valence structures is of critical importance[39] and several generalized[40, 41] or system specific computer algorithms[42] are available to enumerate the number of Kekulé valence structures even for very large systems, which is found to be a fair indicator of stability. In condensed aromatic systems, it is found that the delocalized π-electrons are shared among the individual aromatic units.

B. Macrotransition Metal Clusters

There are numerous high-nuclearity transition metal clusters in which two or more individual polyhedral units interact together to form the macroaromatic system. As bonding in simple transition metal clusters can be understood by Wade's rule using the isolobal analogy, Mingos extended these ideas to cover the transition metal clusters.[34, 43] According to this rule, the overall electron requirement of a macropolyhedral cluster is the sum of the electronic requirements of the individual units minus the electron count characteristic of the atom, pair of atoms or triangular face shared between them. The

characteristic requirement of the shared atoms is defined as 18 electrons for vertex sharing polyhedra, 34 for edge sharing polyhedra and 48 for face (triangle) sharing polyhedra. It is to be noted here that the electronic requirement of individual cluster is taken as the total number of electrons in the cluster including the *exo* 2c-2e bonds. This methodology gives 4n+2 electrons for (*closo*) borane clusters and 14n+2 electrons for (*closo*) transition metal clusters.

Using this axiomatic basis, the total number of electron pairs, in the condensed polyhedra having two interacting aromatic units can be expressed[34] as

$$N = (7n+1) + (7m+1) - (9v-e) \quad . \quad . \quad . \quad . \quad (2.5)$$

Where

n $\rightarrow$ number of vertices in the first fragment

m $\rightarrow$ number of vertices in the second fragment

v $\rightarrow$ number of shared vertices

e $\rightarrow$ number of shared edges

This rule derives the electronic requirement of individual aromatic units by using the Wade's rule. The second term (9v-e) is referred as the electronic characteristic of the shared fragment. An example to illustrate this rule is the complex $[Ru_{10}C_2(CO)_{24}]^{2-}$, which is essentially two octahedra fused by an edge. Eqn (2.5) is derived based on the assumption that the condensed polyhedron can be viewed as a complex between two individual polyhedra, with one polyhedron acting as a ligand donating electrons to the second polyhedron. If the condensed system of two interacting units can be separated into individual fragments in such a way that one of the fragments retains the shared atom and the other fragment without the shared atom, the second fragment acts as a ligand. The

33

number of electrons donated from the 'ligand' fragment is defined to be 6 for single vertex sharing systems owing to its *nido* framework. For edge sharing system, the ligand fragment is treated as 10-electron donor owing to its *arachno* pattern. Using this axiomatic basis, the number of electron pairs in the condensed polyhedron having two interacting aromatic units can be expressed as

$$N = (7a+1) + (7b+x+1)-y \quad . \quad . \quad . \quad (2.6)$$

Where

a → number of vertices in the (*closo*) first fragment

b → number of vertices in the second fragment

x → number of shared vertices

y → number of electrons donated from the ligand fragment.

For vertex and edge shared systems this equation can be reduced to eqn (2.5). Extending this implication further for a face-shared system, the ligand fragment should act as a 14-electron donor.[34] However, electronic characteristic of the shared face becomes 25 electron pairs, which is one more than the value used by Mingo's for face-sharing system. Though an MO theoretic justification is still lacking, this rule explains the charges of several macropolyhedral transition metal carbonyls successfully. It is interesting to note that bridging carbonyl groups of transition metal clusters acts like bridging hydrogens in boranes donating two electrons to the skeletal bonding.

C.   Condensed Polyhedral Boranes

In the case of condensed clusters of main block elements the polyhedral skeletal electron counting rules of Mingo's had to be reformulated.[43"45] In the place of the eighteen-electron rule, the octet rule was employed for clusters of main group elements

and the electronic characteristic becomes 4v - e. The electronic characteristic for the shared fragment then is 8, 14 and 18 respectively for vertex, edge and face sharing main block clusters. The resulting predictions were found to be inappropriate, even for characteristic structures. Later, these values were modified suitably to 4, 12 and 18 respectively.[44, 45] A clear justification for the choice of these numbers is yet to emerge. The six and ten electron donation based explanation, which works for vertex and edge shared transition metal clusters, is also inapplicable in the domain of condensed clusters of main block elements.

The studies on different modes of condensation of relatively simple individual aromatic clusters of main block elements revealed the nature of the interaction between the BMOs in a systematic manner and successfully predicted the electronic requirements of the condensed main block clusters in specific instances.[46] Here the electronic requirement can be conveniently expressed in terms of the total number of skeletal atoms n and the number of individual aromatic fragments (or polyhedra) m that constitutes the macro-aromatic system.

$$N = n + m \quad \ldots \ldots \ldots \ldots \ldots \ldots \quad (2.7)$$

With the exception of single vertex sharing, this definition includes all the macroaromatic systems characterized so far including 'very condensed' systems[17] where more than two aromatic units are interacting with each other. The first *closo* macropolyhedral borane. $B_{20}H_{16}$ stands as an evidence for this rule. This kind of interaction results in the overall decrease in the charges when macropolyhedral boranes are concerned.

$B_{20}H_{16}$

$m = 1, n = 20$
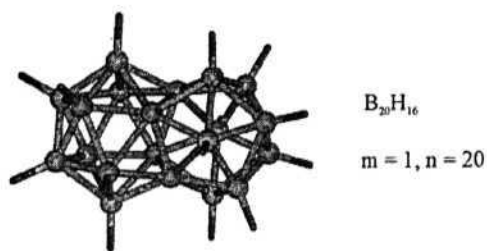
Figure 2

The structure of $B_{20}H_{16}$ involving the fusion of two icosahedra through four boron atoms.

The above summary shows that bonding in sandwiched compounds of polyhedral boranes is not accounted for. Also an electron counting rule, which can merge the various modes of condensations in polyhedral boranes as well as different classes like metallocenes and metallaboranes with polyhedral boranes is lacking. This thesis includes our attempts towards these and further studies on mono, condensed and extended polyhedral boranes to support our findings.

REFERENCES

1. (a) Pauling, L., *The Nature of the Chemical Bond and the Structure of Molecules and Crystals,* Cornell University Press, U.S.A., **1960.** (c) Lewis, G. N.,*J. Am. Chem. Soc,* **1916,** *38,* 762. (b) Abegg, R. *Z. Anorg. Chem.,* **1904,** *39,* 330.

2. Klein, D. J.; Trinajstic, N., *Valence Bond Theory and Chemical Structure,* Elsevier, Amsterdam, **1990.**

3. (a) Lipscomb, W. N., *Boron Hydrides;* Benjamin, New York, **1963.** (b) Muetterties, E. L. *Boron Hydride Chemistry;* Academic Press, New York, **1975.**

4. Longuet-Higgins, H. C; Roberts, M. de. V. *R. Soc. London, Ser. A* , 1955, *230, 110.*

5. (a) Streitwieser, Jr., A. *Molecular Orbital Theory for Organic Chemists,* John Wiley & Sons, Inc., New York, **1961.** (b) Woodward, R. B.; Hoffmann, R. *The Conservation of Orbital Symmetry,* Verlag Chemie, GmbH, Weinheim/Bergstr, Germany, **1971.**

6. (a) Levine, 1. N. *Quantum Chemistry,* 2nd Edition Allyn and Bacon, Boston (b) McQuarrie, D. A. *Quantum Chemistry,* Oxford University Press, California, 1983. (d) Pilar, F. L. *Elementary Quantum Chemistry,* Mc-Graw Hill Publishing Co., New York, **1968.** (e) Chandra, A. C. *Introductory Quantum Chemistry,* Tata Mc-Graw Hill Publishing Co., New Delhi, **1988.** (f) Szabo, A.; Ostlund, N. S. *Modern Quantum Chemistry,* Mc-Graw Hill Publishing Co., NewYork, **1982.**

7. (a) Hehre, W. J.; Radom, L.; Schleyer, P. v. R.; Pople, J. A. *Ab-initio Molecular Orbital Theory,* John Wiley & Sons, Inc., New York, **1986.** (b) Pople, J. A.; Beveridge, D. L. *Approximate Molecular Orbital Theory,* Mc-Graw Hill Publishing Co., NewYork, **1970.** (c) Lowe, J. P. *Quantum Chemistry,* Academic Press, New

York, 1978. (d) Schaeffer III, H. F. *Electronic Structure of Atoms and Molecules,* Addison-Wesley, Massachusetts, USA, **1972.** (e) Foresman, J. B.; Frisch, A. *Exploring Chemistry with Electronic Structure Methods,* Gaussian Inc. Pittsburgh, USA. (f) Richards, W. G.; Cooper, D. L. *Ab initio Molecular Orbital Calculations for Chemists,* Clarendon Press, Oxford, **1983.** (g) Jensen, F. *Introduction to Computational Chemistry,* John Wiley & Sons, New York, **1999.**

8. (a) Parr, R. G.; Yang, W. *Density Functional Theory of Atoms and Molecules,* Oxford University Press, Oxford, **1989.** (b) Dreisler, R. M.; Gross, E. K. V. *Density Functional Theory: An Approach to the Quantum Many-body Problem,* Springer-Verlag, Berlin, **1990.** (c) Hohenberg, P. C.; Kohn, W.; Sham, L. J. *Advances in Quantum Chemistry,* vol. 21, Academic Press, 1990. (d) Kohn, W.; Becke, A. D.; Parr, R. G. *J. Phys. Chem.* 1996, *100,* 12974. (e) Hohenberg, P. C; Kohn, W. *Phy. Rev.* 1964, *136,* B864. (f) Kohn, W.; Sham, L. *J. Phys. Rev.,* 1965, *A140.* (g) Geerlings, P.; De Proft, F.; Langenaeker, W. *Chem. Rev.,* 2003, *103, 1793.*

9. (a) Hoffmann, R.; Lipscomb, W. N. *J. Chem. Phys.,* **1962,** *36,* 2179. (b) Hoffmann, R. *ibid.,* 1963, *39, 1397.* (c) Hoffmann, R. *ibid.,* **1964,** *40,* 2474. (d) Hoffmann, R. *ibid.,* **1964,** *40,* 2480. (e) Hoffmann, R. *ibid.,* **1964,** *40,* 2745. (f) Hoffmann, R. *Angew. Chem. Int. Ed Engl.* 1982, *21, 711.*

10. Albright, T.A.; Burdett, J.K.; Whangbo, M. *Orbital Interactions in Chemistry,* John Wiley & Sons, Inc, **1985.**

11. (a) Payne, M. C; Teter, M. P.; Allan, D. C.; Arias, T. A.; Joannopoulos, J. D. *Rev. Mod. Phys.,* **1992,** *64,* 1045. (b) Perdew, J. P.; Chevary, J. A.; Vosko, S. H.; Jackson, K. A.; Pederson, M. R.; Singh, D. J.; Fiolhais, C. *Phys. Rev. B,* **1991,** *46,* 6671.

12. (a) Price, W. C. *J. Chem. Phys.,* **1947,***15,* **614.** (b) Price, **W. C.** *ibid.,* **1948,***16,* **894.**

13. **Hedberg,** K.; Schomaker, **V.** *J. Am. Chem. Soc,* **1951,** *73,* **1482.**

14. **Sidgwick,** N. V. *The electronic theory of Valency,* Cornell University, Ithaca, **1927.**

15. Grimes, R. N. J. *Organomet. Chem.,* **1999,** 581,1.

16. (a) Fehlner, T. **P.** *Structure and Bonding,* **1997,** *87,* 112. (b) Fehlner, T.P. *Organometallics,* **2000,** 19,2643.

17. Kennedy, J. D, *Advances in Boron Chemistry:* Siebert, W., Ed.; Royal Society of Chemistry; Cambridge, UK, **1997: p** 451.

18. (a) Aihara, J.-I *J. Am. Chem. Soc,* **1978,** *100,* 3339. (b) Aihara, J.-i I *J. Am. Chem. Soc,* **1976,** *98,* 2750. (c) Aihara, J.-i I *J. Am. Chem. Soc,* **1976,** *98,* 2750. (d) Aihara, J.-i I *J. Org. Chem.,* **1977,** *99,* 2048. (e) Aihara, J.-i I *Bull Chem. Soc. Jpn.,* **1977,** *50,* 2010. (f) Gutman, I.; Milun, M.; Trinajstic, N. *J. Am. Chem. Soc,* **1977,** PP, 1692.

19. Hückel, E. Z. *Physik,* **1931,** *70,* 204.

20. Coulson, C. A.; Longuet-Higgins, H. C. *Proc. R. Soc,* **1947,** *192A,* 16.

21. Hückel, E. *International Conference on Physics,* Vol II London, **1934.**

22. Williams, R. E. *Inorg. Chem.,* **1971,** *10,* **210.**

23. Williams, R. E. *Adv. Inorg. Chem. Radiochem.,* **1976,** *18,* 67.

24. (a) Wade, K.; *Chem. Commun.,* **1971,** 792. (b) Wade, K. *Adv. Inorg. Chem. Radiochem.,* **1976,** *18,* **1.**

25. **Rudolph,** R. W.; Pretzer, W. P. *Inorg. Chem.,* **1972,** *11,* 1974.

26. Mingos, D. M. P.; *Nature (London) Phys. Science,* **1972,** *236,* **99.**

27. (a) Aihara, J.-I. *Bull. Chem. Soc. Jpn.* **1983,** *56,* 335. (b) Fowler, P. W. *Polyhedron,* **1985,4,2051.**

28. Kennedy, J. D. in *The Borane, Car borane, Carbocation continuum* Casanova, J., Ed.; John Wiley & Sons Inc, New York, **1998.** p. 85.

29. Mingos, D. M. P.; Welch, A. J. *J. Chem. Soc. Dalton Trans.* **1980,** 1674.

30. Mason, R.; Thomas, K. M.; Mingos, D. M. P. *J. Am. Chem. Soc,* **1973,** *95,* 3802.

31. McKee, M. L.; Wang, Z.; Schleyer, P. v. R../. *Am. Chem. Soc,* **2000,***122,* 4781.

32. Fox, M.; Wade, K. *The Borane, Carborane, Carbocation continuum* Casanova, J., Ed.; John Wiley & Sons Inc, New York, **1998.** p. 57.

33. Grimes, R. N. *Metal Interactions with Boron Clusters,* Plenum Press, New York, **1982.**

34. Mingos, D. M. P. *Acc. Chem. Res.,* **1984,** *17,* 311.

35. Mingos, D. M. P. *J. Chem. Soc, Dalton Trans.,* **1974,** 133.

36. (a) Jemmis, E. D. *J. Am Chem. Soc.* **1982,** *104,* 7017. (b) Jemmis, E. D., Schleyer, P. v. R. *J. Am. Chem. Soc.,***1982,** 104, 4781.

37. Jemmis, E. D.; Jayasree, E. G. *Submitted.*

38. Jemmis, E. D; Balakrishnarajan, M. M.; Pancharatna, P. D. *J. Am. Chem. Soc,* **2001,** 123,4313.

39. Dewar, M. J. S; Dunitz, J. D; Hafner, K; Heilbronner, E; Ito, S; Lehn J. -M.; Niedenzu, K; Raymond, K. N.; Rees, C.W.; Vogtle, F. (Ed.), *Topics Curr. Chem.,* **1989,** *153.*

40. Balakrishnarajan, M. M.; Venuvanallingam, P. *Computers. Math. Applic,* **1995,** *29,* 115.

41. Balakrishnarajan, M. M.; Venuvanalingam, P. *Appl. Math, Lett.,* **1996,** 9, 49.

42. Balakrishnarajan, M. M.; Venuvanalingam, P. *Comput. Chem.,* **1995,***19,* **101.**

43. Mingos, D. M. P. *J. Chem. Soc. Chem. Commun.,* **1983,** 706.

44. Mingos, D. M. P.; Johnson, R. L. *Struct. Bonding (Berlin)* **1987,** *68,* 31.

45. Mingos, D. M. P.; Wales, D. J. *Introduction to Cluster Chemistry*; Prentice HalhEnglewood Cliffs, NJ, **1990.**

46. Balakrishnarajan, M. M; Jemmis, E. D. *J. Am. Chem. Soc.* **2000,** *122,* 4516.

CHAPTER 2

BONDING IN CONDENSED (MACROPOLYHEDRAL) BORANES

2.0. INTRODUCTION

Polyhedral boranes have provided excitement in all branches of chemistry.[1] Aesthetically pleasing structures, path breaking bonding characteristics, unusual physicochemical properties, promising materials for the future, Boron Neutron Capture Therapy,[1e] membrane specific spherical structures,[1f] templates for catalysis[1g] - the range of areas spanned by boranes is indeed vast.[1] Several condensed polyhedra with borane structures are known in literature. Wade's rule, which has been successful in explaining the bonding in monopolyhedral boranes is inapplicable to assess the electronic requirements of condensed systems. Recently, a n+m skeletal electron pair count has been formulated for macropolyhedral boranes where condensation involves sharing of more than one vertex among m cages.[2] $B_{20}H_{16}$ with four atoms in common serves as the best example for this rule. [3] Face sharing polyhedral skeletons are found in extended solids.[4] The majority of the known macropolyhedral boranes are either edge-shared open cages or they share a single vertex.[5] We conducted a thorough survey of all macropolyhedral borane skeletons characterized experimentally so far that resulted in a generalized electron counting scheme, which is applicable to all aromatic systems including metallaboranes, polydecker sandwiches and any combination of these structural motifs. The generalizations and illustrations of the rule are discussed in the first section followed by a justification considering various modes of fusion. The second part also demonstrates the importance of the electron counting rule as a guiding tool, specifically taking an experimentally reported macropolyhedral borane, the molecular formula of which is estimated erroneously.

2.1. A GENERALIZED ELECTRON COUNTING *mno* RULE

In recent years, it is increasingly felt that there are several common features among two-dimensional aromatic organic molecules and three-dimensionally aromatic polyhedral boranes. There are also attempts to merge another thriving area viz.. organometallics with boranes through the * intermediacy of metallaboranes and metallocenes.[6] A generally applicable electron counting rule should help in this process. We provide here such a generalization that brings polyhedral boranes, polycondensed polyhedral boranes and metallocenes under the same umbrella.

The variety of bonding patterns exhibited by polyhedral boranes was explored by Lipscomb (styx)[1a], Wade[7a-7c], Williams[7d] and many others in the second half of the last century. A major breakthrough came from William's perception that the experimentally isolated *arachno* and *nido* boranes can be viewed as being derived from the nearest *closo* structures by the removal of a vertex rather than as fragments of icosahedral $B_{12}H_{12}$ skeleton. Wade's n+1 electron pair rule for a polyhedron exhibiting a *closo* pattern. $(B_{12}H_{12}{}^{2}$', 1 Figure 1) where n is the number of vertices was derived simultaneously. Application of the rule generated a Paradigm for the Electron Requirements of Clusters (PERC approach) by Rudolph.[9] The often reproduced chart of Rudolph gave a mnemonic way to correlate the different cluster patterns both by the debor approach and the seco approach and has been text book material for years.[10] According to the debor approach, a *nido* cluster will have one BH group (one vertex) less with respect to its nearest *closo* form. The seco approach treats a *nido* unit as derived from its *closo* analogue by the removal of a bond pair. An *arachno* cluster can be differentiated from its

nido in a similar fashion. The Wade's rule was extended to include electron deficient clusters with capped vertices where each cap normally donates an electron pair."

In this treatment of polyhedral bonding all the boron atoms were treated as sp hybrids. One sp hybrid radiates away from the center of the sphere forming the *exo*-2c-2e bond with the hydrogen atom or other substituents. Another sp hybrid points towards the center of the cage. The two remaining unhybridized AOs are tangential to the sphere. Hence, each atom contributes three orbitals for skeletal bonding. The radial orbitals combine in phase to generate a strong core bonding molecular orbital (BMO). The tangential orbitals upon linear combination produce the remaining n surface BMOs. The n+1 electron pairs of a *closo* polyhedron occupy all BMOs so that a favorable structure results. The n+1 rule was justified using graph theory by King and Rouvray.[12] Stone[13] derived it using the Tensor Surface Harmonic Theory. Chemistry of boranes flourished along with this easily applicable electron-counting rule.[1, 10, 14]

Early on there were examples of borane structures with condensed polyhedra. The first macropolyhedral borane, $B_{20}H_{16}$, (2, Figure 1) was isolated as a neutral species in the sixties.[3] It involves the sharing of four atoms between two icosahedra. This gave a clear indication that polycondensation of polyhedral boranes would reduce the electron requirement. Until then polyhedral boranes were known with negative charges and the neutrality of $B_{20}H_{16}$ was a mystery. Condensed structures, where the delocalized electronic **structure** of the individual polyhedron is not disturbed, can be understood by the **Wade's n+1 electron pair rule.** For example, Structure 3 (Figure 1), may be visualized as a combination of **two** polyhedra where the electronic structure of the individual icosahedral units is retained. However there are many other ways in which the

44

condensation can take place (Figure 2). The absence of an electron-counting rule, which can be applied to all these condensed structures is immediately felt. An analysis on the nature of interaction between individual aromatic units of polyhedral boranes in all the possible modes has already resulted in an electron-counting scheme[2] applicable to the whole range of main group elements. The rule gives the requirement of electron pairs as n+m for a *closo* macropolyhedral borane cluster, where m is the number of individual polyhedra involved in the condensation and n is the total number of vertices. For example the n+m electron pair count for $B_{20}H_{16}$ (2) is 20+2=22. The number of available electron pairs is also 22 (16 electron pairs from 16 BH groups and six from four boron atoms). *Nido* and *arachno* arrangements call for additional electron pairs.

Attempts to modify the n+m rule to include the single vertex condensations as well, have paved the way for a new rule, which is christened as the *mno* rule. It unifies polycondensed polyhedral boranes, metallaboranes, metallocenes and any of their combinations. With the new parameter 'o' standing for the number of single vertex bridging, the rule states that m+n+o skeletal electron pairs are required for the stability of condensed polyhedral boranes involving *closo* arrangements.

A generalized electron counting rule, which also takes into account the open structures and capping vertices[11] is given by N = m+n+o+p–q, where N is the skeletal electron pairs, m and n have the same implications as above, p is the number of missing vertices from its corresponding *closo* structure and q is the number of capping vertices. The electron-counting rule presented here is applied to a wide variety of boranes, heteroboranes and metallaboranes.

45

1. $[B_{12}H_{12}]^{2-}$

2. $B_{20}H_{16}$

3. $(C_2B_{10}H_{11})_2$

4. $[(C_2B_9H_{11})_2M]^{n-}$
M=Fe, Co, Ni, Al, Si n=0, 1, 2

5. $[(C_2B_9H_{11})_2M]^{n-}$
M=Ni, Cu, Au. n=1, 2

6. $[B_{22}H_{20}]^{2-}$

7. $B_{18}H_{20}^{2-}$

8. $[B_{21}H_{18}]^{1-}$

9. $[Cp^*IrB_{18}H_{20}]$

10. $[Cp^*IrB_{18}H_{19}S]^{1-}$

11. $[Cp_2^*Rh_2B_{17}H_{19}]$

12. $[Cp_2^*Rh_2S_2B_{18}H_{14}(OH)]$

13. $[Cp_2Fe]$

14. $[Pt(B_{18}H_{20})_2]^{2-}$

15. $[(PMe_2Ph)_3Pt_2B_{26}H_{28}]$

16. $[Cp_2^*Ru_3(B_4H_{10})_2]$

17. $[C_{23}H_{42}B_6CoRh]$
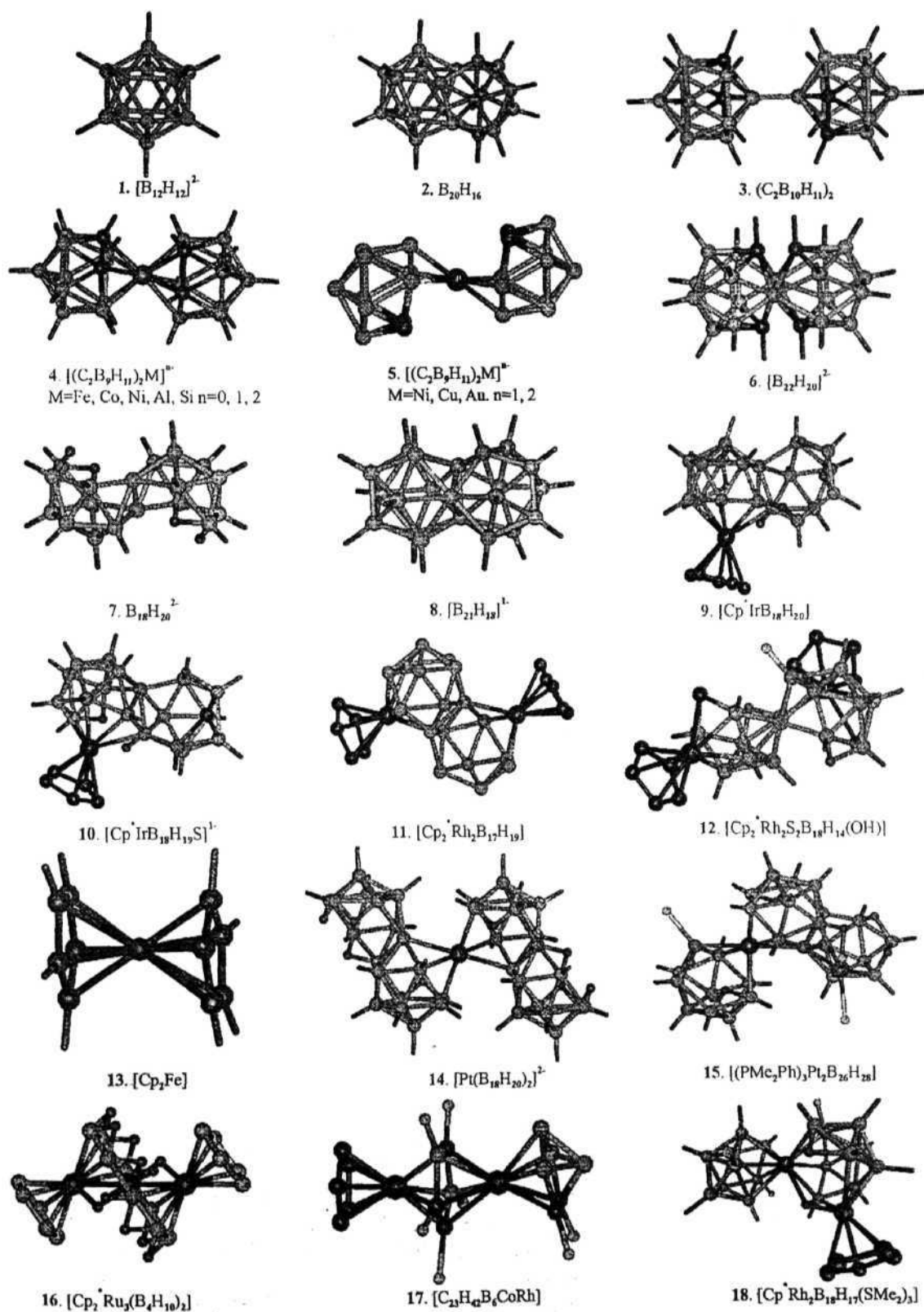
18. $[Cp^*Rh_2B_{18}H_{17}(SMe_2)_3]$

Figure 1

Representative examples (Structures 1-18) illustrating the *mno* rule are given.
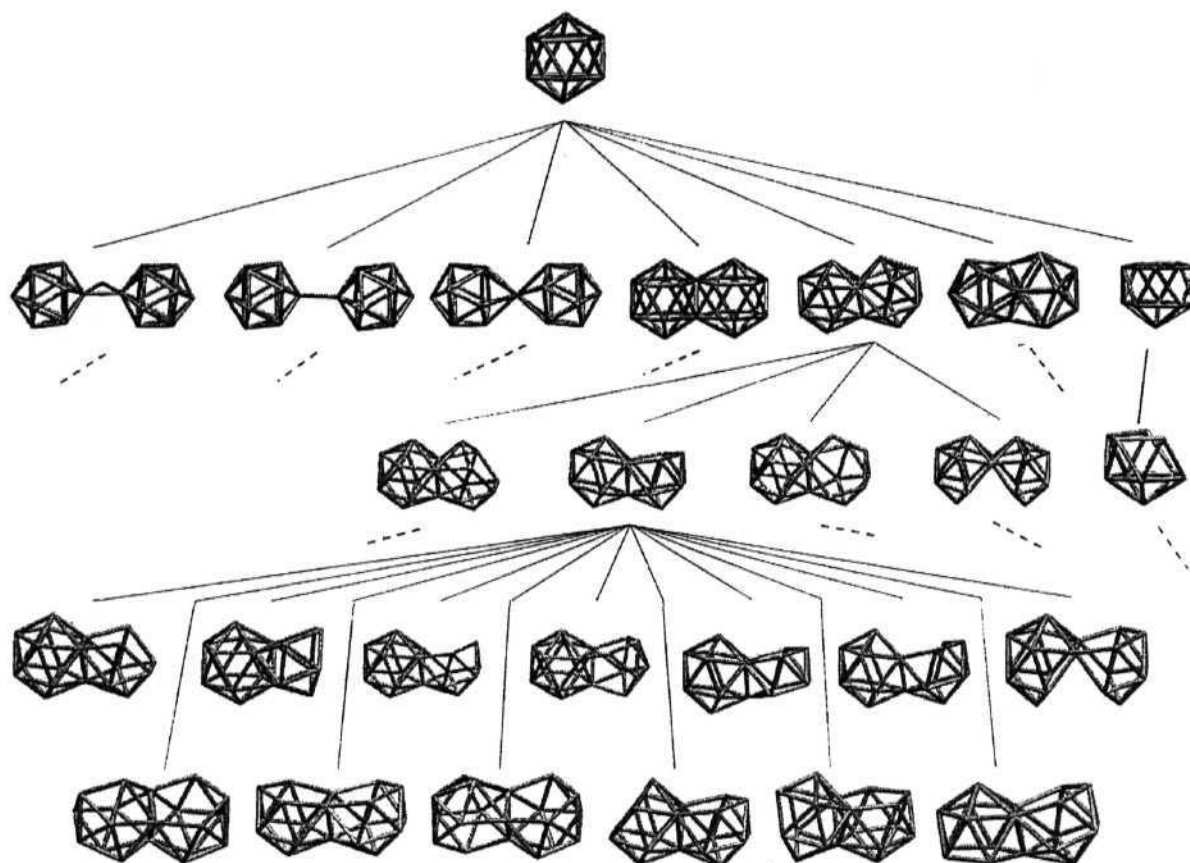
Figure 2

A comparison of the variety of polyhedral bonding exhibited by simple polyhedral boranes and its polycondensed analogues. A correlation between *closo, nido* and *arachno* patterns of macropolyhedral borane systems are shown. The last set includes both the *arachno* and *bisnido* structures. At each level one structure is expanded. Others too branch off in a similar fashion as shown by dotted lines.

Condensation of polyhedra provides infinite variety. Figure 2 demonstrates this using two polyhedra with different modes of condensation. For simplicity the correlation has been drawn considering only an icosahedral fragment though it will be applicable to other polyhedral clusters in any possible combinations. Expansion of a macropolyhedral *closo* form to different *nido* patterns has been done only on a single cluster. The possibility of open structures starting with an icosahedron alone grows exponentially and hence only one structure is expanded at a given level of this tree-diagram. Similarly the

arachno and *bisnido* structures emerging from a single *nido* pattern have been shown. The branch at the extreme right hand side starting from the icosahedron indicates the *closo*, *nido* and *arachno* path for monopolyhedral boranes discussed in the Rudolph diagram. Terminal hydrogens are omitted for clarity. The variety available in polycondensation is immediately obvious.

The success of any electron counting rule is in its applicability to a range of experimentally known systems and projections for the unknown. The generality of the *mno* rule by applying it to a large set of structures is demonstrated. Despite the success it is good to remember that electron-counting rules are just that - electron counting rules. Just as the $B_nH_n^{2-}$ (n=5-12) exhibit varying stability, the detailed thermodynamic and kinetic stability of the favorable condensed structures depend on many factors and need to be studied individually. However, the evaluation of the number of cluster electrons from the constituent elements and its comparison with that predicted from the electron counting rules help in arriving at the charge of an unknown molecule, thus providing a tool for rationalizing data and exploring new avenues.

2.1.1. Illustration of the *mno* Rule

The icosahedron, $B_{12}H_{12}^{2-}$ (1, Figure 1) can be a good starting point for illustrating the *mno* rule. Here the number of polyhedron m=1, the number of vertices n=12, and the number of single-vertex-sharing o=0, (m+n+o=13), so that the n+1 electron pair rule of Wade for single polyhedra is obtained. Each vertex with one terminal atom contributes all electrons for cluster bonding except one, which is involved in the *exo* covalent bond. Thus in the icosahedral C2B10H12, the BH groups donate one electron pair each and the CH contributes three electrons to the polyhedral bonding satisfying the *mno*

rule (m=1, n=12, o=0). Simplest possible condensation is obtained by connecting two icosahedral fragments through a single bond as in Structure 3, represented by $(C_2B_{10}H_{11})_2$. The electron count is twice that of the single polyhedral system (m+n+o=2+24+0). The structure has 26 skeletal electron pairs. Table 1 provides the number of electron pairs needed to satisfy the *mno* rule for structures discussed here.

Let us consider the condensation of two icosahedra through a single vertex to give 4 (Figure 1). The *mno* rule gives 2+23+1=26 electron pairs. For the Aluminacarborane, $[(C_2B_9H_{11})Al(C_2B_9H_{11})]$,[15] with the overall structure **3**, the *mno* electron count predicts a charge of −1, since the electron pairs contributed from the various fragments amount only to 25.5 (BH groups - 18, CH groups - 6, Al - 1.5). The anionic structure is well-characterized.[15] Compounds where Al is replaced by Fe, Co, Ni and Si are also known with appropriate charges.[16] The transition metal sandwich complexes can be approximated to octahedral complexes so that the valence d orbitals of the transition metal is split into the "t_{2g}" and "e_g set". The contribution of a transition metal in sandwich complexes towards skeletal bonding originates from this "e_g set". This is usually found to be true except in cases such as the high spin species, ferrocenyl cation and cobaltocene. The magnetic property is an indicator of the electronic structure of such complexes. A search of Cambridge Crystallographic Database[17] gave over 80 structures with this skeleton, most of which follow the electron count. Examples are known with the same skeleton as 4 having dative bonds, which affect the charge requirements.[18] When an external bond is dative in nature, all the valence electrons on the vertex atom participate in the polyhedral bonding. Compounds are also isolated with bridging groups between two dicarbollide ligands.[19]

Table 1. The Number of skeletal Electron pairs required according to the mno **rule** for **the polyhedra** (m=No. of polyhedra, n=No. of vertices, o=No. of single-vertex-bridge, **p=No.** of missing vertices, **q**=No. of capping vertices, a = No. of electrons from the metal, {3 = No. of electrons from a **main** group element other than boron, a = No. of electron pairs donated by bridging hydrogen atoms and b = No. of electron from a dative bond) and comparison with that provided from the constituent elements. Last column gives the references to experimental structures wherever available. * implies electron count ambiguous for various reasons described in the text.

Structure	m	n	o	p	q	N	BH	B	CH	α/β	a/b	N'	x	Ref
1	1	12	0	0	0	13	12	0	0	0	0	12	-1	
2	2	20	0	0	0	22	16	6	0	0	0	22	0	3
3	2	24	0	0	0	26	20	0	6	0	0	26	0	14
4	2	23	1	0	0	26	18	0	6	Fe-1 Co, Al - 1.5 Ni, Si – 2.0	0	25 25.5 26	-2 -1 0	15,16
5*	2	23	1	0	0	26	18	0	6	Ni – 2.0 Cu, Au – 2.5	0	26 26.5	-2 -1	20
6	2	22	0	0	0	24	20	3	0	0	0	23	-2	
7	2	18	0	2	0	22	16	3	0	0	2^a	21	-2	22
8	2	21	0	0	0	23	18	4.5	0	0	0	22.5	-1	23
9	3	24	1	3	0	31	15	4.5	7.5	1.5^α	2.5^a	31	0	24
10	3	25	1	3	0	32	16	3	7.5	$1.5^\alpha, 2^\beta$	1.5^a	31.5	-1	24
11	4	29	2	4	0	39	14	4.5	15	3^α	2.5^a	39	0	25
12	4	32	2	4	0	42	16	3	15	$3^\alpha, 4^\beta$	1^a	42	0	26
13	2	11	1	2	0	16	0	0	15	1^α	0	16	0	
14*	4	37	1	2	0	44	32	6	0	2^α	4^a	44	-2	27
15*	3	28	1	2	0	34	23	4.5	0	4^α	$3^a, 0.5^b$	35	0	28
16	4	21	3	4	0	32	8	0	15	3^α	6^a	32	0	6c
17	3	18	2	1	0	24	6	0	15	$3^\square$	0	24	0	34
18*	3	25	2	2	0	32	18	0	7.5	3^α	$1^a, 1.5^b$	31	0	40

Structure 5 gives the skeleton of a slipped sandwich complex. The distorted skeleton is known with transition metals such as Ni, Cu, Au etc.[20] All of them have one or more additional electron pairs than expected from the *mno* rule. Consider the slipped complex of nickel. Treating the structure as *closo,* it requires 26 electron pairs. Nickel donates its 2 electron pairs which along with the 24 electron pairs originating from the two dicarbollide ligands lead to an electron pair count of 26. An additional charge of -2 make the electron pair count to exceed the *mno* count for *closo* structures. Alternative is

obviously to have a *nido* arrangement. The detailed electronic structure study of the slipped structures and the occupancy of the metal-ligand antibonding orbitals that cause the distortion in these complexes have been well documented.[21]

Next we consider two atoms (edge) sharing structures. Two *closo* structures condensed by an edge lead to severe steric crowding. The atoms represented in dark colors in 6 (Figure 1) are too close to each other. There is no example of this kind in the literature. However if one or more vertex is removed as it happens in the *nido* arrangements, edge sharing should be practical. For example $B_{18}H_{20}^{2-}$ (7) is well characterized and adheres to the *mno* rule.[22] The compound has 16 BH groups (16 electron pairs), two boron atoms (3 electron pairs) and four bridging hydrogens (2 electron pairs). The molecule achieves the *mno* electron count as a dianion. The steric interaction is reduced in a triangular face sharing (three atoms sharing) polyhedron, $B_{21}H_{18}$ (8)$^-$ and the four atoms sharing polyhedral borane, $B_{20}H_{16}$ (2), which is discussed earlier. In (8) m=2, n=21 and o=0 and hence 23 electron pairs are required. This is accounted from the 18 BH groups, 3 boron atoms and a negative charge.

The importance of the *mno* rule is obvious in its applicability to a variety of polyhedral boranes where condensation has taken place by any combination of one, two, three, or four atom sharing. Let us take the formidable looking structure 9, $[Cp^*IrB_{18}H_{20}]$.[24] With three *nido* arrangements, the *mno* rule leads to 31 electron pairs (m=3, n=24, o=1, p=3). The skeleton gets its electron pairs from 15 BH groups (15), 5 CH groups (7.5), 3 shared boron atoms (4.5), 5 bridging hydrogens (2.5), and Ir atom (1.5). The next structure we consider, $[Cp^*IrB_{18}H_{19}S]^{-1}$ (10) has an additional vertex in the form of a sulphur atom so that the number of electron pairs required is 32. Sulphur is

found to be a four-electron donor with two electrons remaining as a lone pair orienting outward from the cluster. Three bridging hydrogens, 16 BH, two boron atoms, 5 CH groups, the metal and four electrons from sulphur together contribute 31.5 electron pairs to the skeletal framework. Therefore the *mno* rule requires an additional electron, as indeed is observed.[24] $[Cp_2{}^*Rh_2B_{17}H_{19}]$ (11) requires 39 electron pairs (m=4, n=29, o=2, p=4) for stability taking into account the 4 *nido* structures. The complex has five bridging hydrogen atoms which enable it to attain the *mno* electron count and is found to be neutral.[25] $[Cp_2{}^*Rh_2S_2B_{15}H_{14}(OH)]$ (12) is in perfect agreement with the *mno* electron count for a cluster with four *nido* structures and 42 skeletal electron pairs for stability.[26] Metallocenes can be easily included if one considers them as having two open *(nido)* faces. Taking the simplest case, ferrocene (13), the molecule has 16 electron pairs (15 from the ten CH groups and one electron pair from iron). The *mno* rule suggests the same count for a skeleton with two open faces (m=2, n=11, o=1, p=2).

The *mno* rule is necessary to account for the skeletal electron pairs of structures **14** and 15 because the metal platinum is sandwiched between two polyhedral boranes of which either one or both are condensed to one more subcluster.[27,28] A transition metal with external ligands is related to its BH analogue with appropriate charges when it occupies an unshared site. Otherwise it is replaced by boron equivalent. This is done applying the concepts of isolobal analogy[29] followed by deprotonation[29]. Thus, the d^{10} ML_2 fragment at a nonshared position in 15 is isolobally equivalent to a CH2 fragment and in turn to $BH^{2"}$. Hence it is a three orbital - four electron donor. The number of electron pairs in 14 and 15 is 45 and 35 respectively. The *mno* rule suggests an electron pair count of 44 and 34 respectively for a skeleton with two absent vertices. The extra

electrons lead to a slipped geometry around the metal as is found in the nickel complex, 5.[20] The highly mixed up organometallaborane skeleton, 16, finds its 32 electron pairs in $[Cp^*Ru(B_4H_{10})Ru(B_4H_{10})RuCp^*]$.[6]

The non-bonding interactions expected in single vertex sharing polyhedra become prominent when the shared vertex is a boron atom. The smaller size of the central atom results in the shortening of the distance between the neighboring ring atoms, which are bridged by a single vertex. This raises the energy of some of the BMOs where the antibonding interactions become significant. As a result the number of BMOs will be fewer than m+n+o and such systems deviate from the electron counting rule. To achieve a boron atom sandwiched borane the size of the ring has to be reduced. Even with four-membered ring the interactions are significant enough to cause deviations as has been observed in octahedral aluminium clusters.[30-33] No isolated molecule is experimentally characterized with this framework though this pattern is observed in solid state for aluminum clusters of the type AeM_2Al_9 (Ae=Ba, M=Fe, Co, Ni; Ae=Sr, M=Co; Ae=Ca, M=Co) and $CaNiAl_9$.[30-32] With heavier elements in the ring such a possibility has been suggested.[33] The only known structure with a sandwich type bonding to boron is found as part of the B_{10}-B-B_{10} unit of the β-rhombohedral boron unit cell where the *mno* rule is successfully applied to account for its bonding.[4]

The mismatch between a bridged atom and the ring size is seen in simple multidecker sandwiches where a single five membered ring bridges two metals. They are exceptions to the *mno* rule in the sense that complexes are known with a range of electronic requirements including the ones dictated by the *mno* rule.[21] When the shared metal is of smaller size there will be the usual nonbonding interactions mentioned earlier.

If the metal atom is of bigger size there is a tendency towards metal-metal bond formation. Both these are factors which bring in additional interactions than what is considered in the formulation of the *mno* rule. Molecules with the *mno* electron count as in the example, $[C_{23}H_{42}B_6CoRh]^{34}$ (**17**) and with less and more electrons are known. The requirement of 24 electron pair in 17 is met with the building fragments of the polyhedral cluster.

Compounds are known with fewer electrons than the Wade's electron count and are called 'hypercloso' or 'isocloso' compounds.[35] They are well-debated structures and have been studied theoretically.[36] Similarly isonido[37] and isoarachno[38] structures also exist where they are stable with n+1 and n+2 electron pair count respectively. The hypothetical *closo* eleven vertex $B_{11}H_{11}^{2-}$ species is found to be highly fluxional suggesting other open structures for the complex.[37] Results of Mingo's calculations on two models of $B_{10}H_{10}^{2-}$, a spherical deltahedron and a polar deltahedron gave a clear MO picture.[36, 39] A deltahedra, which can be approximated to a sphere has equal number of bonding and antibonding π MOs, whereas once it is distorted a *n* and a *n** orbital become approximately non bonding and are at the frontier range. Obviously the nonbonding MO need not be filled so that the molecule prefers one electron pair fewer than the Wade's n+1 count. When this anomalous behavior is extended to condensed clusters many of the apparently anomalous structures can be accounted for. Structure 18 $[Cp^*RhB_9(SMe_2)H_{10}RhB_9H_7(SMe_2)_2]$, is a case in point. This compound consists of a *closo* B_9Rh unit conjoined through rhodium atom to an open RhB_9 unit. Considering Cp ligand as part of the cluster, the total electron requirement is 32 electron pairs (n=25,

m=3, o=2, p=2). But the electron pairs obtained by the skeletal fragments are only 31. Thus the open part has some *isonido* characteristics.[40]

Considering the plethora of structures known, the selection of the structures given in Table 1 is arbitrary. Attempts were made to cover one example, each involving different modes of fusion and then to present representative examples with any combinations of the possible fusion modes. Emphasis is given to bring out structures that have ambiguities. We have applied the rule to all the experimental structures obtained by searching the CSD;[17] only structures with differing structural patterns are listed in table 1.

2.2. JUSTIFICATION AND APPLICATIONS OF THE *MNO* RULE

Macropolyhedral boranes that are formed by the interaction of two or more monomeric units can be broadly classified into two categories. The first category involves the *exo*-interactions where the individual units are connected together by localized bonds. The latter category involves the sharing of one or more atoms between the individual units giving rise to condensed polyhedral boranes. Among the condensed polyhedral boranes, the single vertex sharing systems are treated separately, as their electronic requirements are different from the rest of the condensed systems. To illustrate **the** various possible modes of interactions, we describe the study of two generalized *closo*-polyhedral boranes by bringing them together from a non-interacting distance to form condensed systems, varying the distance periodically. *Exo*-polyhedral interactions arise as the first case, followed by condensed systems.

As an illustration of the applications of the rule, we present the structural error reported experimentally in one of the macropolyhedral boranes. The compound, reported

with a molecular formula of $B_{19}H_{20}{}^{1-}$ exhibits an edge-sharing pattern with two *nido* faces *trans* to each other. Our analysis of their MOs using extended Hückel theory and higher level theoretical calculations found all indications that the reported $B_{19}H_{20}$ to be a stable species only as a tri-anion. The formulation presented for $B_{19}H_{20}{}^{1-}$ requires two additional electrons and hence the correct structure is predicted to be $B_{19}H_{22}{}^{1-}$. Based on the above results the mechanism for the formation of $B_{19}H_{22}{}^{1-}$ is also explained.

2.2.1. Justification for the *mno* Rule

i. Exo-Polyhedral Interactions

Let us assume that one B-H bond each of the two *closo*-polyhedral boranes $B_xH_x{}^{2-}$ and $B_yH_y{}^{2-}$ are brought along a line of interaction. With the decrease in distance, the nonbonding interactions dominate (Figure 3, A), giving a doubly bridging structure (Figure 3, B) as a possibility. The resulting structure is very similar to that of diborane (B_2H_6), but, unlike diborane, has only one hybrid orbital on each bridging boron. It is not sufficient to generate two stable levels. The charge requirements remain the same as four electrons. The electrons that are earlier involved in the exo-B-H bonds are enough to stabilize the one 4c-2e bond. The second pair of electrons necessarily goes to a less stable level resulting in an unstable system. But this shortcoming is alleviated when any one of these two boron atoms is replaced with transition metals, which have diffused orbitals to lower the unstable level. It is even possible with a main group element where the bridging hydrogens are replaced by groups like CO or -CH_3 with unoccupied π^* or pseudo π^* orbitals to stabilize the antibonding level. An example which illustrates this type of interaction is $(Be(B_3H_8)CH_3)_2$ (1, Figure 4).[41] This linkage can also be viewed as the equivalent of the doubly protonated C_2H_4, the neutral analogue being B_2H_6.
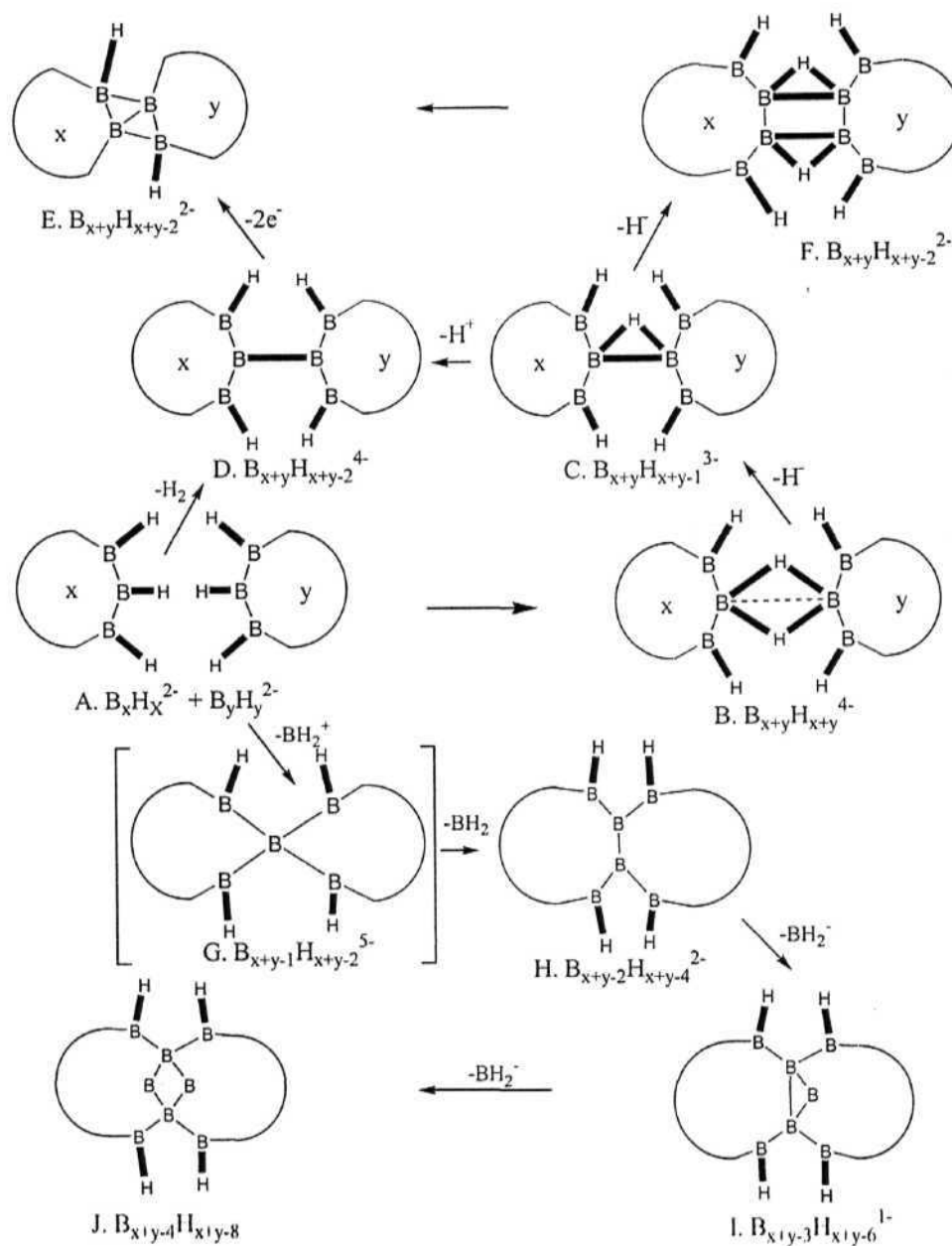
Figure 3

Different modes of interaction (A-J) between two polyhedra ranging from exopolyhedral to condensed ones are depicted. All patterns except G is known experimentally. Structural pattern G is observed in the unit cell of β-rhombohedral boron and also when the central boron atom is replaced by heavier elements.

Another way to arrive at a stable structure from B (Figure 3) is to remove one of the hydrogen atoms, which leads to structure C (Figure 3). Here, the two sp-hybridized

57

orbitals of boron and the s-orbital of hydrogen will interact together to form a stable BMO and two antibonding MOs. Three electrons are available, one with each atom involved in the three-center interaction. As only two electrons are required for this 3c-2e bond, one electron has to be expelled from the system, which reduces the charge to (3-). This pattern is a fairly stable mode of interaction provided the nonbonding interactions between adjacent B-H groups are minima. $(B_{10}H_9)_2H$ involves a protonated B-B linkage between two of its B_{10} units and exemplifies such type of linkage[42] (B20H19'^{3}, 2).

1. $[Be(B_3H_8)CH_3]_2$ 2. $(B_{20}H_{19})^{3-}$

3. $(B_{20}H_{18})^{4-}$ 4. $B_{20}H_{26}$

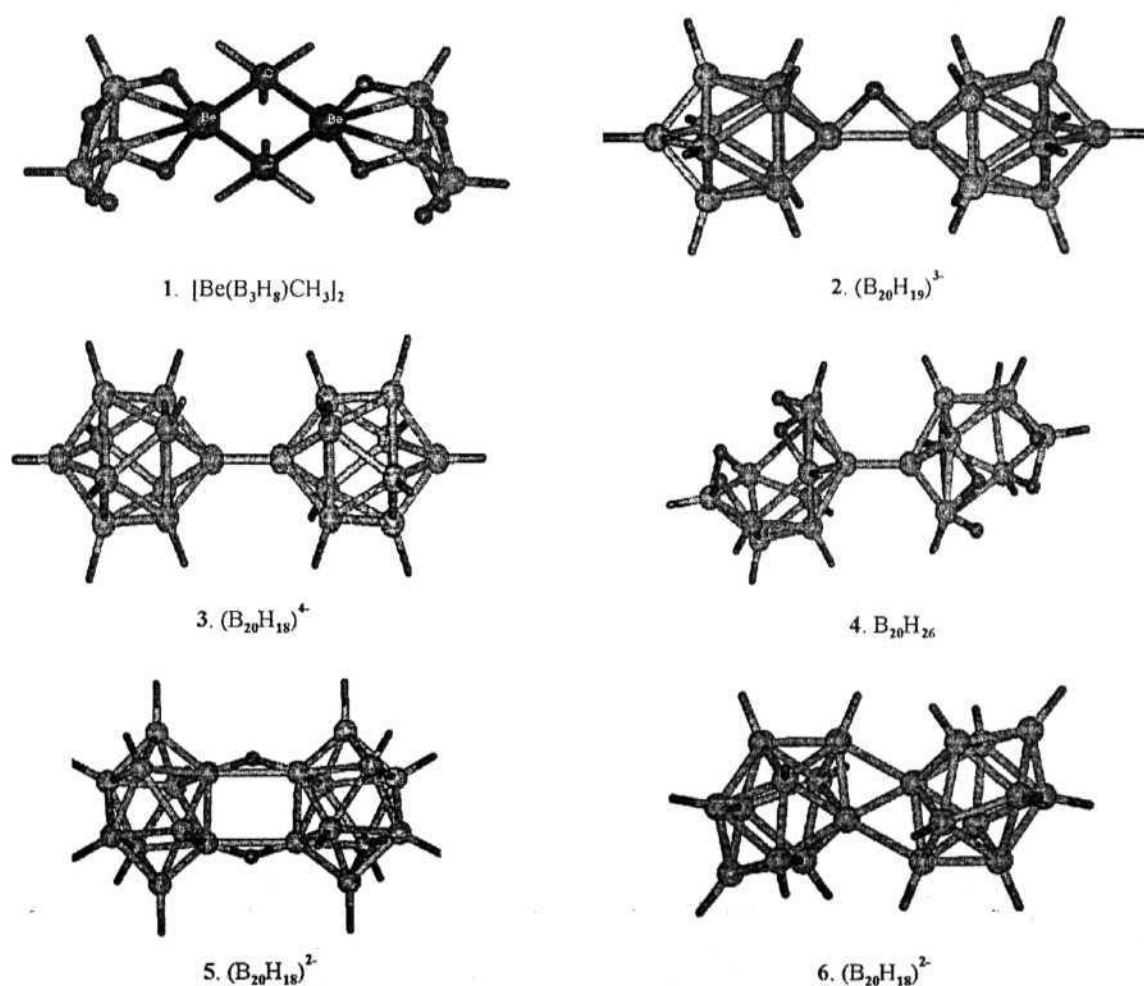5. $(B_{20}H_{18})^{2-}$ 6. $(B_{20}H_{18})^{2-}$

Figure 4

Representative examples illustrating exopolyhedral interactions between two polyhedra.

Removal of a proton from C leads to the most familiar form of condensation, resulting in a new 2c-2e B-B bond (Figure 3, D). Here the electron count is the sum of the electron counts for two polyhedral systems. Thus $B_{12}H_{11}$-$B_{12}H_{11}$ requires m+n+o (2+24+0=26) electron pairs supporting the anticipated four negative charges. With several arms ready for condensation, dendrimers are a natural extension as is found experimentally.[43] These systems have got rid of the unfavorable enhanced charge requirement by replacing borons by carbons.[43] Two B_{10} units arc known to have this type of linkage exhibiting *closo* or *nido* patterns (3, 4).[44]

Alternatively, structural pattern C (Figure 3) can be bent to have more than one interacting centers, by the linking of two or more adjacent centers with a 3c-2e or 2c-2e bond as in pattern F. In the case of 3c-2e linkages, every such bond will reduce the total charge by one, whereas the 2c-2e bonds keep the charge requirements constant. Such multiple linkages are quite possible even with pure borane clusters. Occasionally, atoms other than hydrogen may also bridge the two aromatic units by forming 2c-2e bonds on both the sides. It is fairly easy to recognize and evaluate the electron requirement in these cases as they seldom form 3c-2e bonds. Cases where two B_{10} units interact through this type of multiple linkage, have been experimentally characterized (5).[45]

Conversely, if one of the boron atoms in pattern D is brought closer so that two adjacent boron atoms of the other borane unit are within bonding distance as represented in E, the nature of interaction dramatically changes. This interaction gives rise to the capping of an edge by a boron atom, where the two *exo*-hydrogens of the boron atoms that are connected by the concerned edge are still retained. Since capping interactions will not add any BMOs than that is already present in the polyhedra, the extra electron

available on boron atom can be used to fill up the BMOs of the polyhedra. These types of interactions occur pairwise, if the cluster geometry is favorable, where one boron atom from each borane unit caps an edge of the other boron, as depicted in E. These systems exhibit true macropolyhedral skeleton, as localized bonds do not separate these interacting borane units anymore. This pattern depicts the intermediate skeletal nature between connected and condensed polyhedral boranes, as they neither share any vertices nor are separated by localized bonds. Many examples are known with this type of bonding. One among them is $(B_{20}H_{18}{}^{2-}, 6)$.[46] Capping interaction should be differentiated from 3c-2e interactions where none of the edges of the 3c-2e bond are common with the individual polyhedral units formed during the interaction. The interactions discussed so far are all *exo*-polyhedral and seldom affect the nature of the skeletal bonding of both the polyhedra. All these patterns were observed experimentally, in varying numbers. The careful identification of the nature of these interactions is necessary before employing the electron counting rules. In the following section, interactions where the interacting borane units share one or more vertices is considered, a situation that is entirely different from what was discussed so far.

ii. Condensed Polyhedral Boranes

Though the structures discussed so far may be categorized as products of condensation, here those structures where the process of condensation has reduced at least one vertex in comparison to the isolated polyhedra is discussed. As in the previous section, the number of vertices that are shared will be systematically increased, considering all the possibilities of condensation.

The first mode of condensation is through a single vertex (G, Figure 3) leading to a sandwich. The BMO pattern and hence the electronic requirement is very much dependent on the distance between the two polyhedral fragments when they are allowed to share a single vertex. When the distance between the non-bonded vertices is reasonably large, the number of BMOs remains the same. This is achieved by replacing the central atom by atoms larger than boron. The electron count here depends on the central atom. While assigning the charge of (-5) to the system G (Figure 3) it was assumed that the nonbonding interactions were absent. With smaller central atom the nonbonding interactions involving B-H groups on neighboring polyhedra raise some of the BMOs. The details of these destabilizing interactions and the consequent reduction in the negative charge to (-1) are discussed below.[30, 32, 33] In these sandwich systems the central atom is assumed to be sp hybridized. The two sp hybridized orbitals of the central atom are ideally directed towards the center of each cluster that is shared. One of the sp hybrid interacts with the inwardly pointing sp hybrids of the other boron atoms in one cage to form a single strongly bonding MO, as in the case of mono-polyhedral boranes. One more strongly bonding MO is formed by the interaction with the other cage AOs. So the number of core orbitals formed by the overlap of the radial orbitals on each vertex equals the number of cages in the polycondensed system, m. The two tangential orbitals on the shared vertex are mutually perpendicular to each other and they contribute to the surface BMOs. Each sub cluster retains its electronic requirement. If the number of vertices on each sub-cluster of a two polyhedra condensed complex, excluding the shared atom are 'a' and 'b' respectively such that a+b+1=n, the total number of vertices, then the bonding surface MOs formed from the tangential orbitals on each sub-cluster will be a+1

and b+1 respectively. The total amounts to n+1 which when generalized gives n+o, where o is the total number of single vertex condensations. So the total bonding MOs is m+n+o, which is the basis of the rule.

The electronic requirements of single vertex sharing can also be rationalized using a fragment molecular orbital approach, starting with a ring-cap division used in explaining the relative stability of *closo* borane isomers.[47] This approach simplifies the problem by reducing the number of BMOs to be considered.
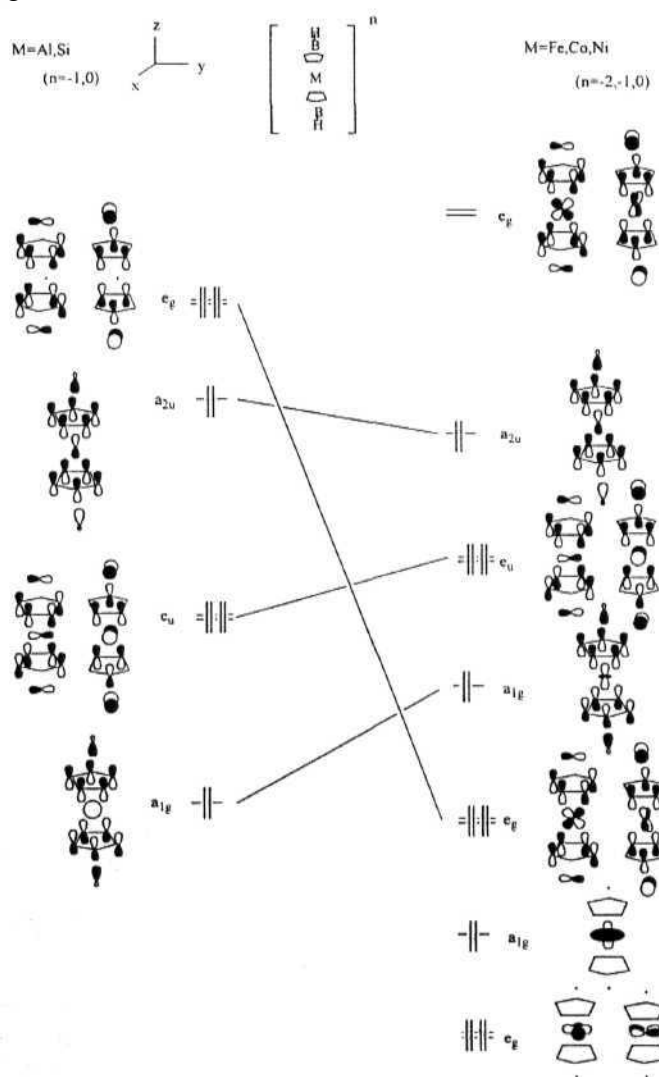
Figure 5

A molecular orbital diagram of sandwich complexes correlating main group sandwiches and corresponding transition metal systems.

The ring atoms are considered as sp^2 hybrids, interacting with a sp hybrid cap. The frontier MOs of the ring will be the *n* molecular orbitals formed by the linear combination of the unhybridised p orbitals similar to conjugated hydrocarbons. Figure 3 gives a correlation between the simplified MO pattern of both main group sandwich complex and transition metal complex.

The L.H.S. of the Figure 5 shows the MO pattern for a main group sandwich where the central atom is larger than boron. It is correlated with the transition metal compound on the R.H.S. The *mno* rule can be well understood from the BMO pattern of $(B_6H_6)_2M$ where M=A1, Si etc. An extension of any rule to transition metal complexes usually results in additional terms to account for the d-orbitals. But it can be seen from Figure 5 that the BMOs which have a major contribution from the polyhedral skeleton remain the same whether M is a main group or a transition metal and hence the constancy in the rule.

There are no major changes in the BMO pattern of the two correlated systems except in the "e_g"and "e_u"set. The "e_g" set of the first system do not have a proper match from the orbitals of the main group element and is the highest among the occupied levels. It is this "e_g" set which is affected when a larger central atom is replaced by boron leading to a charge of (-1) instead of (-5) as given in Figure 3, G. This, in addition to other repulsive interactions, makes the existence of single boron bridged condensation unlikely. The d_{xz} and d_{yz} orbitals of transition metals are of proper symmetry to interact with these particular orbitals and hence stabilize the "e_g" set, bringing it below the "e_u" set (Figure 5, RHS). The LUMO of the second system is doubly degenerate. When the number of electrons exceeds the *mno* count, this antibonding MO has to be occupied. The resulting

antibonding interactions can be reduced with slipping. The distortion provides some bonding character to the otherwise antibonding orbital. This explains the additional requirement of the slipped sandwiches, which results in excess electrons than that required according to the rule.[21]

One more atom at the shared position between two monomeric units leads to an edge shared polyhedron (H, Figure 3). As discussed earlier the *closo* form is not practical for these systems. The core BMOs of this polycondensed polyhedron that are formed by the strongly bonding interaction of the inward pointing sp hybrid orbitals remain unchanged. But, the two surface BMOs are shared between both the units since they share more than one atom. Edge sharing allows the existence of hamiltonian circuits[12] that span the entire macropolyhedral framework which enables the stabilization of exactly the same number of surface bonding orbitals as to the number of vertices in the system. A similar effect is observed in the three and four vertex sharing macropolyhedral systems (I, J, Figure 3). But the sp hybrids of the boron atoms in these systems, unlike in the case of single vertex sharing systems, will not be ideally oriented towards each polyhedron. This necessitates a rehybridization of the shared boron to have more p character to relieve strain and essentially reduces the s orbital contribution. The core BMOs of these systems are stabilized by rehybridization due to the increased overlap. In some very condensed systems like $B_{28}H_{21}^{1+}$ which is found in J3-rhombohedral boron, the p character of the hybrid orbitals of the central atom sharing the three polyhedra are close to sp^2 hybridization, since three radial orbitals are required. Polycondensation by sharing five atoms leads to boron nanotubes. This arrangement makes the system cylindrical in shape with a uniform radius of curvature. Such a system emerges as a single polyhedra

id the rule can be applied.[48] Higher fusions are not possible due to the poor ring-cap mpatibility of boron.

All the various types of fusions discussed here starting from structures B to I igure 3) are isolated experimentally. All-borane structures are lacking only for B and , the reasons for which have been discussed. Theoretical calculations on the same rstems (B-I) with the predicted charge by *mno* rule also provide reasonably fair HOMO-UMO gap supporting the qualitative explanations given in the above section.

2.2. Application of *mno* Rule for Edge Shared Macropolyhedral Boranes

When two B_{12} units are forced to share an edge, the proximity between the non-onding boron atoms of the two polyhedra is very small as illustrated in 7 (Chart 1) . /ith the experimental B-B distances of $B_{12}H_{12}{}^{2-}$, the distance between the boron atoms :presented by dark spheres is less than 1.5 A°. This distance is not improved even in dge sharing octahedra.[31] But these steric interactions caused by condensation will be :lieved by the removal of one or more vertices near the shared atoms leading to *nido* ructures. An additional electron pair is required for compensating every vertex that is :moved from the non-adjacent positions.[49] Hence these molecules acquire bridging ydrogens between two adjacent borons at the open face to acquire extra electrons or else ley must be anions with appropriate charges.
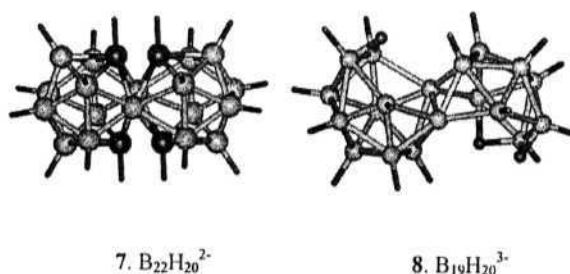

7. $B_{22}H_{20}{}^{2-}$ 8. $B_{19}H_{20}{}^{3-}$

Chart 1

9.$B_{12}H_{16}$

10. $B_{13}H_{19}$

11.$B_{16}H_{20}$

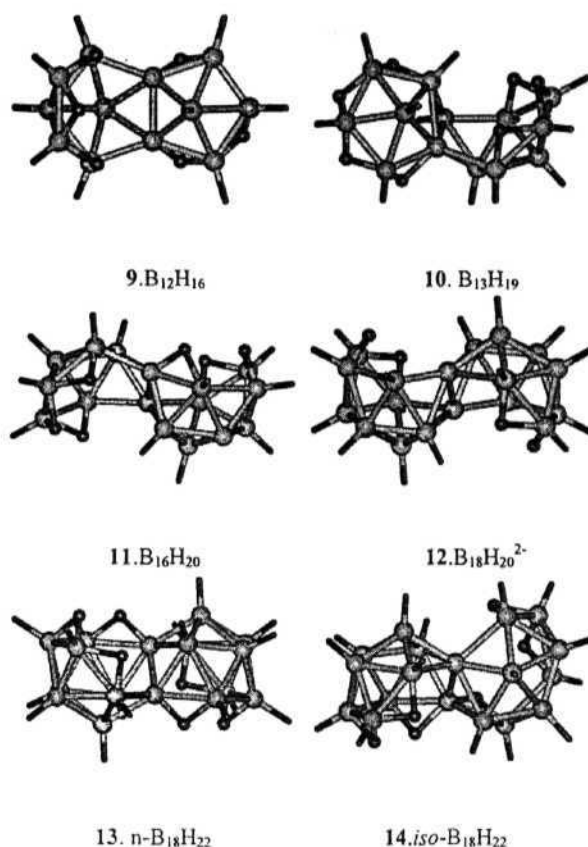12.$B_{18}H_{20}^{2-}$

13. n-$B_{18}H_{22}$

14.*iso*-$B_{18}H_{22}$

Chart 2

Several molecules (Chart 2, 9-14) are known to exhibit this edge-sharing *nido* pattern and all of them require n+m electron pairs for stability. The charge requirement for all these structures is evaluated in Table 1. For example, the isomers of $B_{18}H_{22}$ (13, 14) have 18 boron atoms distributed over two *nido*-cages.[50] Hence n=18, m=2 and two more electron pairs are needed to compensate the two absent vertices. The polyhedral skeleton requires (n+m+2) 18+2+2=22 electron pairs. The 16 B-H groups give 16 electron pairs and six bridging hydrogen atoms give 3 electron pairs to the skeletal bonding. Two shared boron atoms each give three electrons (all its valence electrons as there is no *exo*-2c-2e bond) to make the total electron pairs 22. All the other structures can be worked out in a similar way (Table 2).

66

Table 2. Skeletal electron pairs for edge sharing *nido*-boranes. [a]Boron atoms at the shared position, [b]Two isomers, [c]the species observed must be $B_{19}H_{22}^{-}$, p the number of missing vertices, b-H bridging hydrogens, q the net charge.

Borane	Electron pairs required by rule				Skeletal Electron pairs contributed by fragments				Q	Ref.
	n	m	p	Sum	BH	B[a]	b-H	Sum		
$B_{12}H_{12}$	20	1	0	13	12	0	0	12	-2	
$B_{20}H_{16}$	20	2	0	22	16	6	0	22	0	3
$B_{21}H_{18}$	21	2	0	23	18	4.5	0	22.5	-1	23
$B_{22}H_{20}$	22	2	0	24	20	3	0	23	-2	
$B_{12}H_{16}$	12	2	2	16	10	3	3	16	0	51
$B_{13}H_{19}$	13	2	2	17	12	1.5	3.5	17	0	52
$B_{16}H_{20}$	16	2	2	20	14	3	3	20	0	53
$B_{18}H_{20}$	18	2	2	22	16	3	2	21	-2	22
$B_{18}H_{22}$[b]	18	2	2	22	16	3	3	22	0	50
$B_{19}H_{20}$[c]	19	2	2	23	17	3	1.5	21.5	-3	54

A recently reported edge sharing condensed polyhedral borane $B_{19}H_{20}^{1-}$ does not fit the *mno* electron counting rule.[54] Here we point out an alternative to this structure. As per the n+m rule, this structure requires (n=19 and m=2) 19+2+2=23 electron pairs taking into account of the two *nido* fragments. However, $B_{19}H_{20}$ is reported to be a mono anion having 17 + 3 + 2 (3H + $^{-}$e) = 22 electron pairs. In the absence of electron count, there were no guidelines to estimate the number of electrons. The number of hydrogen atoms was therefore assumed to be 20 and their initial positions were generated from the skeletal geometry for the X-ray structure analysis. During the refinement of diffraction data, the number of hydrogens was unaltered as there were no bonding considerations to do so. The MALDI mass-spectra of the ions showed two additional mass units consistently. The authors prefer a different interpretation for the two additional mass

units, which is not convincing. The mechanistic schemes that gave rise to the $B_{19}H_{20}{}^{1-}$, with two hydrogen atoms less than necessary are also not convincing. One of them required an elimination of one mole of H_2, while the maximum observed was $0.13 mol$ only. The other two pathways had improbable mechanistic steps.

We have calculated the energy levels at the extended Hückel[55] and B3LYP/6-31G* levels[56, 57] and found all indications for the reported B19H20 to be a stable species only as a tri-anion. Frequency calculations at the same level characterized the structure $B_{19}H_{20}{}^{3-}$ as minima on the potential energy surface. But the same structure with -1 charge failed to converge. The formulation presented for $B_{19}H_{20}{}^{1-}$ requires two additional electrons and hence most likely the correct structure is $B_{19}H_{22}{}^{1-} \bullet$ The authors discounted this fact, as they assumed that the additional two hydrogen atoms would lead to *arachno* structures.

Based on the above results the mechanism for the formation of $B_{19}H_{22}{}^{1-}$ can be explained. The reaction of $B_{18}H_{20}{}^{2-}$ with $(CH_3)_2SBH_2Cl$ results in the formation of $B_{19}H_{22}{}^{1-}$ in which, a $BH_2{}^{+}$ caps the triangular face of $B_{18}H_{20}{}^{2-}$ skeleton. In the case of (CH3)$_2$SBHCl$_2$, the equivalent intermediate is $B_{19}H_{21}Cl^-$ where the cap is BHX^+ instead of $BH_2{}^{+}$. It has been proved that a capping B-H or $BH_2{}^{+}$ group in a polyhedral skeleton[11, 30] does not alter the electronic requirement of the polyhedral skeleton and the number of electron pairs for this skeleton, (18+2+2) 22, remain the same as that of $B_{18}H_{22}$. The migration of the BH2 or BHX groups from the capping position to the polyhedral skeleton results in the final $B_{19}H_{22}{}^{1-} \bullet$ In the process one of its *exo*-hydrogen atom is moved to the bridging position to satisfy the increased requirement of 23 electron pairs of $B_{19}H_{22}{}^{1-}$. In the case of $B_{19}H_{21}Cl^-$, migration of BHCl group takes place in a similar manner followed

by the substitution of hydrogen in the place of chlorine. The importance of an electron-counting rule in exploring the chemistry of macropolyhedral boranes, is thus obvious.

2.3. CONCLUSIONS

A unifying electron counting rule - the *mno* rule - explains the bonding patterns exhibited by single and condensed polyhedral borane clusters. According to this *mno* rule, m+n+o elecron pairs are necessary for a *closo* polycondensed polyhedral system. Here m= number of polyhedral clusters, n=number of vertices, o=single vertex fusions. Wade's n+1 rule is a special case of *mno* rule where m=1 and o=0. Similarly the m+n rule is a special case with o=0. The rule can also be extended to metallocenes, which can be merged with the borane systems. The rules of condensation envisage infinite possibilities. A glimpse of the dimension of the problem is seen in Figure 2, which treats condensation of icosahedral fragments alone. There are endless mixing and matching possible. The *mno* rule will be a useful guide to achieve the different goals wherein efforts are made to unify the two fields.

A justification based on MOT is provided for the *mno* rule. The variety of bonding patterns observed in terms of the modes of condensation of macropolyhedral boranes are accounted for. Application of the rule to rectify an error in a recently reported edge sharing macropolyhedral borane, $B_{19}H_{20}^{1-}$ illustrates the importance of the *mno* rule in the further exploration of polyhedral borane chemistry. The mechanism for the formation of the structure with the exact molecular formula, $B_{19}H_{22}^{1-}$ is also revised based on the *mno* rule.

REFERENCES

1. (a) Lipscomb, W. N. *Adv. Inorg. Chem. Radiochem.*, **1950,** 7, 117. (b) Lipscomb, W. N. *Boron Hydrides,* Benjamin, New York, **1963.** (c) Muetterties, E. L. *Boron Hydride Chemistry,* New York, **1975.** (d) Mathias, J. P.; Stoddard, J. F. *Chem. Soc. Rev.,* **1992,** *21,* 215. (e) Soloway, A. H.; Tjarks, W.; Barnum, B. A.; Rong, F. G.; Barth, R. F.; Codogni, I. M.; Wilson, J. G. *Chem. Rev.,* **1998,** *98,* 1515. (f) Colquhoun, H. M.; Lewis, D. F.; Herbertson, P. L.; Wade, K. *Polymer,* **1997,** *38,* 4539. (g) Hong, E.; Kim, Y.; Do, Y. *Organometallic*,* **1998,** *17,* 2933.

2. Balakrishnarajan, M. M; Jemmis, E. D. *J. Am. Chem. Soc.* **2000,** *122,* 4516.

3. (a) Friedman, L. B.; Dobrott, R. D.; Lipscomb, W. N. *J. Am. Chem. Soc.* **1963,** *85,* 3505. (b) Dobrott. D. R.; Friedman, L. B.; Lipscomb, W. N. *J. Chem. Phys.* **1964,** *40,* 866. (c) Miller, H. C; Muetterties, E. L. *J. Am. Chem. Soc.* **1963,** *85,* 3506. (d) Miller, N. R.; Forstener, J. A.; Muetterties, E. L. *Inorg. Chem.* **1964,** *3,* 1690.

4. Jemmis, E. D; Balakrishnarajan, M. M. *J. Am. Chem. Soc,* **2001,** *123,* 4324.

5. Jemmis, E. D; Balakrishnarajan, M. M.; Pancharatna, P. D. *Chem. Rev.,* **2002,** *102,* 93.

6. (a) Kennedy, J. D. *Advances in Boron Chemistry,* Ed. Siebert, W.; Royal Society of Chemistry, **1997,** 451. (b) Grimes, R. N. *Advances in Boron Chemistry,* Ed. Siebert, W.; Royal Society of Chemistry, **1997,** 321. (c) Lei, X.; Shang, M.; Fehlner, T. P. *Angew. Chem. Int. Ed. Engl.* **1999,** *38,* 1986 and references there in. (d) Yan, Y. K.; Mingos, D. M. P. Chem. Soc. Rev. **1995,** 203.

7. (a) Wade, K.; *Chem. Commun.,* **1971,** 792. (b) Wade, K.; *Adv. Inorg. Chem. Radiochem.,* 1976, *18,* 1. (c) Wade, K.; *Inorg. Nucl. Chem. Letters,* 1972, *8,* 563. (d)

Williams, R. E. *Adv. Inorg. Chem. Radiochem.*, **1976,** *18,* 67.

8. Williams, **R. E.** *Inorg. Chem.*, **1971,** *10,* 210.

9. **Rudolph, R. W.** *Acc. Chem. Res.,* **1976,** *9,* 446.

10. (a) Hugheey, J. E.; Keiter, E. A.; Keiter, R. L. *Inorganic Chemistry : Principles of Structure and Reactivity,* New York, **1993.** (b) Shriver, D. F.; Atkins, P. W.; Langford, C. H. *Inorganic Chemistry,* Oxford, **1990.** (c) Grimes, R. N. *Comprehensive Organometallic Chemistry* I (Abel, E.; Stone, F.; Wilkinson, G. A.), Oxford, **1982,** Chap. 9

11. Mingos, D. M. P.; *Nature (Phys. Science),* **1972,** *236,* 99.

12. **King,** R. **B.;** Rouvray, D. H. *J. Am. Chem. Soc,* **1977,** *99,* 7834.

13. (a) Stone, A. J. *Mol. Phys.,* **1980,** 41, 1339; Stone, A. J. *Inorg. Chem.,* **1981,** *20,* 563. (b) Stone, A. J; Alderton, M. J. *Inorg. Chem.,* **1982,** *21,* 2297.

14. Rathke, J.; Schaeffer, R. *J. Am. Chem. Soc,* **1973,** *95,* 3402.

15. Schubert, D. M.; Bandman, M. A.; Rees, W. S., Jr.;Knobler, C. B.; Lu, P.; Nam, W.; Hawthorne, M. F. *Organometallics,* **1990,** *9,* 2046.

16. (a) Kang, H. C; Lee, S. S.; Knobler, C. B.; Hawthorne, M. F. *Inorg. Chem.* **1991,** *30,* 2024. (b) Deboer, B. G.; Zalkin, A.; Templeton, D. H. *Inorg. Chem.* **1968,** 7, 2288. (c) Warren, L. F., Jr.; Hawthorne, M. F. *J. Am. Chem. Soc.* **1970,** *92,* 1157. (d) Rees, W. S., Jr.; Schubert, D. M.; **Knobler,** C. B.; Hawthorne, M. F. *J. Am. Chem. Soc.* **1986,** *108,* 5369.

17. (a) **Allen, F. H.; Bellard, S.; Brice, M. D.; Cartwright, B. A.; Doubleday, A.;** Higgs, **H.;** Hummelink, T.; Hummelink-Peters, **B.** G.; **Kennard, O.; Motherwell, W. D. S.; Rodgers, J. R.; Watson, D. G.** *Acta Cryst.* **1979,** *B35,* 2331. <b) **Allen, F. H.** *Acta*

Cryst. Sect. A, 1998, *54,* 758. (c) Allen, F. H.; Kennard, O. *Chem. Des. Autom. News,* 1993,5,31.

18. Franken, A.; Plesek, J.; Fusek, J.; Semrau, M. *Collect. Czech. Chem. Commun.,* **1997,** 62, 1070.

19. Churchill, M. R.; Gold, K. *Inorg. Chem.,* **1971,** 10, 1928.

20. (a) Wing, R. M. *J. Am. Chem. Soc.* **1970,** *92, 1187;* Colquhoun, H. M.; Greenhough, T. J.; Wallbridge, M. G. H. *Acta Cryst.* **1977,** *33,* 3604. (b) Wing, R. M. *J. Am. Chem. Soc.* **1968,** *90,* 4828; Wing, R. M. *J. Am. Chem. Soc.* **1967,** *89,* 5599.

21. (a) Lauher, J. W.; Elian, M.; Summerville, R. H., Hoffmann, R. *J. Am. Chem. Soc.* **1976,** 98, 3219. (b) Cox, D. N.; Mingos, D. M. P.; Hoffmann, R. *J. Chem. Soc. Dalton Trans.* **1981,** 1788. (c) Jemmis, E. D.; Reddy, A. C. *Organometallics,* **1988,** 7, 1561. (d) Jemmis, E. D.; Reddy, A. C. *J. Am. Chem. Soc.* **1990,***112,*722.

22. Fontaine, X. L. R.; Greenwood, N. N.; Kennedy, J. D.; MacKinnon, P. *J. Chem. Soc. Dalton Trans.* 1988, 1785

23. (a) Enemark. J. H.; Friedman, L. B.; Lipscomb. W. N. *Inorg. Chem.* **1966,** *5,* 2165. (b) Lipscomb, W. N. *J. Less-Common Met.* **1981,** *82,* 1.

24. Shea, S. L., McGrath, T. D.; Jelinek, T.; Stibr, B.; Thornton-Pett, M.; Kennedy, J. D. *Inorg. Chem. Commun.* 1998, 97.

25. **Fontaine,** X. L. **R.;** Greenwood, N. N.; Kennedy, J. **D.;** MacKinnon, **P. I.;** Thornton-**Pett, M.** *Chem. Commun.* **1986,** 1111.

26. Kaur, P.; Kennnedy, J. D.; Thornton-Pett, M.; **Jelinek,** T.; Stibr, B. *J. Chem. Soc. Dalton Trans.,* **1996,** 1775.

27. McGrath, T. D.; **Jelinek,** T.; Stibr, B.; Thornton-Pett, M.; Kennedy, J. D. *J. Chem.*

Soc. Dalton Trans., **1997,** 2543.

28. Bould, J.; Clegg, W.; Kennedy, J. D.; Teat, S. J. *J. Chem. Soc. Dalton Trans.* **1998,** 2777.

29. Hoffmann, R. *Angew. Chem. Int. Ed. Engl,* **1982,** *21,* 711.

30. Vajenine, G. V.; Hoffmann, R. *J. Am. Chem. Soc.* **1998,** *120,* 4200.

31. Burdett, J. K.; Canadell, J. *J. Am. Chem. Soc.* **1990,** *112,* 7207.

32. Tillard-Charbonnel, M.; Manteghetti, A.; Belin, C. *Inorg. Chem.* **2000,** *39,* 1684.

33. Srinivas, G. N.; Hamilton, T. P.; Jemmis, E. D.; McKee, M. L.; Lammertsma, K. *J. Am. Chem. Soc.* **2000,** *122,* 1725.

34. Fessenbecker, A.; Attwood, M, D.; Bryan, R. F.; Grimes, R. N.; Woode, M. K.; Stephan, M.; Zenneck, U.; Siebert, W. *Inorg.Chem.* **1990,** *29,* 5157.

35. (a) Baker, R. T. *Inorg. Chem.* 1986, *25,* 109. (b) Kennedy, J. D. *Inorg. Chem.* 1986, *25,* 111.

36. (a) Johnston, R. L.; Mingos, D. M. P. *Inorg. Chem.* **1986,** *25,* 3321. (b) Fowler, P. W. *Polyhedron,* **1985,** *4,* 2051.

37. Bould, J.; Clegg, W.; Teat, S. J.; Barton, L.; Rath, N. P.; Thornton-Pett, M.; Kennedy, J. D. *Inorg. Chim. Acta* **1999,** *289,* 95.

38. Bould, J.; Cooke, P. A.; Dorfler, U.; Kennedy, J. D.; Barton, L.; Rath, N. P.; Thornton-Pett, M. *Inorg. Chim. Acta* **1999,** *285,* 290.

39. Johnston, R. L.; Mingos, D. M. P. *J. Organomet. Chem.* **1985,** *280,* 419.

40. Ditzel, E. L.; Fontaine, X. L. R.; Greenwood, N. N.; Kennedy, J. D.; Thornton-Pett, M. *J. Chem. Soc, Chem. Commun.* **1988,** 1262.

41. Gaines, D. F.; Walsh, J. L.; Morris, J. H.; Hillenbrand, D. F. *Inorg. Chem.,* **1978,** *17,*

1516.

42. Watson-Clark, R. A; Knobler, C. B; Hawthorne, M. F. *Inorg. Chem.* **1996,** 55, 2963.

43. (a) Yang, X. G.; Jiang, W.; Knobler, C. B.; Hawthorne, M. F. *J. Am. Chem. Soc.* **1992,** *114,* 9719. (b) Housecroft, C. E., *Boranes and Metallaboranes,* Ellis Horwood, Hemel Hempstead, **1994.** (c) Housecroft, C. E. *Angew. Chem. Int. Ed. Engl.,* **1999,** *38,* 2717.

44. (a) Hawthorne, M. F.; Pilling, R. L.; Stokely, P. F.; Garrett, P. M. *J. Am. Chem. Soc.* **1963,** *85,* 3704. (b) Hawthorne, M. F.; Pilling, R. L.; Stokely, P. F. *J. Am Chem. Soc.* **1965,** *87,* 1893. (d) Ng, L. L; Ng, B. K; Knobler, C. B; Hawthorne, M. F. *Inorg. Chem.,* **1992,** *31,* 3669.

45. DeBoer, B. G.; Zalkin, Z.: Templeton, D. H. *Inorg. Chem.,* **1968,** 7, 1085.

46. Li. F.; Shelly, K.; Knobler, C. B.; Hawthorne, M. F. *Angew. Chem. Int. Ed. Engl.* **1998,** *37,* 1868.

47. Jemmis, E. D. *J. Am. Chem. Soc.* **1982,** *104,* 7017.

48. Schleyer, P. v. R.; Najafin, K.; Mebel, A. M. *Inorg. Chem.* **1998,** *37,* 6765.

49. Burdett, J. K.;Canadell, E. *Inorg. Chem.* **1991,** *50,* 1991.

50. (a) Pitochelli, A. R.; Hawthorne, M. F. *J. Am. Chem. Soc.* **1962,** *84,* 3218. (b) Simpson, P. G.; Folting, K.; Dobrott, R. D.; Lipscomb, W. N. *J. Chem. Phys.* **1963,** *39,* 26. (c) Simpson, P. G.; Lipscomb, W. N. *J. Chem. Phys.* **1963,** *39,* 2339.

51. Brewer, C. T.; Swisher, R. G.; Sinn, E.; Grimes. R. N. *J. Am. Chem. Soc.* **1985,** *107,* 3558.

52. Huffman, J. C; Moody, D. C; Schaeffer, R. *Inorg. Chem.* **1976,** *15,* 227.

53. Friedman, L. B.; Cook, R. E.; Glick, M. D. *Inorg. Chem.* **1970,** *9,* 1452.

54. Dooke, J. A.; Powell, D. R.; Gaines, D. F. *Jnorg. Chem.* **2000,** *39,* 463.

55. Hoffmann, R. *J. Chem. Phys.,* **1963,** *39,* 1397.

56. Frisch, M. J.; Trucks, G. W.; Schelegel, H. B.; Gill, P. M. W.; Johnson B. G.; Robb, M. A.; Cheeseman, J. R.; Keith, T.; Peterson, G. A.; Montgomery, J. A.; Raghavachari, K; Al-Laham, M. A.; Zakrzewski, V. G.; Ortiz, J. V.; Foresman, J. B.; Cioslowsky, J.; Stefenov, B. B.; Nanayakkara, A.; Challacombe, M.; Peng, C. Y.; Ayala, P. Y.; Chen, W.; Wong, M. W.; Andres, J. L.; Replogle, E. S.; Gomberts, R.; Martin, R. L.; Fox, D. J.; Binkley, J. S.; Defrees, D. J.; Baker, J.; Stewart, J. P.; Head-Gordon, M.; Gonzalez, C; Pople, J. A. Gaussian 94, Revision D.1, Gaussian Inc., Pittsburg PA, **1995.**

57. B3LYP is Becke's three parameter hybrid method with LYP correlation functional: (a) Becke, A. D. *J. Chem. Phys.,* **1993,** *98,* 5648. (b) Lee, C; Yang, W.; Parr, R. G. *Phys. Rev. B,* **1988,** *37,* 785. (c) Vosko, S. H.; Wilk, L.; Nusair, M. *Can. J. Phys.,* **1980,** *58,* 1200. (d) Stephens, P. J.; Delvin, F. J.; Chabalowski, C. F.; Frisch, M. J. *J. Phys. Chem.,* 1994, *98,* 11623.

58. (a) Thomas, K. M.; Mason, R.; Mingos, D. M. P. *J. Am. Chem. Soc,* **1973,** *95,* 3802. (b) Jemmis, E. D.; Balakrishnarajan, M. M. *J. Am. Chem. Soc,* **2000,** *122,* 7392.

CHAPTER 3

STABILITY OF MACROPOLYHEDRAL BORANES - A
MOLECULAR ORBITAL STUDY ON THE CAP-CAP
(INTERPOLYHEDRAL) INTERACTIONS

3.0. INTRODUCTION

The development of polyhedral borane chemistry has often involved isoelectronic and isolobal relationships with carbon and metals connecting it to hydrocarbons and to organometallics.[1, 2] Various attempts to merge organometallics with boranes are carried out mostly through the intermediacy of metallaboranes and metallocenes.[3] Here the examples known in organometallic chemistry is used to have a better understanding on bonding in isolobally related and structurally similar polyhedral boranes. The interaction between the non-bonded atoms on adjacent polyhedra in a condensed skeleton is assumed to be one of the major factors that hinder the stabilities of macropolyhedral systems as they are thought to be repulsive. The nature of these intrapolyhedral interactions in the macropolyhedral boranes are explored first followed by the impact due to the presence of hetero atoms.

In sandwich complexes involving boron as the bridging atom, the interaction between non-bonded atoms tend to be antibonding, but a closer analysis of various condensed systems shows that this cannot be generalized. The interactions between proximate atoms in adjacent units of macropolyhedral boranes are studied taking $B_{10}H_{14}$ and isolobal $[C_8H_6(Ru(CO)_2GeMe_3)_2]$ as prototype. In general single-atom bridging with main group elements leads to antibonding interactions between two formally non-bonded pairs of atoms, whereas higher fusions show greater inclination to have bonding interactions. Models to comprehend the nature of cap-cap interactions in heteroboranes were restricted to single vertex and edge shared systems, as all higher fusions are found to share the same trends.

3.1. CONDENSED POLYHEDRAL BORANES

Steric interactions induced between two adjacent vertices of an icosahedron by replacing terminal hydrogen atoms with bulky substituents have been studied previously; a representative example is shown in 1, Figure 1.[4] In these molecules, mostly metallacarboranes, the phenyl groups on two neighboring carbon atoms results in repulsive interactions leading to the cleavage of the C-C bond. The ligands on the metal are mostly Cp or C_6H_6 which makes the molecule a two-cluster system fused through a transition metal vertex. Macropolyhedral boranes formed by the condensation of two or more polyhedral clusters through one or more boron atoms bring additional complexity as the non-bonding interactions are suspected to influence their stability.[5] The nature of these interactions is the subject of the current study. Though there are many ways of fusing polyhedral boranes starting with single vertex to four-atom sharing, mixing the various fusions, alleviating the charges of opened cages by adding bridging hydrogens and so on, progress appears to be hindered due to the suspected steric interactions. The existence of pentalene complexes of metals with both *cis* and *trans* orientations[6] prompted us to have a detailed analysis of such interactions. Taking the same B_{12} skeleton, Figure 1 shows the various condensations (2, 4-6) known in polyhedral borane chemistry. Here the dotted lines indicate the interactions between atoms from two adjacent subclusters, which are linked to the same shared atoms. These atoms are called as caps and the interactions between them as cap-cap interactions (Figure 1).
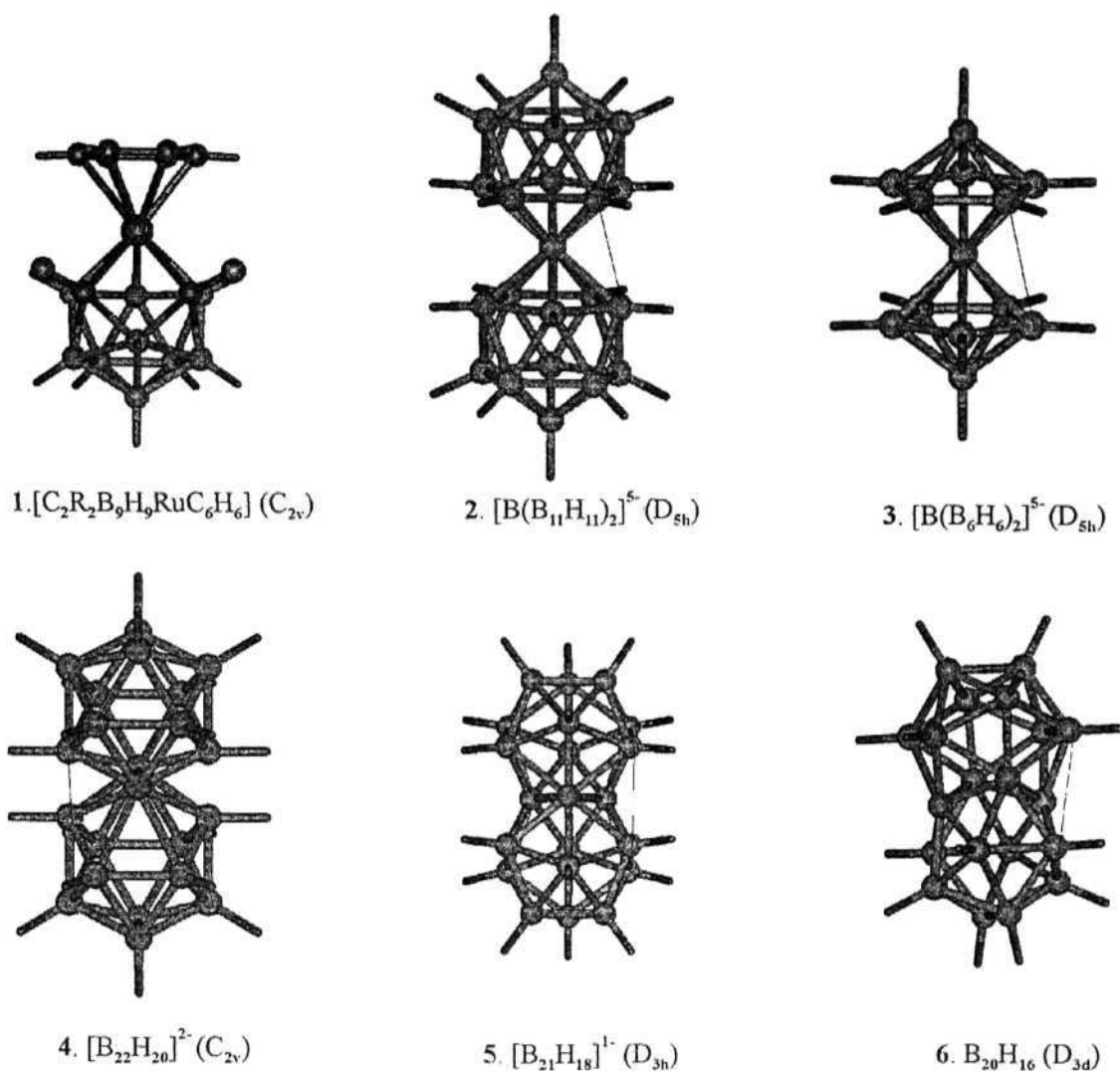
1. $[C_2R_2B_9H_9RuC_6H_6]$ (C_{2v})

2. $[B(B_{11}H_{11})_2]^{5-}$ (D_{5h})

3. $[B(B_6H_6)_2]^{5-}$ (D_{5h})

4. $[B_{22}H_{20}]^{2-}$ (C_{2v})

5. $[B_{21}H_{18}]^{1-}$ (D_{3h})

6. $B_{20}H_{16}$ (D_{3d})

Figure 1

All the fusion modes starting from single vertex to four-atom sharing is shown taking a B_{12} unit: $[B(B_{11}H_{11})_2]^{5-}$ (2), $[B22H20]^{2-}$ (4), $[B_{21}H_{18}]^{1-}$ (5) and $B_{20}H_{16}$ (6). The cap-cap interactions due to condensation are depicted as dotted lines. $[C_2R_2B_9H_9RuC_6H_6]$ (1) corresponds to the monopolyhedral system where such interactions are induced between the vertices of the B_{12} cage. $[B(B_6H_6)_2]^{4-}$ (3) corresponds to a sandwich system based on pentagonal bipyramidal skeleton. Structures 2, 3 and 4 are hypothetical examples. 5 and 6 corresponds to the minimized geometries on the PES. 6 is also known experimentally.

Structure 2 with all boron atoms does not exist in an isolated form. Molecular Orbital (MO) studies on sandwich compounds involving octahedral aluminium clusters by Hoffmann et al have shown that the cap-cap distance and hence their interactions are

major factors in determining the stability of sandwich complexes.[7] A similar approach has been used in studying hypothetical borane clusters based on pentagonal bipyramid, $[B(B_6H_6)_2]$ (3). Structure 4 where two B_{12} skeletons share an edge is not realizable due to the very close distance between the caps (1.5 A with the experimental B-B distances of B12H12$^{2"}$).[8] All the experimentally known structures with edge sharing exhibits either bis*nido* patterns with open faces opposite to each other[9] or the skeleton has been slightly rearranged.[10] Realizable models are taken in edge shared systems from *closo* ($B_{12}H_{10}^{2-}$ 7, $B_{10}H_8^{2-}$ 8), *nido* (B11H13 9), and *bisnido* ($B_{10}H_{14}$ 10, 11) forms where there is the possibility of cap-cap interactions. A comparison across two fusions is possible through 8 which has a *nido* face shared isomer (12). The *closo* form of the face condensation product of two B_{12} skeletons, $B_{21}H_{18}^{1-}$ (5), discussed earlier and which is a subject of many theoretical studies[11] is yet to be isolated. 5 along with its *nido* form, $B_{20}H_{18}^{2-}$ (13)[12] is considered in the studies. Structure 13 is derived from the known $B_{20}H_{16}(NCMe)_2$ by the replacement of $NCMe_2$ groups by H".[5] After the experimental isolation and structural characterization of this molecule by Lipscomb et al., the existence of the *closo* $B_{21}H_{18}^{1-}$ (5) was predicted. According to Lipscomb, the steric interactions between atoms on adjacent clusters in 5 will be larger in relation to that in 6; the non-bonded distance is less than the sum of the van der waal's radii.[5] The only known *closo* form among condensed clusters, $B_{20}H_{16}$ (6) involving four-atom fusion was isolated in the early 1960s.[13] The extent of steric interactions that occur in the different condensation modes and how it affects the stability of these molecules has been studied here.
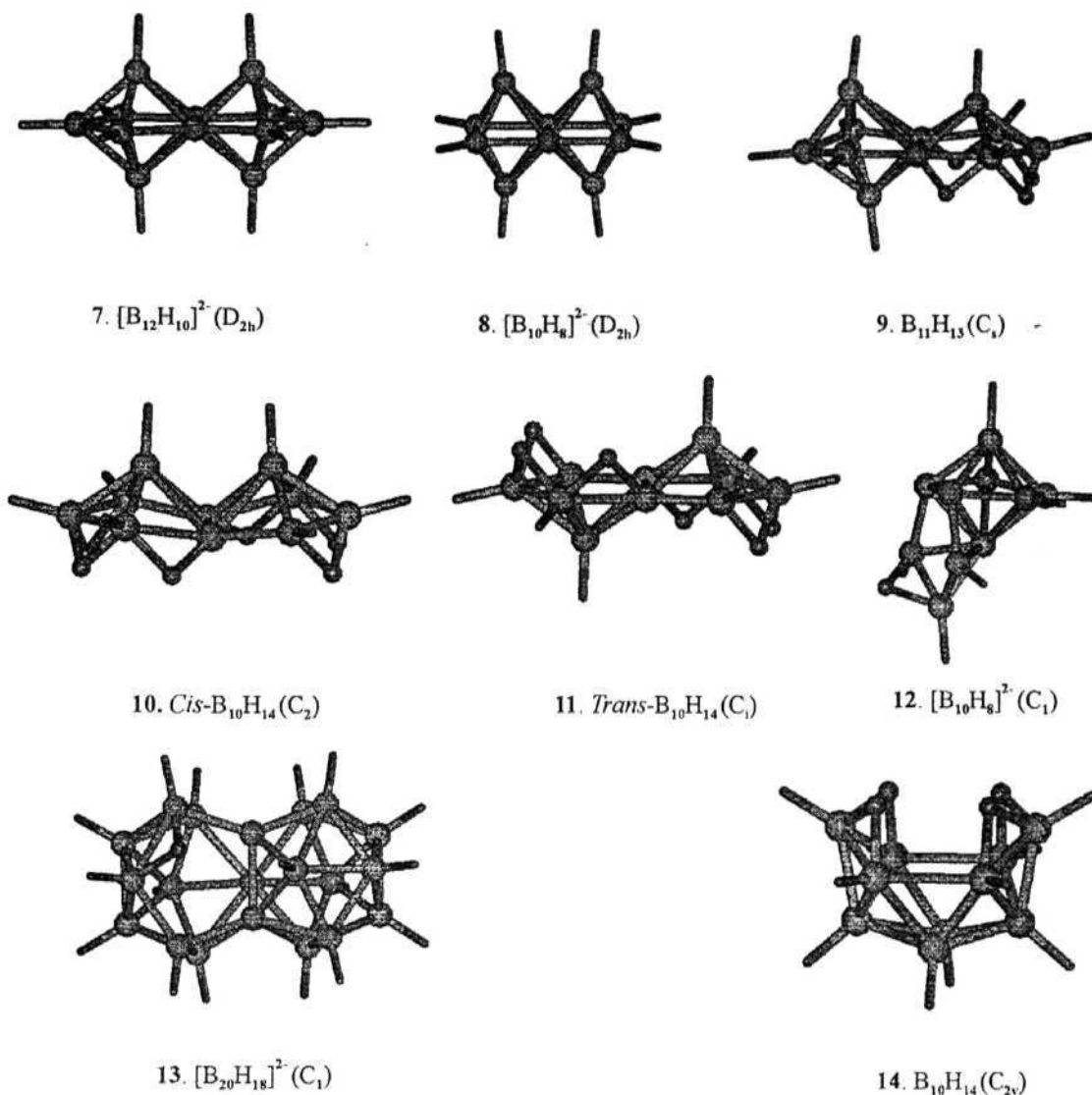
7. $[B_{12}H_{10}]^{2-}$ (D_{2h})

8. $[B_{10}H_8]^{2-}$ (D_{2h})

9. $B_{11}H_{13}$ (C_s)

10. Cis-$B_{10}H_{14}$ (C_2)

11. Trans-$B_{10}H_{14}$ (C_1)

12. $[B_{10}H_8]^{2-}$ (C_1)

13. $[B_{20}H_{18}]^{2-}$ (C_1)

14. $B_{10}H_{14}$ (C_{2v})

Figure 2

The geometries of the optimized structures used for the study. Structures [$[B_{12}H_{10}]^{2-}$ (7), $[B_{10}H_8]^{2-}$ (8 and 12) $B_{11}H_{13}$ (9), Cis-$B_{10}H_{14}$ (10), Trans-$B_{10}H_{14}$ (11), $[B_{20}H_{18}]^{2-}$(13), $B_{10}H_{14}$ (14) are calculated at B3LYP/6-31g* level. All are minima on the PES.

Most of the molecules which have m+n number of skeletal electron pairs are inclined to show the same trend in the nature of Overlap Population (OP). A simplified and realistic model of the isomers of $B_{10}H_{14}$ is taken as representative examples for our detailed MO study. Such a system (10 and 11) can be reduced from the experimentally

80

isolated pentalene complexes of metals by isolobal replacement. While cis $B_{10}H_{14}$ has its equivalent in $[C_8H_6(Ru(CO)_2GeMe_3)_2]$ and $[C_8H_6(Re(CO)_3)_2]$, $trans$ form has many isolobal organometallic molecules; one among them is $[Ni(C_3H_5)_2(C_8H_6)]$.[6] This also enables to compare several classes of isomers ranging from a condensed system with either the presence or absence of the cap-cap interactions *(cis* and *trans bisnido,* **10** and 11) and the known monopolyhedral system (**14**).[14] The single vertex sandwiches, which have m+n+o skeletal electron pairs has a greater tendency towards antibonding interactions between the caps depending on the nature and size of the central atom.

. Mülliken Overlap Population (OP)[15] at both *ab initio* and Extended Hückel (EH)[16] levels on the *ab initio* optimized geometries of selected structures are used to study the nature of the cap-cap interactions. The OP is a rough and ready indicator of bonding and antibonding interactions, especially useful when comparisons involve analogous bonding situations.[17] Hence its use is restricted in similar contexts and expect the conclusions on cap-cap interactions to be qualitatively correct. Wiberg Bond Index (WBI)[18] between the caps in the *cis* arrangements is also computed as a further verification of the quantitative results obtained. The values of OP at both *ab initio* and EH levels, the WBI, total energies and the non-bonding B-B distance and the dihedral angles wherever possible along the shared atoms are given in Table 1. The relative energies of the isomers whenever applicable are given in Table 1. The EH studies have also been used in understanding the bonding and energetics of MOs of some selected systems, which are minima on the PES.

3.1.1. Sandwich complexes involving five-membered rings

Sandwich complexes with all boron atoms are not known so far experimentally, except as a part of β-rhombohedral boron.[19] Let us consider the hypothetical *closo*-$[B(B_6H_6)_2]^{5-}$ (3) with the charge of 5- from the *mno* rule. With boron as the sandwiched atom, the two B5H5 rings are too close with each other and the OP between the caps is -0.138 (cap-cap distance of 2.577 A at B-B bonding distance of 1.786 A). The nature of the cap-cap interaction in 3 is maintained even at a B-B distance found in the experimentally isolated sandwich complexes with heavy atom at the shared site (-0.07 at cap-cap distance of 3.143 A).

The MOs contributing to this antibonding interaction between the caps is shown in Figure 3. In the hypothetical structure obtained from (3) by removing four electrons, $[B(B_5H_5)_2]^{1-}$, where this degenerate pairs of MOs are vacant, the non-bonded interactions become favorable (0.035 and 0.007 at cap-cap distances of 2.577 A and 3.143 A respectively). A sandwich structure involving Si_3H_3 rings and central boron atom, $[(Si_3H_3)_2B]^{1+}$, has been characterized as minima on the PES. This follows the *mno* rule if the tetrahedron is treated as a closed polyhedron.[20]
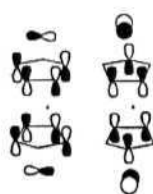
Figure 3

The degenerate e_g MO which is responsible for the antibonding interactions between the caps in a sandwiched complex with a bridging main group atom.

Table 1. The Total energies (T.E.) of 5-16 (**B3LYP/6-31g***) and 17, 18 B3LYP/LANL2DZ, Overlap Populations (OP) between the caps calculated using wave functions obtained at the *ab initio* and EH MO levels and WBI at *ab initio* level of all molecules, corresponding cap-cap distances (D (in A)) and the dihedral angles (A (in °)) between the caps along the shared atoms. The relative energies (R.E. in kcalmol^{-1}) when isomers are present are given with roman numbers within brackets representing each species with a given molecular formula.

Molecule	T.E. (a.u.)	R.E. (kcalmol^{-1})	WBI	OP		D (Å)	A (°)
				Ab initio	EH		
$B_{21}H_{18}^{1-}$ (5)	-533.12037		0.101	0.0514	0.063	2.33	88.3
$B_{20}H_{16}$ (6)	-506.90851		0.043	0.0258	-0.001	2.68	113.7
$B_{12}H_{10}^{2-}$ (7)	-304.28365		0.097	0.0397	0.053	2.54	95.3
$B_{10}H_8^{2-}$ (8)	-253.28709	0.0 (I)	0.250	0.1112	0.213	2.11	67.4
$B_{11}H_{13}$ (9)	-281.17948		0.024	0.0226	-0.002	2.84	63.7
Cis-$B_{10}H_{14}$ (10)	-256.89279	66.9 (II)	0.077	0.0596	0.042	2.49	90.8
Trans- $B_{10}H_{14}$ (11)	-256.95059	30.7 (II)					
$B_{10}H_8^{2-}$ (12)	-253.22851	36.8 (I)	0.233	0.1445	0.152	2.21	93.0
			0.116	0.0777	0.049	2.38	102.6
$B_{20}H_{18}^{2-}$ (13)	-508.19333		0.063	0.0492	0.038	2.43	94.6
			0.060	0.0485	0.039	2.44	92.4
$B_{10}H_{14}$ (14)	-256.99945	0.0 (II)					

3.1.2. Macropolyhedral **boranes** involving higher fusions

The edge shared *closo* structures considered are $B_{12}H_{10}^{2-}$ (7) and $B_{10}H_8^{2-}$ (8). The OP between the caps of the optimized structures of 7 and 8 is positive at both *ab initio* and EH level. The *nido* (9) as well as the *cis bisnido* (10) form derived from $B_{12}H_{10}^{2-}$ has weak bonding interactions between the caps (Table 1). The OP of -0.002 for $B_{11}H_{13}$ at EH level is small. Though *cis* (10) and *trans*-$B_{10}H_{14}$ (11) can exist in many isomeric forms depending on the positions of the bridging hydrogen atoms, 10 and **11** are found to be the most stable ones and are discussed. A comparison of the relative energies of 10 and 11 with its monopolyhedral isomer (14) shows that 14 is the most stable form. The *trans* (11) and the *cis* (10) isomers of $B_{10}H_{14}$ are higher in energy than the monopolyhedron (14) by 30.7 kcal mol^{-1} and 66.9 kcal mol^{-1} respectively. The relative energy shows that the condensation reduces the stability, probably due to the involvement

of larger number of boron atoms at the open area and lesser number of bridging hydrogen atoms to be placed on the open face of the monopolyhedron against 10 or 11. Structure 14 also has the advantage of being a fragment of an inherently stable icosahedron whereas 10 and **11** are derived from pentagonal bipyramids. The trend in the calculated energies at a first sight appears to favor Lipscomb's suggestion about the role of cap-cap interactions in the stability of condensed systems.[5]

The next isomers considered are of $B_{10}H_8^{2-}$ which, exist in a *closo* edge shared form (8) and a *nido* face shared form (12). The cap-cap OPs of these two systems indicate bonding (Table 1). A symmetric form of 12 with an *endo* hydrogen falls back to the C_1 structure, 12 with hydrogen bridging two non-shared boron atoms. Another starting structure where the hydrogen bridges a shared and a non-shared atom (15a, Figure 4) converge to a totally different isomer, which is more like an edge shared system (15b, Figure 4). The energetics show that 12 is less stable than the *closo* edge shared system 8 by 36.8 kcalmol^{-1}, despite the closer cap-cap distance in 8 (Table 1). Structure 15b is found to be less stable than 8 by 19.1 kcalmol^{-1}. Thus short non-bonded distances is not a decisive factor that destabilizes a system.[5] The trend in relative energies of condensed boranes is explained taking $B_{10}H_{14}$ isomers as a model in the next section. Condensed boranes involving three or four atom fusion show similar trends in the nature of OP.

On Optimisation

15a. $B_{10}H_8^{2-}$ 15b. $B_{10}H_8^{2-}$
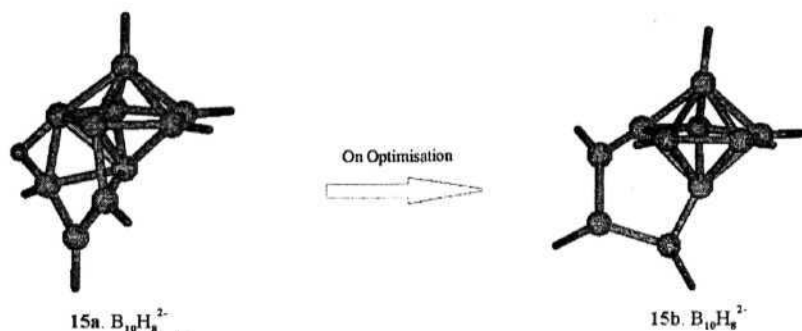
Figure 4

The structure of nido face-shared $B_{10}H_8^{2-}$ (15a, LHS) with the bridging hydrogen between a shared and a non-shared atom converges to structure **15b** on the RHS on optimization. **15b** corresponds to the geometry at B3LYP/6-31g* level of theory.

3.1.3. An MO Theoretical Explanation for cap-cap bonding in higher fusions

The bonding between the caps is studied using the hypothetical $B_{10}H_{14}$ molecule, a model edge shared system. The *cis* and *trans* isomers of $B_{10}H_{14}$ (10 and **11**) is analyzed by a ring-cap fragmentation, emphasizing the differences in the two isomers. The discussion is restricted to those MOs involving combinations of the ring π MOs and various combinations of the cap FMOs.[21]

Figure 5 shows an interaction diagram between the ring FMOs ($B_8H_6^{10-}$, center) and the cap FMOs ($(BH^{2+})_2$; LHS *trans*, RHS *cis*) to give $B_{10}H_8^{6-}$. The skeletons are derived from *closo*-$B_{12}H_{10}^{2-}$ (7) and have point group symmetries of C_{2h} and C_{2v} for *trans* and *cis* respectively. From the diagram it is clear that in the *cis* isomer there is no occupied MO which has an antibonding interaction between the caps resulting from an end-on-overlap between them. On the other hand there are occupied MOs with bonding interactions between the caps explaining the positive OP between the caps. The cap OP value for *cis*-$B_{10}H_8^{6-}$ with C_{2v} symmetry is 0.036, which is less than that in *closo*-$B_{12}H_{10}^{2-}$ (0.053). The bending of the five-membered rings in the optimized form of *cis*-$B_{10}H_{14}$

increases the cap-cap overlap to 0.042. The cap-cap OP in $B_{10}H_{14}$ is greater than that in $B_{12}H_{10}^{2-}$ though WBI between caps is smaller for $B_{10}H_{14}$ according to the *ab initio* results (Table 1).
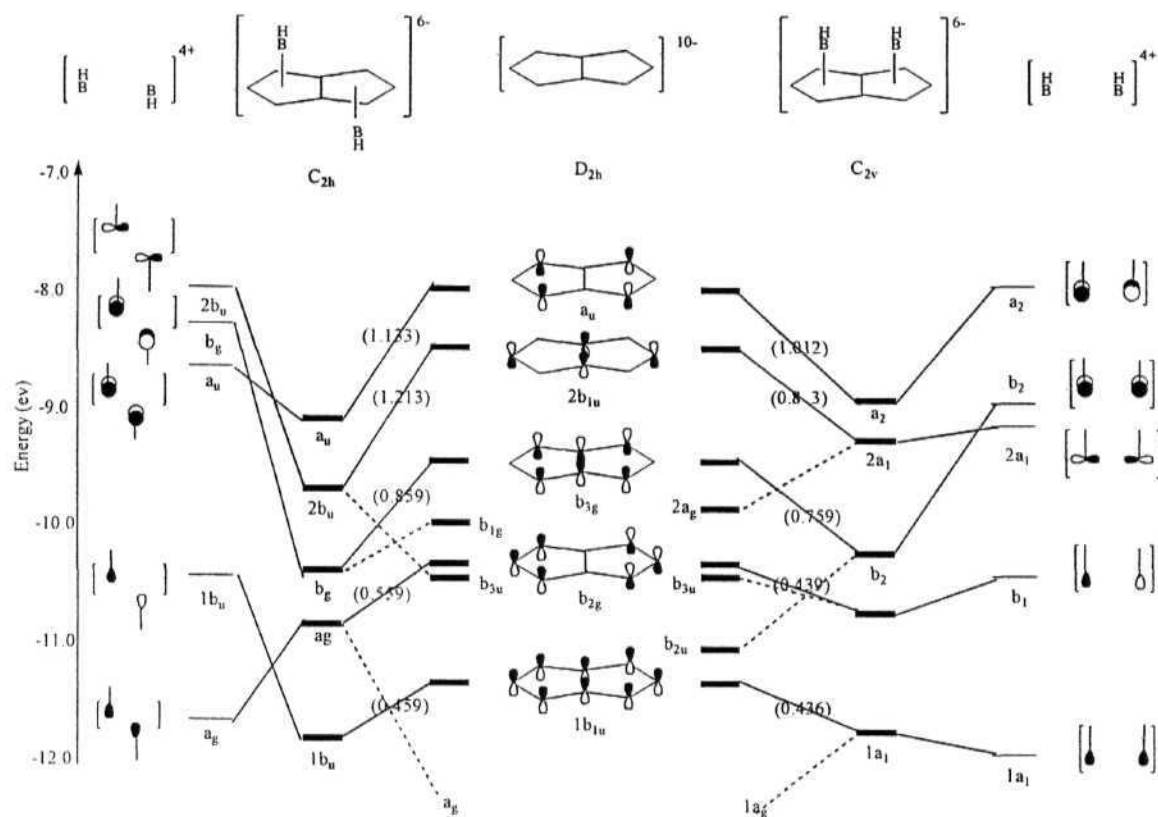
FIGURE 5

The MOs of *cis* and *trans* $B_{10}H_{14}$ (RHS and LHS respectively) obtained by an interaction between an edge shared B_8 ring and two BH groups. Only the MOs involving p orbitals perpendicular to the ring are considered. The magnitude of stabilization of the ring FMOs due to the caps is given in brackets in eVs. The dotted lines correspond to secondary interactions.

The *trans* form of $B_{10}H_{14}$ is found to be more stable than *cis* by 36.3 kcalmol[-1]. In the absence of the cap-cap interaction as a factor in explaining the stability between the two isomers, the MOs are analyzed in detail to describe their relative stability. Figure 5 gives a comparison of the stabilization of the ring FMOs due to capping on the same sides or either sides of the two five-membered rings fused through an edge. Energies of

additional ring FMOs are depicted in Figure 5. These are FMOs involving in-plane orbitals of the ring boron atoms, which influence the energetics of the concerned MOs, by second order interactions. The stabilization energies of the ring FMO due to the cap is given in brackets at appropriate places.

While there are many interactions of varying importance shown in Figure 5, only the strongest among these are considered. These involve the b_{3g}, $2b_{1u}$ and a_u FMOs of the ring. The ring FMO b_{3g} finds its equivalent cap FMO with matching symmetry in b_g of the *trans* arrangement and in b_2 of the *cis* arrangement. b_g (LHS) corresponds to an antibonding cap FMO whereas b_2 (RHS) is a bonding cap FMO. The in-plane ring FMOs which can interact with these cap FMOs will be different in *cis* and *trans*. Thus while in *trans*, b_{3g} is more stabilized due to a second order interaction from b_{1g}, in *cis* form b_{3g} stabilization due to caps is reduced by the second order interaction from b_{2u}. In a similar way, the next ring FMO, $2b_{1u}$ has a second order interaction in both *trans* and *cis; trans* being affected by b_{3u} and *cis* by nearer $2a_g$. The two levels being farther apart in *trans* than in *cis*, the destabilization is less in *trans* than in *cis*. The highest level, a_u of the ring has a lesser stabilization due to caps in *cis* than in *trans* despite the closer interacting levels in *cis* than in *trans*. The symmetry matching cap FMO a_2 in the *cis* form for the ring FMO a_u has antibonding character between the caps which explains the lesser stabilization in *cis* than in *trans*. The analysis show the lower stability of *cis* over *trans* as due to the lesser stabilization of the ring on capping caused by the resulting second order interactions from lower lying levels competing for the same cap FMO. In general it is observed that destabilizing second order interactions are prominent in *cis,* which reduces its stability over the *trans* from.   • •
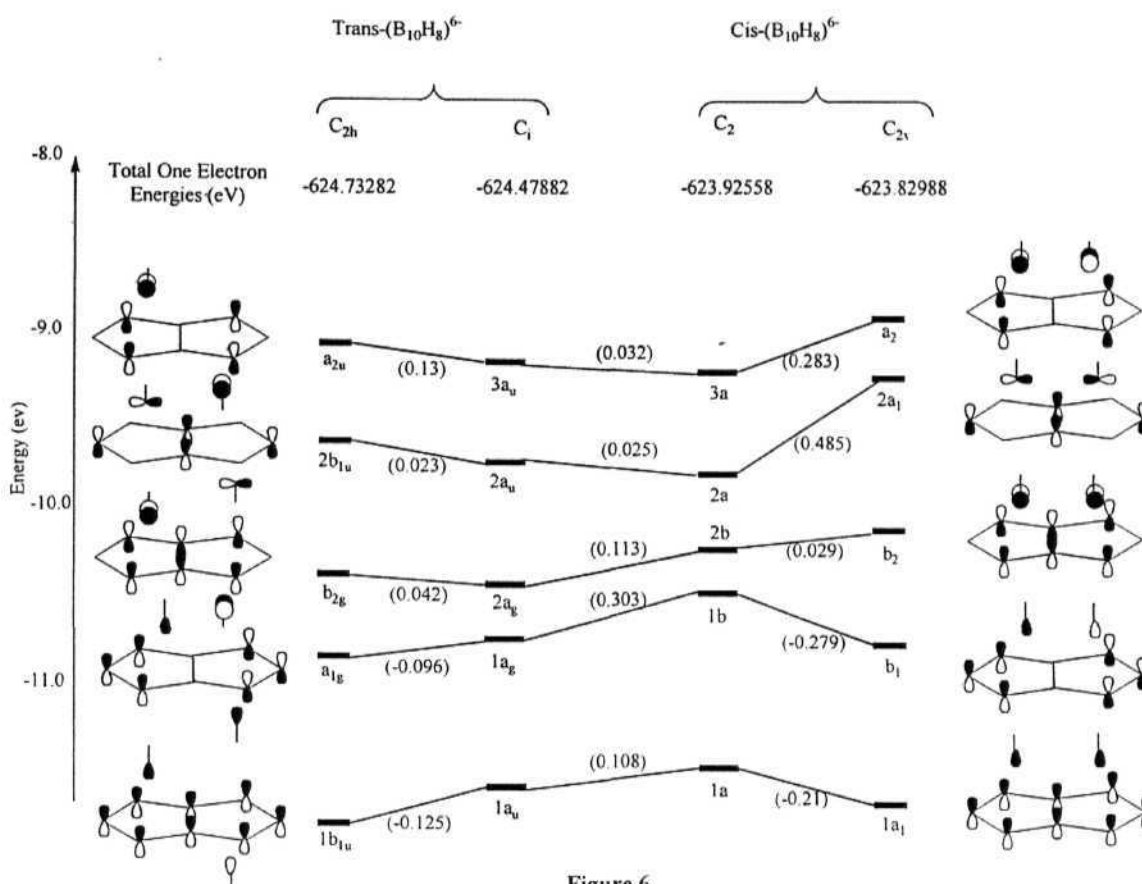
Figure 6

A correlation diagram between the C_{2h} and C_i geometries *of trans* $B_{10}H_8{}^{6-}$ (LHS) and between C_{2v} and C_2 geometries of *cis* $B_{10}H_8{}^{6-}$ (RHS) is given. Only the MOs involving p orbitals perpendicular to the ring are shown.

An EH analysis on *cis*-$B_{10}H_8{}^{6-}$ correlating the initial C_{2v} and the final C_2 geometries (Figure 6) show a decrease in the total one electron energies of the skeleton; C_2 being the optimized geometry of *cis* $B_{10}H_{14}$. The *trans* form has a net destabilization when the one electron energies are correlated between the C_{2h} and the optimized C_i geometries (Figure 6), though the trend in relative energies between *cis* and *trans* remains the same. The two five-membered rings deviates from planarity and subtends an angle of 159.0° instead of 180°.

According to the ring-cap matching principle, the out-of-plane bending of substituents in a ring is to increase its overlap with the cap.[21] Here both the caps benefit from the non-planarity of the two rings. As a consequence the cap-cap distance decreases. There is also a contribution from the cap-cap bonding interaction towards the final geometry. The MOs which are greatly affected in the *cis* form are $2a_1$ and a_2 (Figure 6), with stabilization energy of 0.485 eV and 0.283 eV respectively. In $2a_1$ the bonding between the caps helps in a greater stabilization of the MO when compared to a_2 which has antibonding nature between the caps. Thus the bending of the ring can be partly attributed to the enhancement of cap-cap overlap in addition to the increase in ring-cap overlap.[21] This is also reflected in the shortened cap-cap distance in *cis*-$B_{10}H_{14}$ (10) compared to that of the *closo*-$B_{12}H_{10}^{2-}$ (7) (2.491 A vs. 2.537 A; Table 1).

3.2. CONDENSED POLYHEDRAL HETEROBORANES AND ANALOGOUS ORGANOMETALLIC CLUSTERS

The impact of the hetero atoms on the nature of the cap-cap interactions in macropolyhedral boranes is explored. The various examples used for the qualitative MO study are substantiated with higher level theoretical calculations. Since the condensed polyhedral boranes show striking difference between single vertex and higher fused systems,[22] studies on heteroboranes are done on sandwich systems and edge shared systems representing the higher fusions to inquire the nature of the interactions.

The magnitude and nature of the interactions in single vertex sandwiches is found to depend on the size and nature of the central atom. Single vertex shared complexes always exist in the sandwich form as observed for $[Al(C_2B_4H_6)_2]^{-1}$ (1, Figure 7), and has been selected for our study. Usually they are known with some bulky groups like $-SiMe_3$

on the carbon atoms.[23] The Overlap Populations calculated for $[Al(C_2B_4H_6)_2]^{1-}$ (1) optimized at B3LYP/6-31g* level indicate antibonding interactions between the caps. The skeletal atoms in 1 can also form a different polyhedron as shown in 2(a and b), Figure 1. Though there can be many more isomers for $[Al(C_2B_4H_6)_2]^{-1}$, depending on the position of carbon in both skeletal frameworks discussed (1 and 2), only the experimentally isolated one and its corresponding isomer in the second arrangement are selected for the study. The effect due to transition metals at the sandwich position on the nature of the cap-cap interactions is analyzed taking $[Co(C_2B_4H_6)_2]^{1-}$ (3) as the model.

Analogous organometallic clusters of $B_{10}H_{14}$ is found in $[C_8H_6(Ru(CO)_2GeMe_3)_2]$ and $[C_8H_6(Re(CO)_3)_2]$ for the *cis* form and $[Ni(C_3H_5)_2(C_8H_6)]$ for the *trans* form.[6] Thus the *cis* and *trans* forms of $[C_8H_6(Ru(CO)_2Me)_2]$ (4, 5) are also considered. The large $GeMe_3$ group is replaced by Me for computational ease. $[C_8H_6(Ru(CO)_2Me)_2]$ (4), studied at B3LYP/LANL2DZ level[24, 25] have weak Ru-Ru interactions. DFT calculations using Double Zeta functional without polarization (DZ) and Triple Zeta functional with Polarization (TZP) are also carried out on the transition metal complexes at Becke Perdew level using Amsterdam Density Functional (ADF) package version 2002.03.[26] Taking the same skeleton the isoelectronic borane-transition metal systems $[B_8H_{12}(Ru(CO)_2Me)_2]$ (6, 7) and isolobal carbon-boron systems $[C_8H_6(BH)_2]^{2+}$ (8, 9) are also optimized to understand how the nature of the cap-cap interactions varies with different substitutions. The nature of cap-cap interactions in transition metal systems is substantiated by a detailed Extended Hückel[16] based MO study taking 4 and 5 as the model. $C_2B_8H_{12}$ (10) which is topologically equivalent and isoelectronic to the edge shared $B_{10}H_{14}$ is also considered for the study, the nature of the cap-cap interactions of

which can also be compared with 8 as 10 is just an interchange of the ring and cap atoms, except for the bridging hydrogens in 10. The negative OP between the carbon atoms in 10 is substantiated by a Fragment Molecular Orbital (FMO) analysis. The values of OP at both *ab initio* and EH levels, the Weiberg Bond Index (WBI),[18] total energies and the non-bonding B-B distance and the dihedral angles wherever possible along the shared atoms are given in Table 2. The relative energies of the isomers are also given in Table 2.

3.2.1. Sandwich Complexes involving heteroatoms at the shared position

A well characterized structure is available where four boron atoms of two pentagonal rings shared by a vertex are replaced by carbon and the sandwiched boron atom by a larger atom Al. The optimized geometry of this structure, $[Al(C_2B_4H_6)_2]^{1-}$ (1), Figure 7, is close to that of the experimental geometry.[23] The non-boned B-B distances are much larger (3.65 A) but the OP is negative, though small in magnitude (Table 2). The e_g set of $[B(B_5H_5)_2]$ loses its degeneracy in 1 due to the lack of symmetry, but still remains at the frontier region and is responsible for the antibonding interactions between the caps.

The other isomer 2a, on optimization converges to 2b. The relative energy of 2b when compared to 1 is 71.04 $kcalmol^{-1}$. The higher stability of 1 is quite obvious from the ring-cap matching principle.[21] In 2, aluminum caps a four membered ring, which is less favorable for a bulky atom with more diffused orbitals. On optimization the coplanarity of the two rings are lost; one ring makes an angle of 88° with the other. This may be to reduce the antibonding cap-cap interactions that are greater in magnitude in 2 compared to that in 1 since both the ring atoms and cap atoms are proximate.
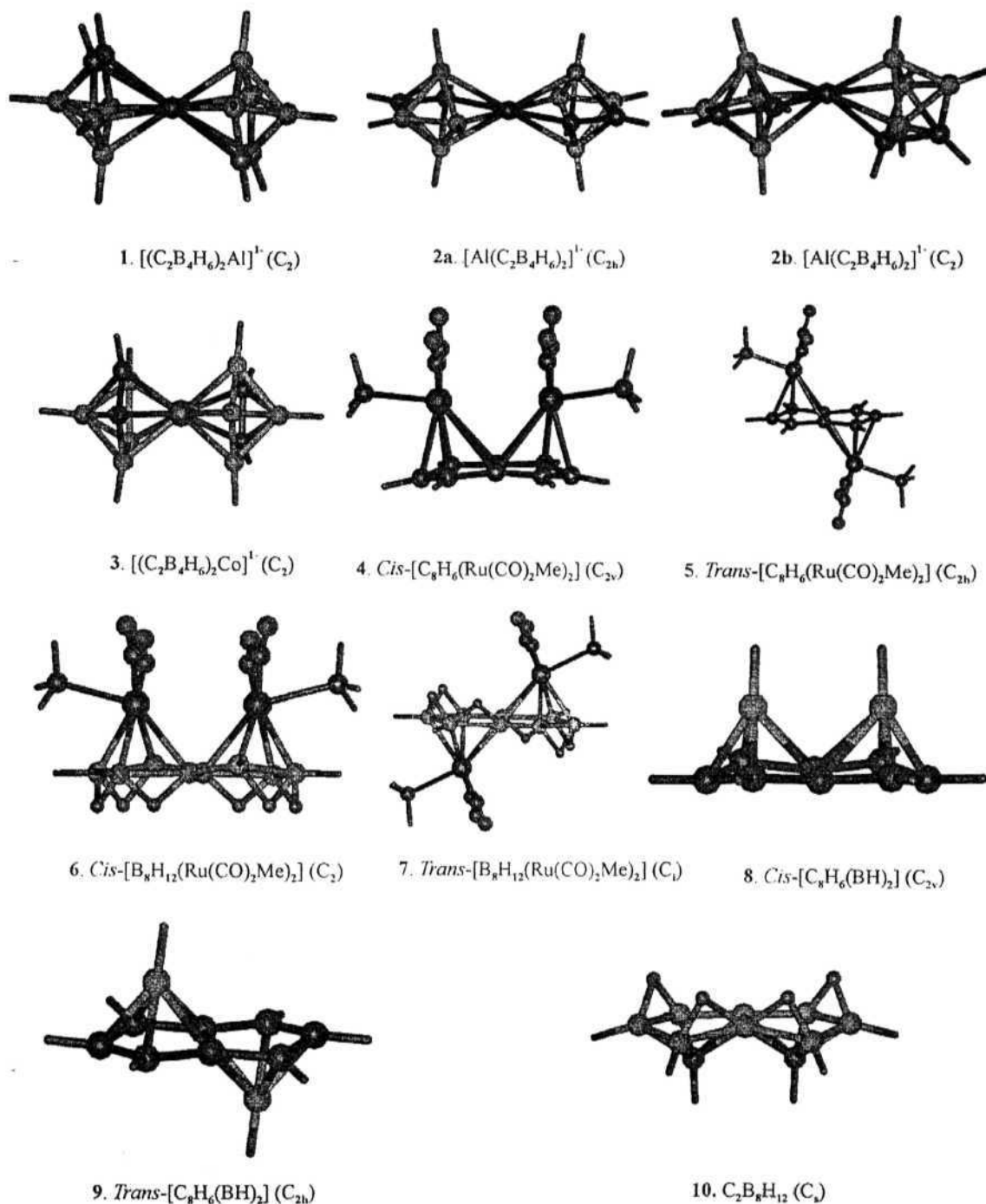
1. $[(C_2B_4H_6)_2Al]^{1-}$ (C_2)

2a. $[Al(C_2B_4H_6)_2]^{1-}$ (C_{2h})

2b. $[Al(C_2B_4H_6)_2]^{1-}$ (C_2)

3. $[(C_2B_4H_6)_2Co]^{1-}$ (C_2)

4. Cis-$[C_8H_6(Ru(CO)_2Me)_2]$ (C_{2v})

5. $Trans$-$[C_8H_6(Ru(CO)_2Me)_2]$ (C_{2h})

6. Cis-$[B_8H_{12}(Ru(CO)_2Me)_2]$ (C_2)

7. $Trans$-$[B_8H_{12}(Ru(CO)_2Me)_2]$ (C_i)

8. Cis-$[C_8H_6(BH)_2]$ (C_{2v})

9. $Trans$-$[C_8H_6(BH)_2]$ (C_{2h})

10. $C_2B_8H_{12}$ (C_s)

Figure 7

The geometries of the optimized structures used for the study. Structures $[(C_2B_4H_6)_2Al]^{1-}$ (1, 2), $[(C_2B_4H_6)_2Co]^{1-}$ (3), $[C_8H_6(Ru(CO)_2Me)_2]$ (4, 5), $[B_8H_{12}(Ru(CO)_2Me)_2]$ (6, 7), $[C_8H_6(BH)_2]$ (8, 9), $C_2B_8H_{12}$ (10),; compounds involving transition metals are calculated at B3LYP/LANL2DZ level and others at B3LYP/6-31g* level. All are minima on the PES.

92

Transition metals are also observed at the sandwich site, instead of larger main group elements. Such an optimized structure of $[Co(C_2B_4H_6)_2]^{1-}$ (3) at B3LYP/LANL2DZ has a positive OP between the caps. This is not surprising as the MO involving antibonding interactions between the caps, which remain as the HOMO and H0M0-1 in 1, is stabilized by the symmetry equivalent d orbitals of the transition metal and becomes a low lying MO. These MOs which are split from e_g of the more symmetric D_{5d} form into b and a of C_2 symmetry in 1 and 3 are shown in Figure 8, A and B respectively.

Table 2. The Total energies (T.E.) of 1-10, Overlap Populations (OP) between the caps calculated using wave functions obtained at the *ab initio* and EH MO levels and WBI at *ab initio* level of all molecules, corresponding cap-cap distances (D (in A)) and the dihedral angles (A (in °)) between the caps along the shared atoms. The relative energies (R.E. in kcalmol^{-1}) when isomers are present are given with roman numbers witliin brackets representing each species with a given molecular formula.

Molecule	T.E. (a.u.)	R.E. (kcalmol^{-1})	WBI	OP Ab initio	OP EH	D (Å)	A (°)
$[Al(C_2B_4H_6)_2]^{1-}$ (1)	-601.05742	0.0 (I)	0.001	-0.0068	-0.012	3.72	
$[Al(C_2B_4H_6)_2]^{1-}$ (2b)	-600.94421	71.0 (I)	0.003 0.003	-0.0053 -0.0120	-0.015 -0.013	3.90 3.46	
$[Co(C_2B_4H_6)_2]^{1-}$ (3)	-503.55700		0.0444 0.0468	0.0216 0.0031	0.020 0.028	3.27 3.21	
$Cis[C_8H_6(Ru(CO)_2Me)_2]$ (4)	-1029.31659	0.0 (II)	0.058	-0.1592	0.048	3.27	77.0
$Trans[C_8H_6(Ru(CO)_2Me)_2]$ (5)	-1029.31420	1.5 (II)					
$Cis[B_8H_{12}(Ru(CO)_2Me)_2]$ (6)	-926.89733	26.5 (III)	0.050	-0.1657	0.048	3.27	83.4
$Trans[B_8H_{12}(Ru(CO)_2Me)_2]$ (7)	-926.93916	0.0 (III)					
$Cis[C_8H_6(BH)_2]$ (8)	-358.58476	7.6 (IV)	0.073	0.0410	0.019	2.59	87.9
$Trans[C_8H_6(BH)_2]$ (9)	-358.59692	0.0 (IV)					
$C_2B_8H_{12}$ (10)	-282.11141		0.029	-0.0104	-0.041	2.55	63.6

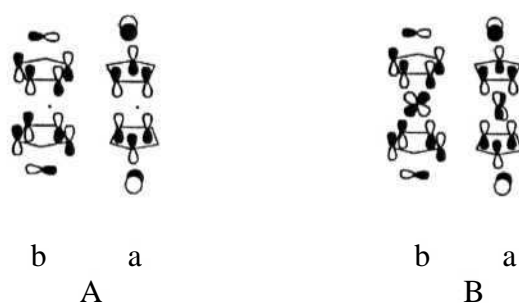| b | a | | b | a |
| A | | | B | |

Figure 8

The MOs corresponding to the Mulliken's symbol b and a of 1 and 3 are shown in A and B respectively. While 1 has these MOs as HOMO and H0M0-1, in 3 they are low lying MOs.

3.2.2. Higher Fusions involving Hetero atoms

A comparison is attempted between $B_{10}H_{14}$ and its isolobal analog, the pentalene-Ru complex which is known in its *cis* form (**4**).[6a][6c] The experimental report on the *cis* form suggests the presence of a bond between the two Ru atoms at a distance of 3.0 A. A bond between the metals is presumed based on the 18 electron rule (Ru^{2+} have 6 electrons, 2 COs donate 4 electrons, Me^{1-} - 2, $C_8H_6^{2-}$ - $10/2 = 5$; leading to the 17 electron count); the M-M a bond completes the 18 electron. The *trans* orientation of 4 is also predicted on the basis of reported geometries of isoelectronic molecules like *trans*-$[Ni(C_3H_5)_2(C_8H_6)]$. The *trans* arrangement is explained as a structure resonating between two forms with one of the metal having 16 and the other 18 electrons around it.[6b] The understanding of the bonding in these systems can be simplified by the application of *mno* rule where one considers the entire cluster to be delocalized.[27] Thus according to the *mno* rule, m = 2, n = 10, o = 0 and there are two *nido* faces which predicts a total of 14 (2 + 10 + 2) skeletal electron pairs for stability. This is achieved from 6 CH (9 electron pairs), two carbons (4) and two d^7 ML_3 fragments isolobal to BH^+ (1). Thus cluster electron count remains the same for the *cis* and *trans* structures. The metal as well as the

94

cluster attains its stable electron count without invoking resonance in the *trans* structure alone. Thus the *mno* rule is more preferred for complexes with condensed ligands.

On optimization of $[C_8H_6(Ru(CO)_2Me)_2]$ at *cis* (4) and *trans* (5) orientations, the *cis* is found to be more stable than *trans* by 1.5 kcalmol^{-1} at B3LYP/LANL2DZ level and by 1.3 kcalmol^{-1} at Becke Perdew level using DZ basis set. The optimized structure of 4 has a somewhat longer metal-metal distance of 3.27 A and 3.20 A at B3LYP/LANL2DZ and BP86/DZ levels respectively. Inclusion of polarization functions, (a triple zeta basis (BP86/TZP)), changes the M-M bond distance marginally to 3.21 A. Some of the important structural parameters of 4 at the experimental geometry and at various levels of theory are given in Table 3 for comparison. The dihedral angle C_m-C_s-C_s-C_m (Table 3) in 4 is the angle subtended by the two planar five membered rings and is bent away from the caps. While the calculated value in all the three levels is around 174°, the experimental structure has an average value of 176.6° (values varying from 173° to 178°). The bending of the ring away from the caps in contrast to that observed in *cis*-$B_{10}H_{14}$ is due to the more diffused metal orbitals with a smaller carbon ring.[21] The OP between the metals in the experimental and the LANL2DZ optimized geometry is found to be positive at EH with a value of 0.041 and 0.048 respectively. But a higher *ab initio* level show antibonding interaction with an OP of -0.1592. The repulsive nature between the metals identified at higher levels of theory is an added reason for bending of the five membered rings in pentalene than that observed in the experimental geometry. This helps in increasing the M-M distance thereby overcoming the possible repulsion between them. The NBO studies[18] on the optimized geometry suggest that there is no bond between the

two metals. Further, the near equal stability of the *trans* form leads us to conclude that there is practically no bonding interaction between the two metals in the *cis* form.

Table 3: Some important parameters of *Cis* - $[C_8H_6(Ru(CO)_2Me)_2]$ at the experimental and theoretical geometries at B3LYP/LANL2DZ, BP86/DZ and BP86/TZP. C_s is the shared carbon. C_m connects C_s and a non shared carbon. C_t bonds two C_m. R.E. is the relative energy with its *trans* isomer. Distances are in Å, dihedral angles in (°) and R.E. in kcalmol^{-1}. The distances and dihedrals are averaged in the experimental geometry.

Parameters	Expt.al	B3LYP/LANL2DZ	BP86/DZ	BP86/TZP
Ru-Ru	3.06	3.27	3.20	3.21
Ru-C_s	2.52	2.65	2.64	2.61
Ru-C_m	2.22	2.37	2.37	2.33
Ru-C_t	2.17	2.27	2.30	2.24
C_s-C_s	1.43	1.46	1.46	1.45
C_s-C_m	1.44	1.45	1.45	1.44
C_m-C_t	1.35	1.45	1.45	1.43
C_m-C_s-C_s-C_m	176.3	174.5	173.5	174.3
R.E.		1.5	1.4	1.8

A boron ring with the transition metal as caps also produces similar results as the pentalene complex. Here bridging hydrogens are added to compensate for the electronic requirement of the skeleton which results in the molecular formula of $[B_8H_{12}((Ru(CO)_2Me)_2]$. The relative stabilities between the *cis* (6) and *trans* (7) isomers is found to be very high. The *trans* form (7) is found to be more stable than the *cis* (6) by 26.5 kcalmol^{1} at B3LYP/LANL2DZ level. Since pure DFT studies with and without polarization gave almost similar results for 4 and 5, the calculations for 6 and 7 are carried out only at B3LYP/LANL2DZ level. The Ru-Ru distance of 6 are almost identical to 4 with a value of 3.27 Å, but the two B5 rings are bend towards the caps as in $B_{10}H_{14}$ making an average angle of 172° between each other.

A detailed FMO analysis is done on 4 and 5 to account for the observations in transition metal capped edge shared cluster compounds. An FMO analysis is done on the optimized geometries of both *cis* and *trans* forms by following the fragmentation of rings and caps. Similar EH studies have been done for sandwich complexes of pentalene $[M_2(C_8H_6)_2]$; (M=Co, Ni), where the OP between metals is found to be zero.[28] The important interactions in the *cis* and *trans* form (4 and 5) which leads to the stabilization of the ring FMOs are shown in Figures 9 and 10 respectively.

The Mülliken symbols assigned to the orbitals are based on the symmetry of the resultant molecule and assuming similar coordinate system in the fragments. The d^7L3M-d^7ML_3 bimetallic part with three ligands arranged in a conical manner on each metal has its octahedral remnants, the bonding and antibonding contribution of the t_{2g} sets; $(t_{2g}+t_{2g})$ and $(t_{2g}-t_{2g})$, occupied. The remaining two electrons will occupy the most bonding FMO $(a_1$, Figure 9) between the metals. In Figure 9, a_1 is shown to be empty as the binuclear metal fragment is considered to be dicationic donating the two electrons to the C_8H_6 ligand. The $2b_2$ and a_2 orbitals of the *cis* structure stabilize the ring FMOs (Figure 9). The $(t_{2g}-t_{2g})$ remains almost non-bonding here, while the $(t_{2g}+t_{2g})$ participates in two orbital - four electron interactions. One such combination is depicted in Figure 9, where two $1b_2$ fragments interact. Here the antibonding combination is stabilized by the high lying $2b_2$ level on the metal side. The HOMO (a_1) of the molecule has bonding interaction between the metals. Removal of two electrons from this MO results in zero OP between the metals by EH studies.
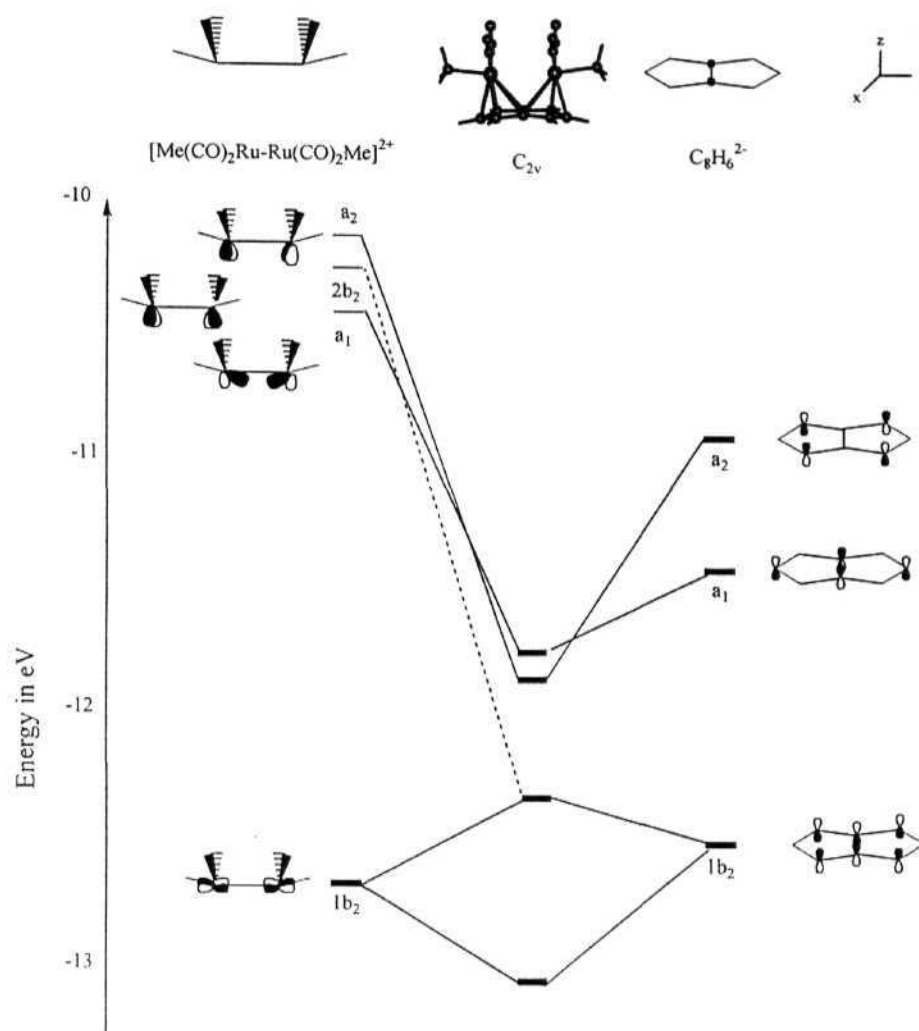
Figure 9

The interaction diagram between the ring and caps of the cis isomer of [$C_8H_6(Ru(CO)_2Me)_2$]. All the stabilizing interactions and one representative 2o-4e interaction are shown. Here (t_{2g}-t_{2g}) remains almost non-bonding and (t_{2g}+t_{2g}) is involved in 2o-4e interactions. The geometry of cis-[$C_8H_6(Ru(CO)_2Me)_2$] corresponds to the optimized one at B3LYP/LANL2DZ.

In the *trans* form (5) the stabilizing interactions are decreased (Figure 10). Here the (t_{2g}+t_{2g}) set remains almost non-bonding whereas the (t_{2g}-t_{2g}) is involved in two orbital - four electron interactions. The HOMO of 5 is one such antibonding **level** resulting from the interaction between two $1b_u$ orbitals. The HOMO is stabilized by a higher lying $2b_u$ FMO on the metal fragment. Only one level (a_u) is involved in a two

orbital - two electron interaction. Though the second order stabilizing interactions are present even in the *trans* structure, its magnitude is less because interactions comes from MOs with antibonding character between the metals and are high in energy.
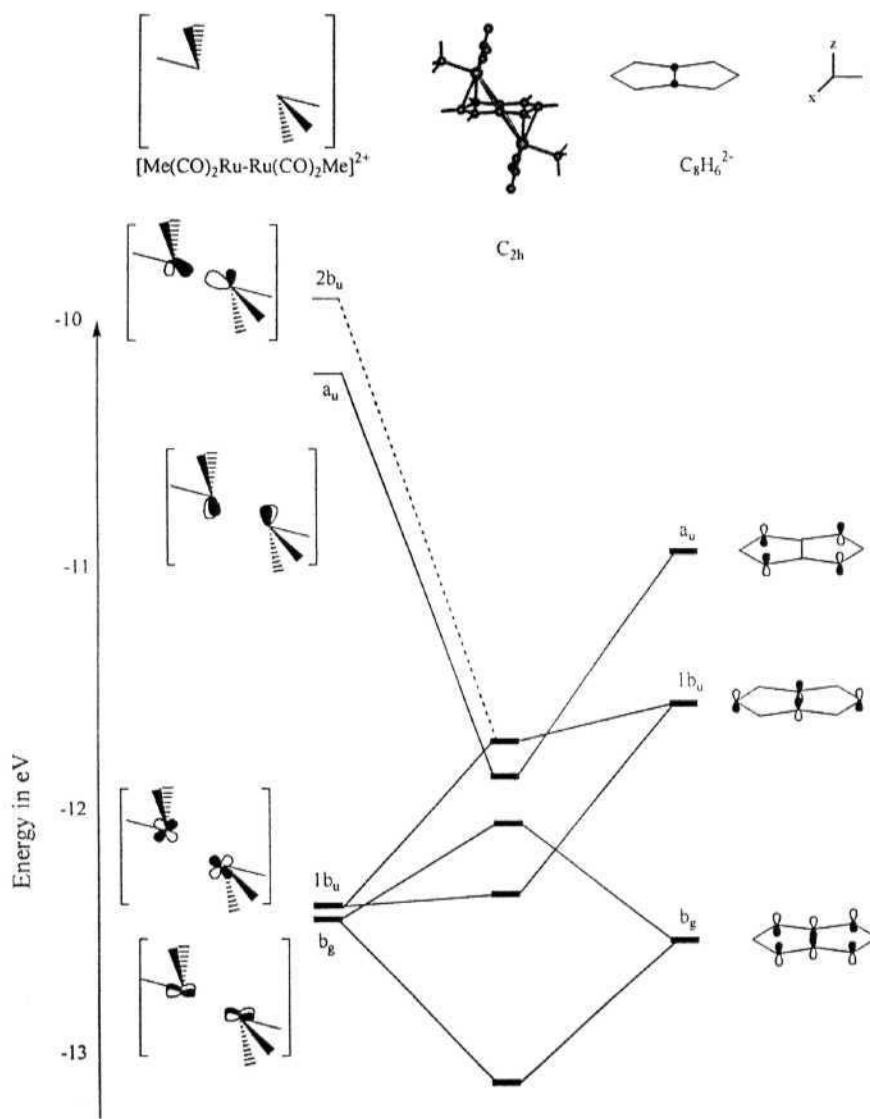
Figure 10

The interaction diagram showing the formation of trans isomer of $[C_8H_6(Ru(CO)_2Me)_2]$ from the ring and caps. All the stabilizing interactions and one representative of the 2o-4e interaction are shown. Here $(t_{2g}+t_{2g})$ remains almost non-bonding and $(t_{2g}-t_{2g})$ is involved in 2o-4e interactions. The geometry of trans-$[C_8H_6(Ru(CO)_2Me)_2]$ corresponds to the optimized one at B3LYP/LANL2DZ.

An isolobal replacement of the metal fragment of 4 and 5 to BH^+ to give $[C_8H_6(BH)_2]^{2+}$ (8 and 9) reduces the relative stability to 7.6 kcalmol^{-1}; *trans* being more

stable than the *cis* form. The plane of the two C5 rings are shifted towards the BH caps subtending an angle of 171° with each other. The nature of the cap-cap interaction is also similar to that of $B_{10}H_{14}$. 8 and 9 are optimized at B3LYP/6-31g* level of theory and the results can be comparable more with $B_{10}H_{14}$. Hence the MO justifications of $B_{10}H_{14}$ are equally valid for 8.

When the two cap BH groups of *cis*-$B_{10}H_{14}$ are replaced by CH groups, the molecular formula becomes $C_2B_8H_{12}$ and structure 10 results. Such a system differs from 8 in the interchange of the atom types between the ring and cap, except for the bridging hydrogens in 10. The special case of $C_2B_8H_{12}$ (10) which has anitbonding interactions between the caps is analyzed comparing the FMO interactions with $B_{10}H_{14}$. In 10, where the caps are CH groups, the OP is found to be negative (Table 2). This suggests that the MOs responsible for the negative OP in 10 corresponds to the in plane FMOs of the ring, rather than the perpendicular set which is common for all higher fusions. Among the various isomers possible for $C_2B_8H_{12}$ depending on the position of bridging hydrogens, 10 is the most stable one where the *cis* arrangement is retained, others converging to a skeleton where one of the carbon occupies a lesser coordination site. A comparative analysis between the interaction diagrams when CH and BH caps show that the difference lies in an MO with contribution from an in plane ring FMO. The interaction that results in this MO is shown in Figure 11 which clearly illustrates the higher contribution of the antibonding cap FMO when CH becomes the caps. The reason is obviously the greater electronegative nature of carbon which brings down the energy levels. Thus the cap FMO shown in Figure 11, which is responsible for the antibonding nature between the caps is very close to the ring FMO and has strong interaction resulting

in the greater stabilization of the ring FMO. This is clear from the percentage contribution of the cap FMOs to this particular MO in the two compounds. While in $B_{10}H_8{}^{6-}$, there is only 12% contribution, $C_2B_8H_8{}^{4-}$ has 43% contribution from the cap FMO to the resultant MO as shown in Figure 5.
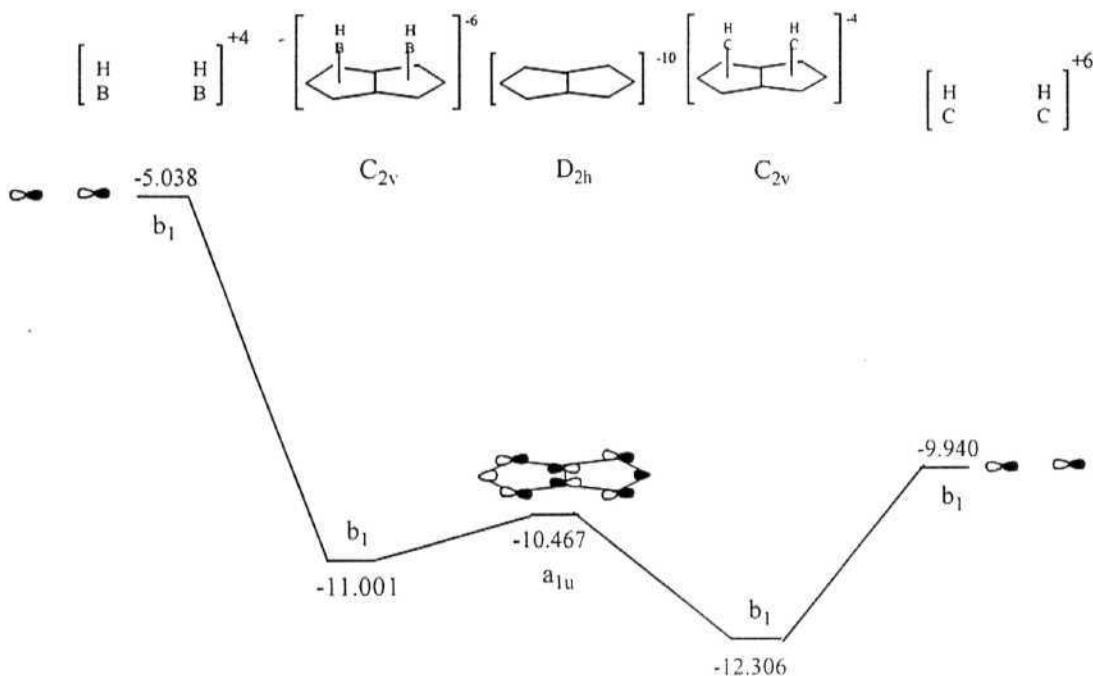

Figure 11

Comparison of the interaction when two BH (LHS) and two CH (RHS) caps the B_8 ring in the cis form leading to b_1. The cap FMO (b_1, RHS) is very close to the ring FMO (a_u) when CH is used as caps. The higher contribution of the CH cap FMO results in an antibonding interaction between the caps.

3.3. CONCLUSIONS

The common belief that the interactions between two non-bonded proximate atoms are repulsive in polycondensed boranes is not found to be generally true. This problem is analyzed using $B_{10}H_{14}$ as the model system. This enabled a further analysis among various isomers of $B_{10}H_{14}$. The energy changes involved due to the condensation

101

of open polyhedral boranes has thus been explored using $B_{10}H_{14}$ as the model. The relative stability between the two isomers of $B_{10}H_{14}$ has been explained based on a detailed FMO approach. The difference in the nature of OP between the caps in sandwich and higher fusions involving borons has been understood by MO study. The nature of bonding between the caps is attributed to the absence of cap-cap end on overlap which is antibonding, unlike in sandwich complexes. The additional MO in sandwich compounds has predominant antibonding character between the caps, which result in a negative OP in these systems. The results of the study demonstrate the significance of cap-cap interactions in the stability of higher fusions, regardless of the experimental abundance of only *trans* isomers in edge shared systems. The higher stability of *closo* edge shared $B_{10}H_8^{2-}$ over its *nido* face shared isomer is a further support for this argument.

Single vertex sandwiches with main group hetero-atoms retain the antibonding nature between the caps as in boranes despite the longer nonbonding distances. Transition metal sandwiched systems on the other hand reverse the cap-cap nature by stabilizing the MOs responsible for the antibonding interactions with its symmetry equivalent d orbitals. Heteroboranes as caps in edge shared systems tend to be antibonding unlike in boranes. The negative OP in edge shared dicarbaboranes with two CH as caps is due to the greater contribution of the cap-cap antibonding FMO to one of the in plane ring FMO. This arises from the greater electronegativity of carbon which brings down the cap FMO closer to the interacting ring FMO. Interchange of the boron and carbon atoms between the ring and caps results in positive OP between the BH caps making it similar to boranes. The positive OP at EH between ruthenium atoms in the

102

transition metal capped pentalene and borane complexes reflects weak bonding interactions between them; this becomes slightly antibonding at higher levels. It is therefore better to treat the pentalene complex under the *mno* rule rather than the 18 electron rule where a localized concept of M-M bond has to be considered. The almost equal stability of *cis* and *trans* forms of $[C_8H_6(Ru(CO)_2GeMe_3)_2]$ supports this conclusion. Appropriate macropolyhedral borane equivalents await experimental scrutiny.

REFERENCES

1. Casanova, J. (Ed.) *The Borane, Carborane, Carbocation Continuum,* John Wiley & Sons, Inc. New York, **1998.**

2. Hoffmann, R. *Angew. Chem. Int. Ed. Engl.* 1982, *21,* 711.

3. (a) Lei, X.; Shang, M.; Fehlner, T. P. *Angew. Chem. Int. Ed. Engl.* **1999,** *38,* 1986 and references therein. (b) Kennedy, J. D. *Advances in Boron Chemistry,* Seibert, W. (Ed.) Royal Society of Chemistry, London, **1997,** 451. (c) Grimes, R. N. *Advances in Boron Chemistry,* Seibert, W. (Ed.) Royal Society of Chemistry, London, **1997,** 321.

4. McWhannell, M. A.; Rosair, G. M.; Welch, A. J.; Teixidor, F.; Vinas, C. J. *Organomet. Chem.* 1999, *573,* 165.

5. Enemark, J. H.; Friedman, L. B.; Lipscomb, W. N. *Inorganic Chem.* **1966,** *5,* 2165.

6. (a) Brookes, A.; Howard, J.; Knox, S. A. R.; Stone, F. G. A.; Woodward, P. *J. Chem. Soc. Chem. Commun.* 1973, 587. (b) Harris, P. J.; Howard, J. A. K.; Knox, S. A. R.; McKinney, R. J.; Philips, R. P../. *Chem. Soc. Dalton.* 1978, 403. (c) Howard, J. A. K.; Woodward, P. *J. Chem. Soc. Dalton.* **1978,** 412. (d) Jones, S. C; Hascall, T.; Barlow, S.; O'Hare, D. *J. Am. Chem. Soc.* **2002,** *124,* 11610.

7. Vajenine, G. V.; Hoffmann, R. *J. Am. Chem. Soc.* **1998,** *120,* 4200.

8. Jemmis, E. D.; Balakrishnarajan, M. M.; Pancharatna, P. D. *Inorg. Chem.,* **2001,** *40,* 1730.

9. (a) Pitochelli, A. R.; Hawthorne, M. F. *J. Am. Chem. Soc.* **1962,** *84,* 3218. (b) Simpson, P. G.; Folting, K.; Dobrott, R. D.; Lipscomb, W. N. *J. Chem. Phys.* **1963,** *39,* **26.** (c) Simpson, P. G.; Lipscomb, W. N. *J. Chem. Phys.* **1963,** *39,* 2339.

10. Hosmane, N. S.; Franken, A.; Zhang, G.; Srivastava, R. R.; Smith, R. Y.; Speilvogel, B. F. *Main Group Metal Chem.* **1998,** *21,* 319.

11. Lipscomb, W. N. *J. Less-Common Met.* **1981,** *82,* 1.

12. (a) Jemmis, E. D.; Balakrishnarajan, M. M.; Jayasree, E. G. Manuscript under Preparation. (b) Jemmis, E. D.; Balakrishnarajan, M. M.; Pancharatna, P. D.; *Chem. Rev.* **2002,** *102,* 93.

13. (a) Friedman, L. B.; Dobrott, R. D.; Lipscomb, W. N../. *Am. Chem. Soc.* **1963,** *85,* 3506. (b) Miller, H. C; Muetterties, E. L. *J. Am. Chem. Soc.* **1963,** 55, 3506.

14. (a) Moore Jr., E. B.; Dickerson, R. E.; Lipscomb, W. N. *J. Chem. Phys.* 1957, *27,* 209. (b) Brill, R.; Dietrich, H.; Dierks, H. *Acta Cryst.,* **1971,** *B27,* 2003.

15. Mulliken, R. S. *J. Chem. Phys.* **1955,** 23, 1481.

16. (a) Hoffmann, R.; Lipscomb, W. N. *J. Chem. Phys.* **1962,** *36,* 2179. (b) Hoffmann, R. *J. Chem. Phys.* **1963,** *39,* 1397.

17. (a) Albright, T. A.; Burdett, J. K.; Whangbo, M. -H. (Eds.), *Orbital Interactions in Chemistry,* Wiley-Interscience, New York, **1985.** (b) Glassey, W. V.; Hoffmann, R. *J. Chem. Phys.* **2000,** *113,* 1698.

18. (a) Reed, A. E.; Weistock, R. B.; Weinhold, F. *J. Chem. Phys.* **1985,** *83,* 735. (b) Reed, A. E.; Curtiss, L. A.; Weinhold, F. *Chem. Rev.* **1988,** *88,* 899. (c) Weiberg, K. B. *Tetrahedron* **1968,** *24,* 1083.

19. Jemmis, E. D.; Balakrishnarajan, M. M. *J. Am. Chem. Soc,* **2001,** *123,* 4324.

20. Srinavas, G. N.; Hamilton, T. P.; Jemmis, E. D.; McKee, M. L.; Lammertsma, K. *J. Am. Chem. Soc,* **2000,** 722,1725.

21. (a) Jemmis, E. D.; Schleyer, P. v. R. *J. Am. Chem. Soc.* **1982,** *104,* 4781. (b) Jemmis, E. D. *J. Am. Chem. Soc.* **1982,** *104,* 7017. <c) Jemmis, E. D.; Pavankumar, P. N. V. *Proc. Ind. Acad. Sci. (Chem. Sci.)* **1984,** *93,* **479.**

22. Jemmis, E. D.; Pancharatna, P. D. *Applied Organomet. Chem.,* **2003,** *17,* 480.

23. (a) Siriwardane, U.; Islam, M. S.; West, T. A.; Hosmane, N. S.; Maguire, J. A.; Cowley, A. H. *J. Am. Chem. Soc.* **1987,** *109,* 4600. (b) Hosmane, N. S.; Meester, P. de; Siriwardane, U.; Islam, M. S.; Chu, S. S. C. *J. Chem. Soc, Chem. Commun.* **1986,** 1421. (c) Hosmane, N. S.; Lu, K. J.; Zhang, H.; Maguire, J. A. *Organometallics,* **1997,** *16,* 5163. (d) Hosmane, N. S.; Meester, P. de; Siriwardane, U.; Islam, M. S.; Chu, S. S. C. *J. Am. Chem. Soc.* **1986,** *108,* 6050. (e) Islam, M. S.; Siriwardane, U.; Hosmane, N. S.; Maguire, J. A.; Meester, P. de; Chu, S. S. C. *Organometallics,* **1987,** *6,* 1936. (f) Hosmane, N. S.; Zhu, D.; McDonald, J. E.; Zhang, H.; Maguire, J. A.; Gray, T. G.; Helfert, S. C. *J. Am. Chem. Soc.* **1995,** *117,* 12362. (g) Hosmane, N. S.; Yang, J.; Zhang, H.; Maguire, J. A. *J. Am. Chem. Soc.* **1996,** *118,* 5150.

24. B3LYP is Becke's three parameter hybrid method with LYP correlation functional: (a) Becke, A. D. *J. Chem Phys.* **1993,** *98,* 5648. (b) Lee, C; Yang, W.; Parr, R. G. *Phys. Rev.* **1988,** *B 37,* 785. (c) Vosko, S. H.; Wilk, L.; Nusair, M. *Can. J. Phys.* **1980,** 55, 1200. (d) Stephens, P. J.; Delvin, F. J.; Chabalowski, C. F.; Frisch, M. J. *J. Phys. Chem.* **1994,** *98,* 11623.

25. (a) Hay, P. J.; Wadt, W.R. *J. Chem. Phys.* **1985,** *82,* 270. (b) Wadt, W.R.; Hay, P. J. *J. Chem. Phys.* **1985,** *82,* 284. (c) Hay, P. J.; Wadt, W. R. *J. Chem. Phys.* **1985,** 82, 299.

26. (a) Baerends, E. J.; Ellis, D. E.; Ros, P. *Chem. Phys.* **1973,** *2,* 42. (b) Boerrigter, P. M.; Velde, G.; Baerends, E. J. *Int. J. Quantum Chem.* **1988,** *33,* 87. (c) Becke, A. D. *Phys. Rev.* **1988,** *A 38,* 2398. (d) Perdue, J. P. *Phys. Rev.* **1986,** *B 33,* 8822. (e) teVelde, G.; Bickelhaupt, F. M.; van Gisbergen, S. J. A.; Guerra, C. F.; Baerends, E. J.; Snijders, J. G.; Ziegler, T. Chemistry with ADF , *J. Comput. Chem.* **2001,** *22,* 931. (f) Guerra, C. F.; Snijders, J. G.; teVelde, G.; Baerends, E. J. *Theor. Chem. Acc.* **1998,** *99,* 391. (g) ADF2002.03, SCM, Theoretical Chemistry, Vrije Universiteit, Amsterdam, The Netherlands, http://www.scm.com.

27. (a) Balakrishnarajan, M. M; Jemmis, E. D. *J. Am. Chem. Soc.* **2000,** *122,* 4516. (b) Jemmis, E. D.; Balakrishnarajan, M. M.; Pancharatna, P. D. *J. Am. Chem. Soc.* **2001,** *123,* 4313.

28. (a) Burdett, J. K.; Canadell, E. *Organometallics,* **1985,** *4,* 805. (b) Cloke, F. G. N.; Green, J. C; Jardine, C. N.; Kuchta, M.C. *Organometallics* **1999,** *18,* 1087.

CHAPTER 4

BONDING IN TUBULAR BORANES

4.0. INTRODUCTION

Wade's rules for monopolyhedral boranes have enjoyed huge success in rationalizing the diverse structural patterns exhibited by polyhedral boranes, and in predicting new structures.[1] Earlier MO calculations on polyhedral boranes involved in the development of extended Hückel theory[2] were followed by HF-SCF calculations[3]. Since then many experimental and hypothetical $B_nH_n^{2-}$ systems (n=4-17) were characterized at several levels of theory[4], and the stable isomers and their geometries were reported. But the underlying reasons for the geometries and stabilities have been afforded only a cursory view using topology-based arguments. Understanding the multicentered bonding in these systems remains a challenge.

Here an analysis of the ring stacking in the most common *closo* borane dianions and the hypothetically predicted to be stable capped borane nanotubes is done in a perturbation theoretic way. A 'staggered' building up of rings to form nanotubes is explored for four and five-membered B_nH_n rings. Arguments are given for the stacking of B5H5 rings being energetically more favorable than B4H4 rings. Elongated B-B distances of the central rings are predicted for some higher members and the necessity to optimize ring-cap bonding is found to be responsible for this elongation. This effect reaches a maximum in $B_{17}H_{17}^{2-}$; the insertion of additional rings will reduce this elongation. The nature of orbital interactions shows that all these *closo*-boranes obey Wade's n+1 rule, but the traditional explanation based on a partitioning into radial/tangential molecular orbitals is found wanting. Our studies indicate a generalized picture starting from molecules to extended nanotubes.

4.1. *CLOSO*-MONOPOLYHEDRAL BORANES

As a part of our approach to a general theory of boron hydrides[5], a systematic perturbation theory based MO investigation of the effect of stacking four and five-membered boron rings is presented. The nature of all the BMOs which are mainly responsible for polyhedral bonding, are investigated. These MOs are conveniently derived by using the starting point of the radial sp hybrid and the two tangential p orbitals. For simplicity, other MOs that are primarily B-H bonding and those lying in the antibonding region are excluded. This choice avoids the complications of mixing of the *exo* bonding and antibonding MOs (really present but less important) that have the same symmetries as the n radial sp hybrids. The energies of the MOs for the molecules as well as those of fragments are derived from extended Hückel calculations[2,6] with the experimental distances found in the respective *closo* boranes; *ab-initio* calculations also give the same ordering of levels for all the selected systems.

Beginning with the well-studied[7] $B_6H_6^{2-}$ and $B_7H_7^{2-}$ to illustrate ring-cap interactions, we proceed to stacked systems by exploring the experimentally characterized $B_{10}H_{10}{}^{2-}$, $B_{12}H_{12}^{2-}$ and the as yet hypothetical $B_{17}H_{17}{}^{2-}$, $B_{22}H_{22}{}^{2-}$ and $B_{27}H_{27}{}^{2-}$. The equilibrium B-B bond lengths for these species (illustrated in Figure 1) were obtained from optimizations of the dianions at the B3LYP/6-31G* level of theory[8,9], which reproduces the experimental geometry of known boranes well.[3]
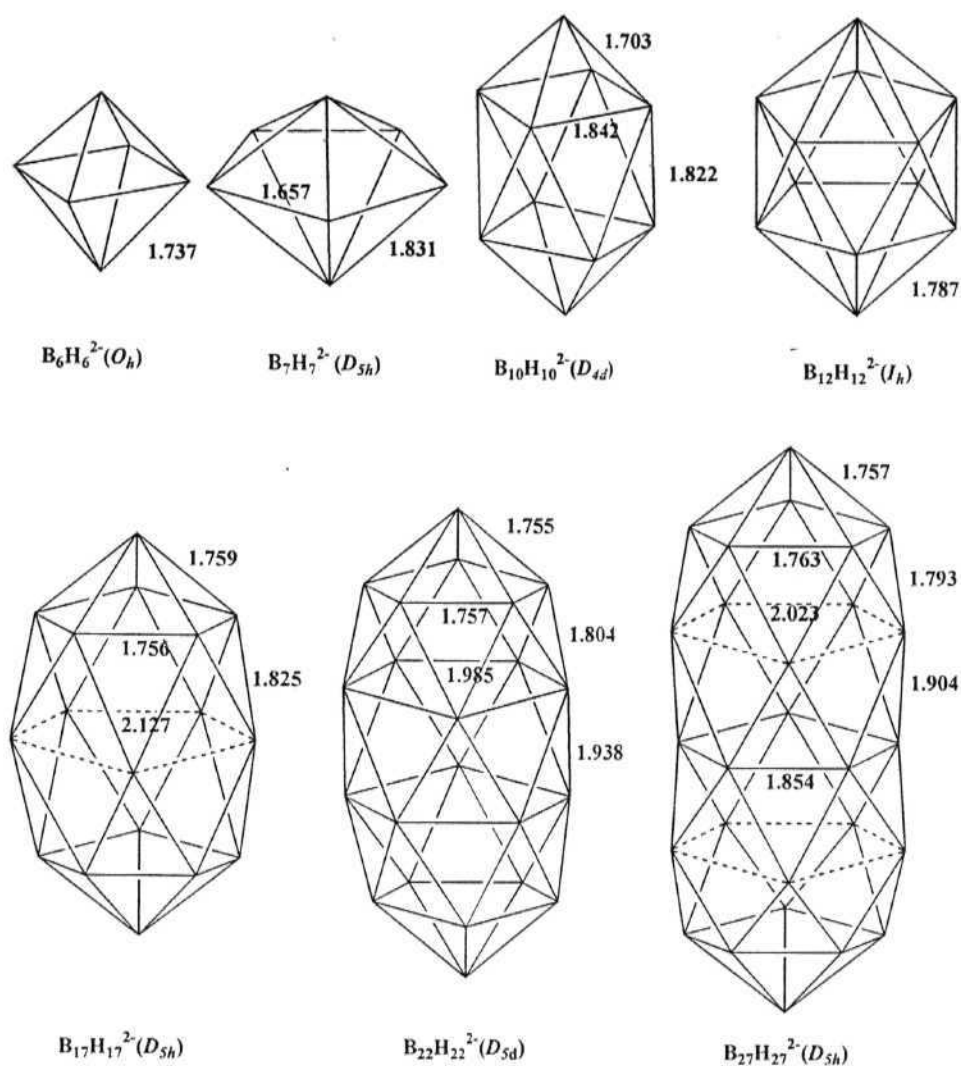
109

Figure 1

Monocage *closo* boranes with bond lengths (in A) as calculated at B3LYP/6-3IG* level of theory. The hydrogens are omitted for clarity.

The aim of the study is a detailed understanding of the general nature of bonding in these polyhedra, the derivation of a general electron counting rule for the larger systems, and an explanation of the geometrical details for these systems. The focus is on how the symmetry dictates the nature of orbital interactions and consequently the geometry and bonding in these systems, with special emphasis on the effect of 'staggered stacking' of borocyclic rings.[10]

110

4.1.1. Intermolecular Interaction of Ring and the Cap Fragments

The formation of the orbitals of $B_6H_6^{2-}$ and $B7H7^{2-}$ from fragments is a good introduction to our analytical process. The molecular orbitals of $B_6H_6^{2-}$ can be constructed from the orbitals of a cyclobutadienoid square $B_4H_4^{6-}$ ring[10] (D_{4h}) and those of two $B-H^{2+}$ caps, as shown in Figure 2.
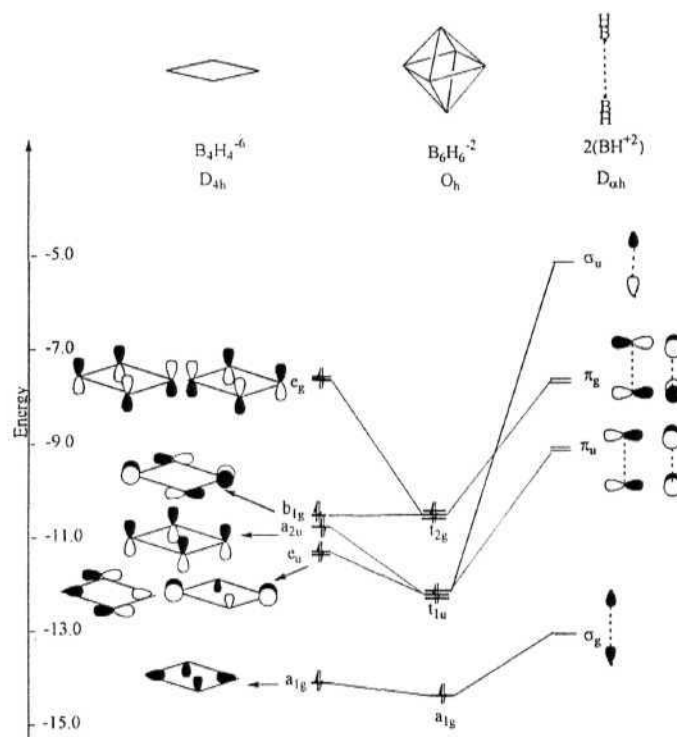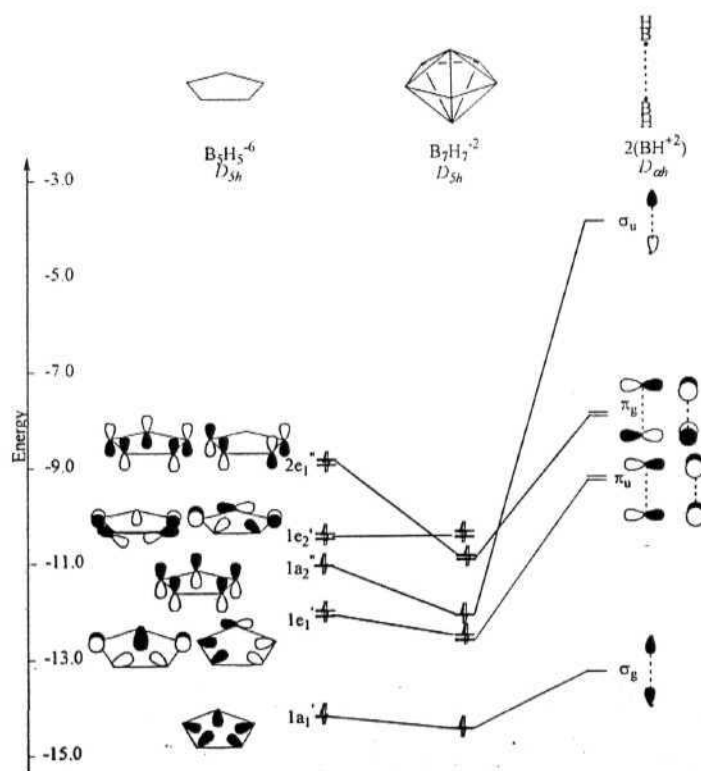

Figure 2

The interaction diagram between an *arachno*-$B_4H_4^{6-}$ fragment with two BH^{2+} caps, resulting in the BMOs of *closo*-$B_6H_6^{-2}$.

The charge assignment in the fragments is, of course, arbitrary. To simplify the diagram, the antibonding MOs of the $B_4H_4^{6-}$ fragment has been tentatively ignored. The interaction between the fragments shown in Figure 2 leads to one strongly bonding radial MO of a_{1g} symmetry and two sets of triply degenerate orbitals (the O_h symmetry forces these degeneracies). The low-lying t_{1u} set has the out-of-phase combination of the cap sp

hybrids interacting with the p orbitals directed towards them. It is interesting to note that radial-tangential mixing enters even in this simple molecuk. The next higher t_{2g} set is made up purely of unhybridized tangential p orbitals of boron, free from any mixing of sp hybrids. It forms the HOMO (Highest Occupied MO). In accord with Wade's simplified explanation, there is one strongly bonding *radial* orbital (a_{1g}) and 6 BMOs (t_{1u} and t_{2g}) that are mainly *tangential* in character.

The orbitals of $B_7H_7^{2-}$ can be constructed in an exactly analogous way by the interaction of two $B-H^{2+}$ caps with the five-membered $B_5H_5^{6-}$ ring, as in Figure 3. As predicted by Wade's rule, this interaction produces seven tangential BMOs (bonding MOs) and one totally symmetric a_1 radial orbital.

Figure **3**

The interaction diagram between an *arachno*-$B_5H_5^{6-}$ fragment with two BH^{2+} caps resulting in the BMOs of *closo*-$B_7H_7^{-2}$.

The $1e_1'$ MO of the ring interacts with the two bonding combination of cap orbitals, whereas the all-bonding perpendicular p_z (π) set of the ring ($1a_2''$) interacts with the out-of-phase combination of the two cap sp-hybrids that are of the same symmetry. However, the degenerate set of high-lying a orbitals of the ring ($1e_2'$ in symmetry) find no matching orbitals from the B-H group and form the HOMO. The $2e_1''$ π set is similar to the HOMO of cyclopentadiene ($C_5H_5^-$) ring. This MO has a nodal plane; it interacts strongly with the out-of-phase combination of the cap p orbitals and hence is pushed below $1e_2'$.

In order to assess the effectiveness of the interaction of the B-H group with four and five-membered rings[12], the group Mulliken overlap populations (group-OP) of all the molecular orbitals of one B-H group with the bonding molecular orbitals of the $B_4H_4^{6-}$ and B5H5^{6-} ring are calculated. keeping the B-B bond lengths fixed at an ideal distance of 1.75Å. The group-OP of the B-H cap with the four and five-membered rings are found to be 1.85 and 1.76, respectively. The group-OP increases from 1.76 to 1.80 when the hydrogens of the ring in *nido*-$B_6H_6^{4-}$($B_5H_5^{6-}$ + BH^{2+}) are bent toward the cap by 15.6 °. This is the optimum angle obtained by following the extended Hückel total energies as a function of the angle of bending. At the MNDO level this value is found to be increased to 17.4°.[12] An energy minimum is also obtained for $B_5H_5^{4-}$ (B4H4^{6-} + BH^{2+}) at a bending angle of 6.4°; here the group-OP is maintained as 1.85. This indicates that irrespective of hydrogen bending, the $B_4H_4^{6-}$ ring is more effective at bonding with the capping B-H group.[7c]

The introduction of one more cap perturbs the hydrogen atoms as they are driven by symmetry to come into the plane of the central ring. Presumably, the overlap

between the ring orbitals and those of the caps **is** greater in $B_6H_6^{2-}$ than in $B_7H_7^{2-}$. The resultant group-OPs are 4.05 and 3.61, respectively.

But, is the overlap between the various FMOs (fragment MOs) of the pentagonal ring and the caps optimal? This point was probed by changing one important remaining geometrical parameter, the ring B-B distances. A reduction in the ring B-B distances of the five-membered ring to the B3LYP/6-31G* optimized distance of 1.657Å increases the stabilization due to bicapping to 5.25eV. Even with this pronounced difference in 'capping' and 'equatorial' (ring) distances, the stabilization due to capping B-H groups is less than for $B_6H_6^{2-}$ by 2.62eV. The B-H caps stabilize the $B4H4^{6-}$ ring orbitals by 7.87eV, whereas the stabilization is only 5.25eV for $B5H5^{6-}$. Though it is not easy to compare the stability of two molecules of different stoichiometry, and the distribution of known structures is not a certain guide to stability, the results point to a special stability for $B_6H_6^{2-}$. This is consistent with the earlier observations and the abundance of octahedral B_6 units in boron-rich solids.

Replacement of one of the BH caps in $B_6H_6^{2-}$ and $B_7H_7^{2-}$ by a *nido*-B_5H_5 and *nido*-B_6H_6, respectively, in a staggered fashion, leads to $B_{10}H_{10}^{2-}$ and $B_{12}H_{12}^{2-}$. As the ring B-H bonds of these fragments are no longer required to be in the plane of the ring by symmetry, they tilt toward the caps. In the next two sections, the nature of these interactions is analyzed systematically using the standard tools of perturbation theory. The intermolecular perturbation of two staggered *nido* fragments is first looked at by keeping the B-H bonds in the plane of the ring, and then proceed to study the effect of geometrical perturbation due to the bending of ring B-H bonds.

4.1.2. Intermolecular Interaction of two Staggered *Nido* Fragments

The molecular orbitals of $B_{10}H_{10}^{2-}$ can be conveniently analyzed by the interaction of its two $B5H5^{4"}$ (C_{4v}) fragments arranged in a staggered fashion. The resulting interaction diagram is illustrated in Figure 4. Here, the ordering of energy levels (while schematic in nature) is derived from extended Hückel calculations using the bond-lengths taken from the optimized geometry of $B_{10}H_{10}^{2-}$ at B3LYP/6-31G* level of theory, but keeping the B-H bonds in the plane of the B4H4 ring. There is a complication in the group theory here, which is a consequence of the general convention employed in C_{4v} to choose σ_d planes as passing through the atoms of the four-membered ring and σ_v to pass between them. In the D_{4d} symmetry of $B_{10}H_{10}^{2-}$, such a choice is impossible to maintain simultaneously for both fragments. This problem affects only the assignment of symmetry labels to b_1 and b_2 orbitals.

The totally symmetric radial MOs ($1a_1$) of the two fragments interact, in a typically destabilizing two-orbital-four-electron interaction. However, the higher lying FMOs ($2a_1$) - the all-bonding combination of perpendicular p_z orbitals of the ring and sp hybrids of the caps - generate orbitals of the same symmetry in the composite molecule. This leads to second-order interactions by which both the out-of-phase combination ($1b_2$) and in-phase combination ($1a_1$) are stabilized. The out-of-phase combination $1b_2$ remains deep inside the bonding region. Hence, contrary to the single radial orbital observed in $B_6H_6^{2-}$ and $B5H5^{2-}$, in $B_{10}H_{10}^{2-}$ two radial MOs are occupied. A similar effect is observed with the interaction of the next degenerate $1e$ set, as both in-phase and out-of-phase combinations remain within the bonding region of $B_{10}H_{10}^{2-}$, due to stabilizing second-order mixing of the $2e$ orbitals. The perpendicular p_z orbitals of $2a_1$, as mentioned above,

interact particularly strongly with each other. As a result, their out-of-phase(b_2) combination is pushed up high into the antibonding region of $B_{10}H_{10}^{2-}$.
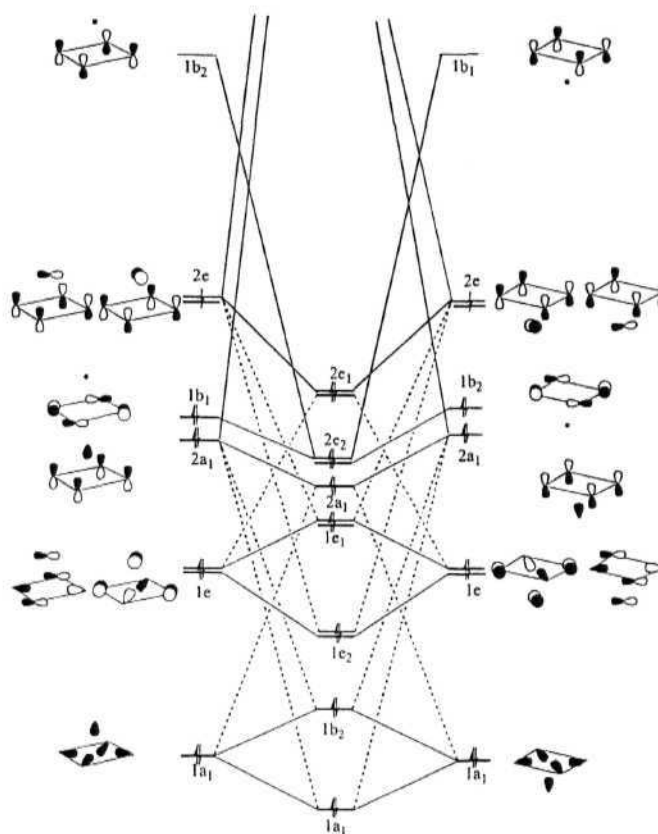

Figure 4

The interaction diagram between two *nido*-$B_5H_5^-$ fragments resulting in the bonding MOs of *closo*-$B_{10}H_{10}^{-2}$. Here dashed lines indicate second order interactions.

The next fragment orbital of the first fragment, $1b_1$ — the all bonding combination of the in-plane p orbitals of the ring - actually is of different symmetry in the two interacting fragments (recall the complication mentioned due to the C_{4v} convention). The same is true in the antibonding region MO, for the totally antibonding combination of the perpendicular p_z orbitals of the ring (illustrated at the very top of Figure 4), i.e., in the first fragment this MO is $1b_2$, while in the second it is $1b_1$. There is a good overlap

116

between these $(2b_1, 2b_2)$ and $(1b_1, 1b_2)$ sets, leading to the occupied degenerate $1e_2$ in the D_{4d} symmetry of $B_{10}H_{10}^{2-}$.

The next degenerate set of MOs (2e) gives one bonding $(2e_1)$ and one antibonding pair of orbitals. The overlap between the 2e FMOs is very large, so that the out-of-phase combination is pushed above the bonding region of $B_{10}H_{10}^{2-}$. This interaction will prove essential in the sequel in the construction of an electron-counting rule for higher polyhedra. A destabilizing second-order mixing of $1e$ keeps the bonding combination pretty high, indeed as the HOMO of $B_{10}H_{10}^{2-}$. When all the interactions are accounted for, 11 MOs lie in the bonding region. The overall number is in adherence with Wade's rule, but note that two (not one) of these bonding MOs ($1a_1$ and $1b_2$) are to be characterized as "radial".

The bonding in $B_{12}H_{12}^{2-}$ is approached in a similar fashion, by analyzing the interaction between its two constituent pentagonal pyramids, the *nido*-$B_6H_6^{4-}$ fragments (Figure 5). At this stage, the B-H bonds lie in the B_5 plane of their respective pyramid, so that the resultant $B_{12}H_{12}^{2-}$ symmetry is not yet I_h, but only D_{5d}.

As was the case for $B_{10}H_{10}^{2-}$, interaction between the totally symmetric $1a_1$ radial FMOs lead to two orbitals, both stabilized by the FMO $2a_1$ combinations through second-order interactions. The interaction between the next degenerate $1e_1$ sets leads to two in-phase and out-of-phase combinations, both stabilized by second-order mixing with the $2e_1$ FMOs. The interaction between the $2a_1$ FMOs forms one bonding and one antibonding MO. Both are destabilized by mixing with the low-lying $1a_1$; as a result, the out-of-phase combination is pushed into the antibonding region of $B_{12}H_{12}^{2-}$.
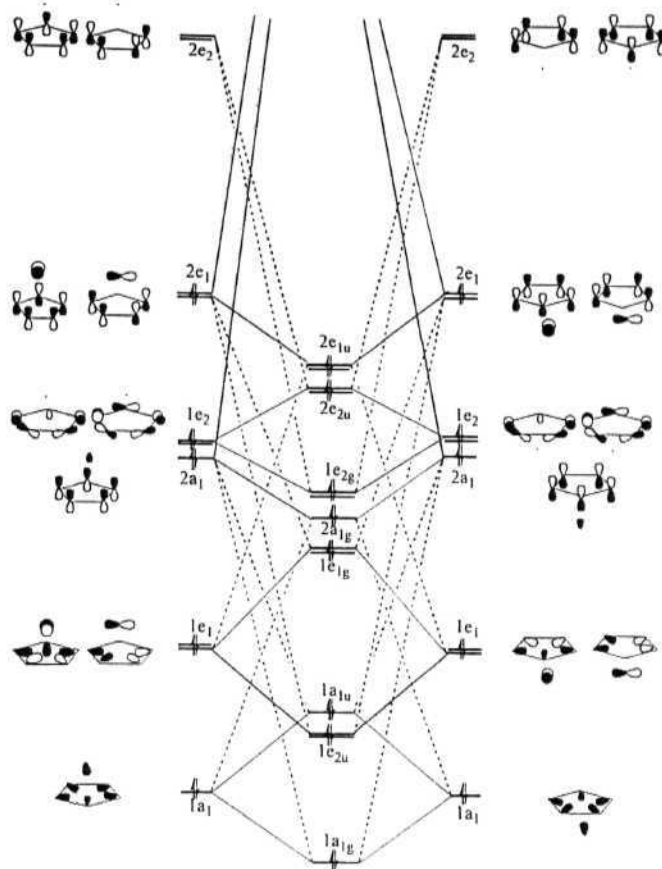
Figure 5

The interaction diagram between two *nido*-$B_6H_6^{1-}$ fragments resulting in the bonding MOs of *closo*-$B_{12}H_{12}^{2-}$. Here dashed lines indicate second order interactions.

So far, the interactions between the FMOs are very similar to what is observed in $B_{10}H_{10}^{2-}$. But unlike the case of $B_{10}H_{10}^{2-}$, the in-plane all bonding combinations of tangential p orbitals do interact with each other (as they are of the same symmetry, despite the rotation of the second fragment by 36°); they form two in-phase and out-of-phase combinations. Though the splitting is not pronounced, due to the lateral nature of the overlap, second-order mixing from the antibonding region MO $2e_2$ stabilizes both the in-phase and out-of-phase combinations. The next pair of $2e_1$ FMOs of the fragments interacts strongly, forming a pair of bonding and antibonding MOs. Mixing with low-

118

lying $1e_1$ destabilizes both of these MOs. Hence, as in the case of $B_{10}H_{10}^{2-}$, the in-phase combination forms the HOMO.

Though the interaction of orbitals of the four and five-membered rings used in the above analysis explains the ordering of energy levels, there is a difference in the orientation of ring B-H bonds in the *nido* fragments for $B_{10}H_{10}^{-}$ and $B_{12}H_{12}^{-'}$ compared to $B_6H_6^{2-}$ and $B_7H_7^{2-}$. The B-H bonds, perforce in the plane of the ring in the case of $B_6H_6^{2-}$ and B7H7$^{2"}$, will be bent towards the caps in the case of $B_{10}H_{10}^{2-}$ and $B_{12}H_{12}^{2-}$.[7d] In other words, the centroid of the molecule, which lies at the ring center for $B_6H_6^{2'}$ and B7H7^{2-}. moves to a position between the rings in $B_{10}H_{10}^{2-}$ and $B_{12}H_{12}^{2-}$ (Figure 6). The bonding and observed geometries of these systems can be more clearly explained if the influence of the geometric perturbation due to this B-H bending is taken into account, as done in the next section.
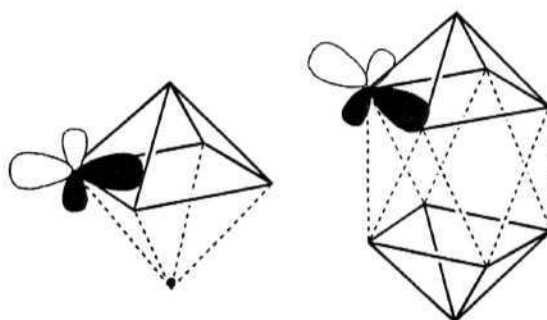
Figure 6

Radial and tangential orbitals in building up $B_6H_6^{2-}$ and $B_{10}H_{10}^{2-}$

4.1.3. Geometric Perturbation Due to the Bending of B-H bonds

If one simply were to bring together two $B_5H_5^{-}$ fragments to form $B_{10}H_{10}^{2-}$, the equatorial B-H bonds in one pyramid would find themselves too close to the B-H bonds of the other. The 6.5° tilt of the B-H bonds of the B_4H_4 unit in $B_5H_5^{-4}$ (C_{4v}) is not

sufFicient to avoid the resulting steric interactions between B-H bonds of the two rings. This results in the calculated bending of the B-H bonds towards the cap by 19.6°, as observed experimentally. Let us assume that the sp "out" hybrid at a given boron atoms follows the motion of the outer hydrogen. This effectively causes a reorientation of the sp hybrid that points toward the center of the ring (it now points towards the 'center' of the polyhedron) as illustrated in Figure 6. One of the tangential orbitals of the ring boron follows the motion, while the other is unaffected.

Table 1. FMO overlap (S) and FMO overlap population (OP) between two $B_5H_5^-$ fragments of $B_{10}H_{10}^{2-}$ (Figure 4), obtained from extended Hückel calculations using the B3LYP/6-31G* optimized geometry. Numbers inside parentheses correspond to the values when the ring B-H bonds are kept in the plane of the four-membered rings in $B_5H_5^-$ fragments. To avoid decimal points, all the values are multiplied by 100.

MO	$1a_1$		$1e$		$2a_1$		$1b_1$		$2e$	
	OP	S	OP	S	OP	S	OP	S	OP	S
$1a_1$	-9(-9)	19(16)	--	--	4(0)	14(14)	--	--	--	--
$1e$	--	--	2(0)	12(1)	--	--	--	--	6(1)	24(15)
$2a_1$	4(0)	14(14)	--	--	37(42)	25(28)	--	--	--	--
$1b_2$	--	--	--	--	--	--	--	--	--	--
$2e$	--	--	6(1)	24(15)	--	--	--	--	44(50)	33(36)
$1b_1$	--	--	--	--	--	--	45(36)	47(41)	--	--

A further inquiry is done as to what will happen to the skeletal orbitals when the B-H bonds, originally in plane with the ring, bend towards the capping group. The resulting correlation diagram (from an extended Hückel calculation for $B_{10}H_{10}^{\,\prime\prime}$) is depicted in Figure 7. It can be easily seen from Figure 7 that the skeletal orbitals perturbed most by B-H bending are $1e_2$, $1e_1$, $2a_1$ and $2e_2$. While $1e_2$, $2a_1$ and $2e_2$ are stabilized, $1e_1$ is destabilized. The net effect is stabilizing.
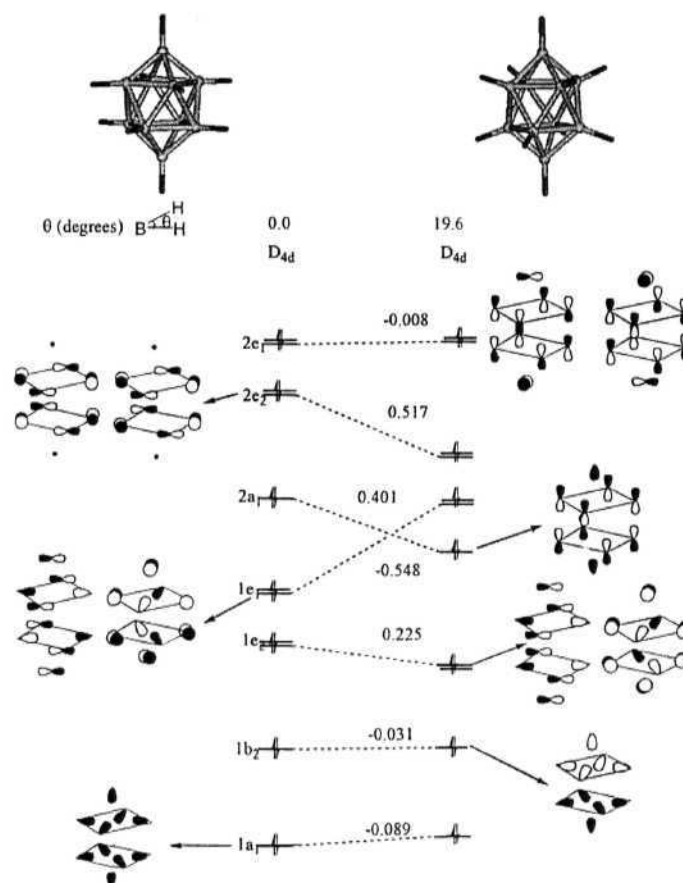
Figure 7

A correlation diagram for $B_{10}H_{10}^{2-}$, showing the variation of energy levels (eV) with respect to bending of hydrogens away from the plane of the rings. The vertical energy scale is schematic. The angle 8, specifying the H-positions, is defined in the text.

The shifting of energy levels can be rationalized from overlap arguments. The FMO overlap (S) and FMO overlap population (OP) values between the skeletal MOs of these fragments (Figure 4) are obtained from extended Hückel calculations by keeping the B-H bonds in the plane of the ring and are given in Table 1 (in parentheses) along with the corresponding values of the optimized geometry.

The $1e_1$ and $1e_2$ orbitals of $B_{10}H_{10}^{2-}$ formed from the $1e$ FMOs of the *nido*-B_5H_5 fragments (Figure 4), has sp hybrid orbitals of two diagonal boron atoms of the ring. If they follow B-H bending, these hybrids will be redirected towards the cage center and

will interact more effectively with the other fragment. Indeed, the overlap between these two FMOs increases from 0.01 to 0.12 (table 1) and hence the in-phase combination $1e_2$ is stabilized and the out-of-phase combination $1e_1$ is destabilized (as a function of bending). It can also be seen from the Figure 7 that the destabilization of $1e_1$ is more pronounced than the stabilization of $1e_2$, as expected from inclusion of overlap in the calculations.

In the case of $2a_1$, which is the bonding combination of FMOs $2a_1$ (Figure 4), the overlap is reduced from 0.28 to 0.25, due to 'out-of-plane' B-H bending. The overlap population between these two FMOs follows and is also reduced, from 0.42 to 0.37 (table 1). This can be attributed to the "splaying out" of ring tangential p_z orbitals of the fragments as the B-Hs move. Surprisingly, Figure 7 shows that this MO is stabilized by B-H bending. Perhaps this is due to the increased overlap between the ring p_z orbitals of the fragments with their respective caps.

MO $2e_2$ is formed from the interaction between the all-bonding combination of the in-plane p orbitals of one fragment and the antibonding region MO that is the out-of-phase combination of the perpendicular p_z orbitals (Figure 4). The overlap between these fragment orbitals increases from 0.41 to 0.47 as a consequence of B-H bending (table 1). Presumably, this change occurs because of the "splaying out" of perpendicular p_z orbitals, increasing their overlap with the in-plane p orbitals which have maximum electron density outside the periphery of the ring. The net overlap population is also substantially increased from 0.36 to 0.45 ($1b_1$ and $1b_2$ in Figure 4). Thus there is a pronounced stabilization of $2e_2$ MOs due to B-H bending. When all the skeletal MOs of $B_{10}H_{10}^{2-}$ are considered, the net effect of B-H bending is found to be stabilizing.

With respect to the *nido* $B_6H_6^{-4}$ (C_{5v}) where the B-H bonds of the B5H5 ring bend towards the cap by 15.6°, the B-H bonds in $B_{12}H_{12}^{2-}$ are bent by an additional 10.9° so that the angle $\theta = 26.5°$ dictated by Ih symmetry is obtained. The similarity of the angles dictated by overlap and the one demanded by symmetry contributes to the high stability of $B_{12}H_{12}^{2-}$. Several MOs become degenerate as a consequence of the increased symmetry, as illustrated in Figure 8. It is evident from the comparison of Figures 7 and 8 that the B-H bending has more pronounced energy consequences in $B_{12}H_{12}^{2-}$. The FMO overlap (S) and FMO overlap population (OP) values between the skeletal MOs of $B_6H_6^{-}$ fragments (Figure 5) are uses to analyze the energy changes. These are obtained from extended Hückel calculations by keeping the B-H bonds in the plane of the ring, and are given in Table 2 (within parentheses), along with the corresponding values for the optimized geometry.

Table–2. MO overlap (S) and FMO overlap population (OP) between two $B_6H_6^{-}$ fragments of $B_{12}H_{12}^{2-}$ (Figure 5), obtained from extended Hückel calculations using the B3LYP/6-31G* optimized geometry. Numbers inside the parenthesis correspond to the values when the ring B-H bonds are kept in the plane of the five-membered ring in $B_6H_6^{-}$ fragments. To avoid decimal points, all the values are multiplied by 100.

1a₁		1e₁		2a₁		1e₂		2e₁	
OP	S	OP	S	OP	S	OP	S	OP	S
-12(-14)	22(20)	--	--	6(1)	13(14)	--	--	--	--
--	--	-2(-2)	22(10)	--	--	--	--	10(1)	21(16)
6(1)	13(14)	--	--	35(40)	25(26)	--	--	--	--
--	--	--	--	--	--	-1(0)	13(1)	--	--
--	--	10(1)	21(16)	--	--	--	--	37(50)	29(35)
--	--	--	--	--	--	42(32)	45(38)	--	--

The $1e_{2u}$ and $1a_{1u}$ orbitals of $B_{12}H_{12}^{2-}$ ($\mathbf{D_{5d}}$) are similar to $1b_2$ and $1e_2$ orbitals of $B_{10}H_{10}^{2-}$, but the icosahedral symmetry forces $\mathbf{t_{1u}}$ degeneracy for these three orbitals. Similarly $1e_{1g}$ (analogous to $1e_1$ of $B_{10}H_{10}^{2-}$) is destabilized, as the overlap between the $1e_1$ orbitals of the fragment (Figure 5) increases from 0.10 to 0.22 (Table 2). The $2a_{1g}$ MO of $B_{12}H_{12}^{2-}$, as in the case of $2a_1$ of $B_{10}H_{10}^{2-}$, is stabilized, though the energy changes are more pronounced in $B_{12}H_{12}^{2-}$ than $B_{10}H_{10}^{2-}$. But in the place of all $2e_2$ orbitals of $B_{10}H_{10}^{2-}$, $B_{12}H_{12}^{2-}$ has in-phase ($1e_{2g}$) and out-of-phase ($2e_{2u}$) combinations of in-plane ring p orbitals of the component $B_6H_6^-$ fragment ($1e_2$, Figure 5), both lying within the bonding region. Though the in-plane p orbitals are not perturbed due to the bending of B-H bonds, both of these degenerate MO pairs $1e_{2g}$ and $2e_{2u}$ are stabilized by B-H bending. This is due to the increased second-order mixing from the antibonding region MO $2e_2$, as in the case of $B_{10}H_{10}^{2-}$.

The overlap between $1e_2$ and $2e_2$ of the fragments is increased from 0.38 to 0.45. and consequently the overlap population is also increased from 0.32 to 0.42 (table 2). Unlike the case of $B_{10}H_{10}^{2-}$, the HOMO of $B_{12}H_{12}^{2-}$ ($2e_{1u}$), is also stabilized by B-H bending, as the overlap between the fragments increases from 0.38 to 0.45. The interesting h_g and g_u degeneracies of all these MOs are forced by the icosahedral symmetry of the molecule.

This analysis also helps to understand why the stacking or the rings always occurs in a staggered fashion, forming the deltahedral framework. An eclipsed orientation would not allow effective mixing of perpendicular p_z orbitals with the in-plane ring orbitals; such mixing is essential to the stability of these systems.
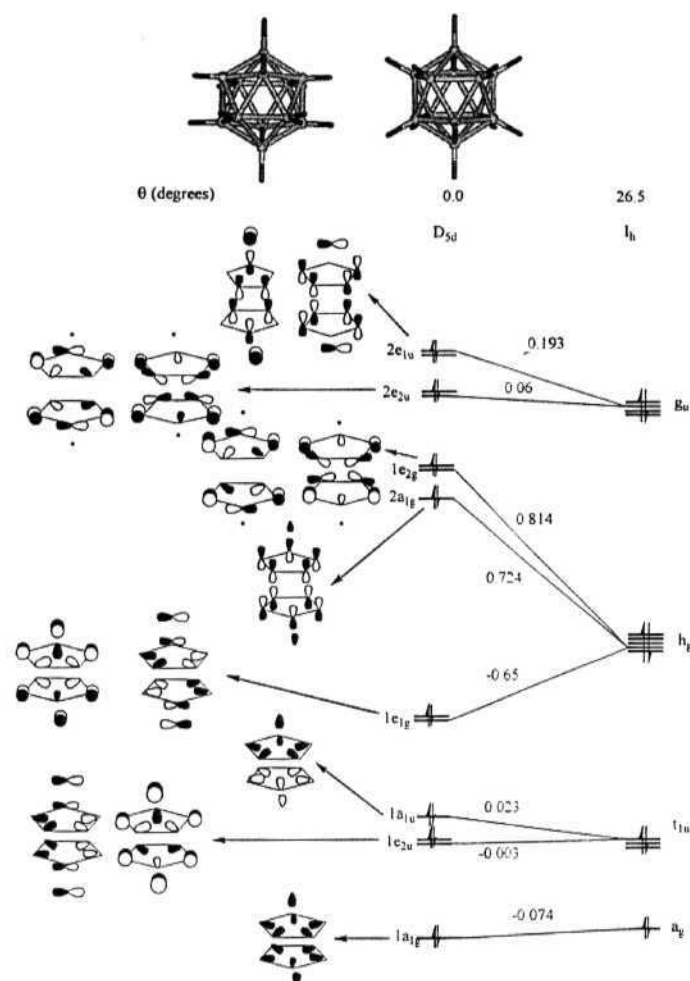
Figure 8

A correlation diagram for $B_{12}H_{12}^{2-}$, showing the variation of energy levels (eV) with respect to bending of' hydrogens away from the plane of the ring. The vertical energy scale is schematic. The angle 8, specifying the H-positions, is defined in the text.

There are some subtle differences in the nature of orbital interactions between four and five-membered ring stacking. The major difference originates from the $2e_2$ of $B_{10}H_{10}^{2-}$. This orbital arises from the interaction of all-bonding in-plane p orbitals of the nido-$B_5H_5^{4-}$ fragment of different symmetry ($1b_1$ and $1b_2$) in the fragment. Stabilization of the $2e_2$ components derives from second-order mixing of an antibonding MO. But in $B_{12}H_{12}^{2-}$, the equivalent orbitals of nido-$B_6H_6^{4-}$ ($1e_2$) do interact, giving a pair of in-phase

125

and out-of-phase combinations, both of which are stabilized by second-order mixing from antibonding $2e_2$ orbitals of the fragment.

Taken as a whole, the interaction between two $B_6H_6^-$ fragments is more pronounced than that of B5H5". In both the cases, the three MOs (a + e) arising from the set of perpendicular p_z orbitals of the ring are primarily responsible for ring-ring bonding. This is reflected in higher OP values for the entries corresponding to these MOs in table 1 and 2. The highest OP values are found for the e set of one fragment interacting with the in-plane MOs of the other. The out-of-phase combinations of the a + e MOs are pushed to the antibonding region. These interactions are more pronounced in $B_{12}H_{12}^{2-}$ than in $B_{10}H_{10}^{2-}$.

All other BMOs arise out of nonbonding or destabilizing four-electron two-orbital interactions, though many of them are stabilized by the second-order mixing from the higher lying MOs of appropriate symmetry. This is well reflected in the group-OP values. Even when the ring hydrogens are kept in the plane of the ring, the group-OP between the *nido* fragments in $B_{12}H_{12}^{2-}$ is 1.60, whereas in B10H10^{2}" it is only 1.50. The bending of the ring B-H bonds towards their cap causes further increase in the group-OP values, and is more pronounced in $B_{12}H_{12}^{2-}$ (2.56) than $B_{10}H_{10}^{2-}$ (2.08). This shows up in the greater distance between the rings in $B_{10}H_{10}^{2-}$ in comparison with $B_{12}H_{12}^{2-}$ (Figure 1). Interaction between the *nido* fragments (taken now as $B_6H_6^-$ and $B_5H_5^-$) results in a net stabilization of 3.55eV in $B_{12}H_{12}^{2-}$, whereas it is only 3.40eV in $B_{10}H_{10}^{2-}$. It can be concluded that staggered stacking of five-membered rings is more favorable than that of the four-membered rings. The dominant contribution to inter-fragment bonding from the

MOs composed of p_z orbitals at the ring atoms will lead to an easy way of deducing favored electron counts for higher boranes.

4.2. BORANE BASED NANOTUBES

Stacking of staggered rings can be extended, in principle leading to borane nanotubes[10, 13]. Conceptually, insertion of one more five-membered B5H5 ring into the icosahedral $B_{12}H_{12}^{-}$ (Figure 9) leads to $B_{17}H_{17}^{-}$ with D_{5h} symmetry, which is a minimum on its potential energy surface at the B3LYP/6-31G* level of theory.[3, 4] The next members in the series will be $B_{22}H_{22}^{2-}$, $B_{27}H_{27}^{2-}$, etc. The number and nature of bonding molecular orbitals for these mini-nanotubes can be easily deduced.

A borane nanotube can be generated by extending the stacking in the above fashion. *Ab initio* calculations at different levels have characterized such smaller molecules of few nanometer tubular size.[14] These have deltahedral arrangement at the sides[10b] contradictory to carbon nanotubes. Carbon nanotubes are usually capped at their ends with hemispherical carbon fullerenes and a side view will have hexagonal rings fused through an edge. Nanotube structures are of great interest in the present era due to its mechanical and one-dimensional electrical properties ranging from semiconductors to metallic.[15-18]

4.2.1. Extended stacking of B₅H₅ rings

Since the MOs arising from the perpendicular p_z orbitals of the ring interact particularly strongly as seen from the previous section, this set of three MOs can be considered exclusively with their effects of stacking on them, for the sake of building up electron counting principles.

In an Aufbau, any member of the series can be generated from its predecessor by the insertion of an *arachno*-B_5H_5 (charge unspecified as yet) planar five-membered ring. For illustration, let us analyze *closo*-$B_{17}H_{17}^{2-}$. This molecule can be conceptually formed by breaking $B_{12}H_{12}^{2-}$ into two *nido*-B_6H_6 (C_{5v}) fragments and inserting a B5H5 (D_{5h}) ring between them (charge not yet specified) in such a way that all the adjacent five-membered rings are in a staggered orientation. This is shown schematically in Figure 9. Before the insertion of the planar B5H5 ring, one of the *nido*-B_6H_6 fragments has to be rotated through the C_5 axis by 36° with respect to the other.
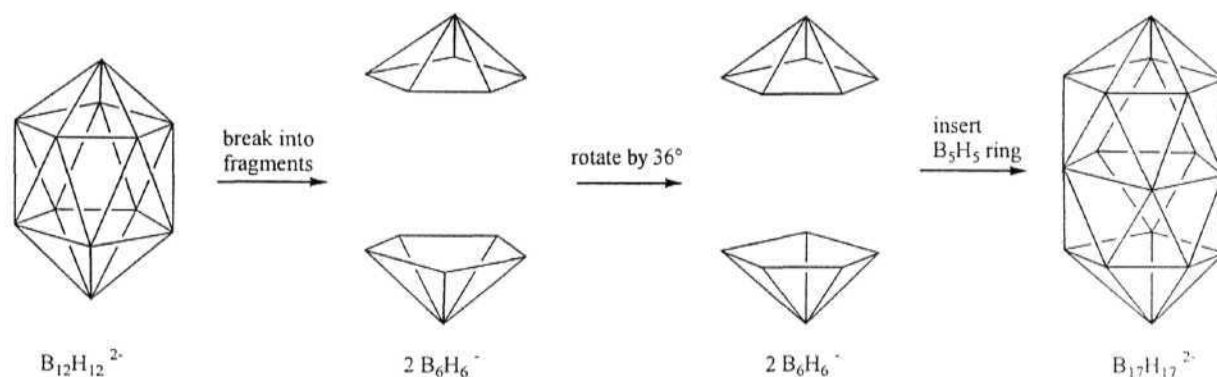
Figure 9

Conceptual construction of $B_{17}H_{17}^{2-}$ from $B_{12}H_{12}^{2-}$ by the insertion of a B_5H_5 ring.

Each of the 'broken' *nido*-B_6H_6 (C_{5v}) fragments requires (n+2) electron pairs by Wade's rule and hence would carry a -4 charge by itself.[1] The frontier BMOs of *nido*-$B_6H_6^{4-}$ are similar to the *n* orbitals of a cyclopentadienyl. The MOs we are interested in are those arising from the perpendicular p_z orbitals of the open face. They correspond to the $2a_1$ and $2e_1$ MOs discussed earlier in Figure 5, and will be referred hereafter as a and e. The B_5H_5 (D_{5h}) fragment, also like cyclopentadienyl anion, has three BMOs of a and e symmetry and will have a −6 charge if those levels are filled (B5H5^{6-} is like $C_5H_5^-$).

128

When the $B_5H_5^{6-}$ ring is inserted between the two $nido$-$B_6H_6^{4-}$ (C_{5v}) fragments, the MOs from different fragments will interact. There arise typical three-orbital interactions, each of the a and e sets generating a bonding, a nonbonding and an antibonding combination, as illustrated in Figure 10. All the levels (nine of them) are filled for the starting point of ($2B_6H_6^{4-}$ + B5H5^{6-}"). But to maximize the bonding, by analogy to smaller $closo$-borane dianions, one should only fill the bonding combinations, i.e., a total of three levels in Figure 10. This results in a -2 charge, or $B_{17}H_{17}^{2-}$ ($2B_6H_6^{4-}$ + $B_5H_5^{6-}$ $\rightarrow$ $B_{17}H_{17}^{14-}$ $\rightarrow$ $B_{17}H_{17}^{2-}$+ 12e-). An extended Hückel calculation on $B_{17}H_{17}^{2-}$ with B-B distances kept 1.79A (B-B bond length in $B_{12}H_{12}^{2-}$) shows a large HOMO-LUMO gap (4.70eV), confirming the above conclusion. Hence Wade's n+1 formula still holds good. Similar interactions and arguments are found in the stacking of three-membered ring $(Pt_3(CO)_6)_n$ fragments, for which chains with n as large as 10 are experimentally characterized, all of them as dianions[1 2].
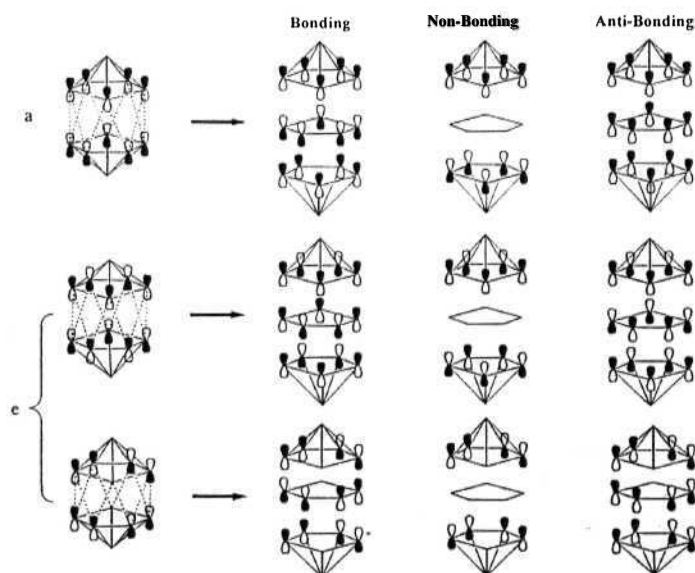
Figure 10

The molecular orbitals arising from the perpendicular p_z orbitals by the insertion of a B5H5 ring between two B_6H_6 fragments in $B_{12}H_{12}^{2-}$.

Note that the nonbonding combinations (third columns from figure 10) are not filled on stacking. This is because there are BMOs of the same symmetry below these MOs, which interact with these combinations and destabilize them. For example, of the three occupied radial BMOs for $B_{17}H_{17}^{2-}$ shown in Figure 11, the a_1' orbital mixes with the lowest nonbonding combination of the p_z set. The same mixing of course leads to stabilization of the radial orbital of the system as shown in Figure 12.
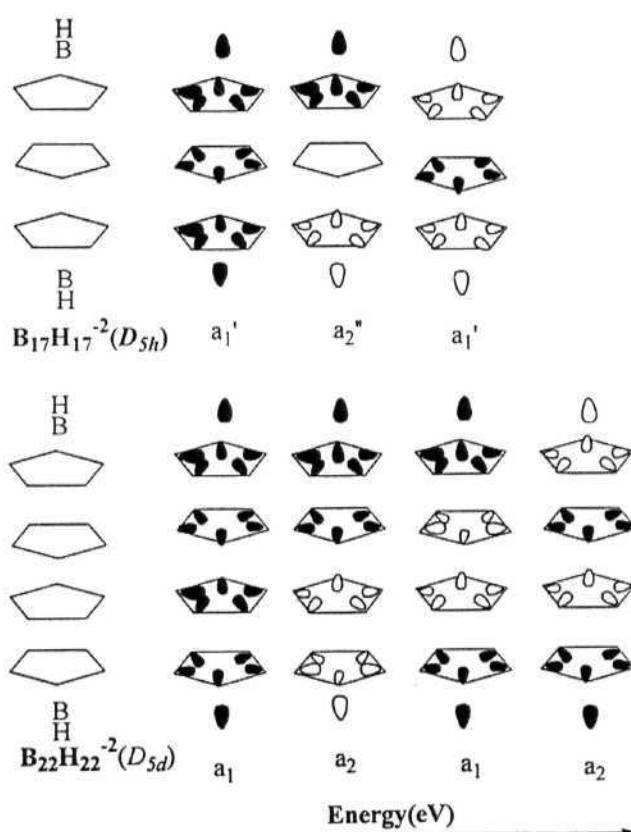

Figure 11

The radial bonding molecular orbitals of $B_{17}H_{17}^{-2}$ and $B_{22}H_{22}^{-2}$

130
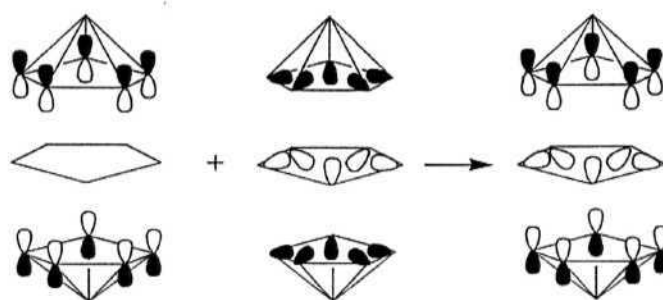
Figure **12**

The mixing of the nonbonding p_z MO with the radial BMO in $B_{17}H_{17}^{2-}$.

Earlier the argument for preferring "staggering" to "eclipsing" in $B_{12}H_{12}^{2-}$ was given. This is also true for the higher nanotubes, which prefer the triangulation that comes from staggering each ring relative to its neighbors.

DFT calculations carried out at B3LYP/6-31G* level of theory[3, 4] on $B_{17}H_{17}^{2-}$ indicate that the B-B bonds of the center ring are elongated substantially, to 2.127Å. This is the import of dashed lines in Fig.1 - the deltahedral framework is, in a way, broken; while there is bonding within the center ring, it is not clear if one should draw a full "bond-line" there. Why does this happen? As noticed earlier, due to the B-H bending in the B_6H_6 fragment towards the capping B-H group, the "perpendicular" p_z orbitals of B_6H_6 fragment will be splayed away from the center on the other side of the cap. The 'splaying-out' of p_z orbitals in borane nanotubes is illustrated schematically for one BMO in Figure 13. In $B_{17}H_{17}^{2}$ * expansion of the center ring makes for more effective overlap with the B_6H_6 fragment p_z orbitals. Calculations shows that the group overlap between the central B5H5 ring with the two *nido*-B_6H_6 fragments increases from 4.03 to 5.72 as a result of the center ring expansion. This offers a plausible explanation for the long B-B distances in the central ring. It can also be seen from Figure 13 that the bending of B-H

131

bonds towards the cap is decreased when compared with $B_{12}H_{12}{}^{2-}$. All these geometry changes are the result of the molecule optimizing cap/center ring group overlaps.
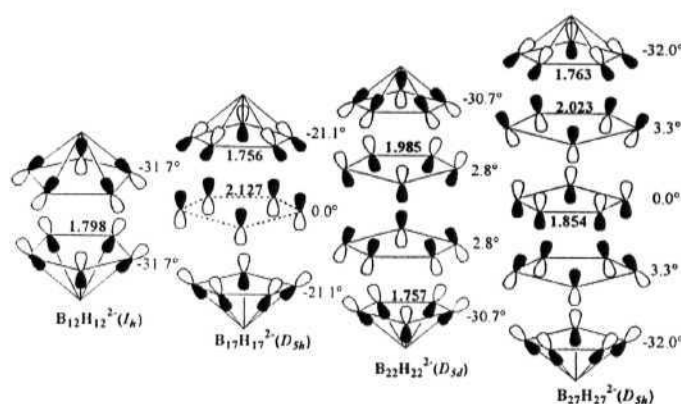

Figure 13

Reorientation of perpendicular p_z orbitals in borane nanotubes is illustrated for the most bonding MO made up of p_z orbitals. The bending of B-H bonds from the plane of the ring is given alongside the rings. The values near the bonds are calculated B-B distances in A.

Despite the expansion of the central ring, $B_{17}H_{17}{}^{2-}$ is predicted to be the most stable among *closo* boranes[19] by B-H increment schemes and highly aromatic by NICS based assessments.[3a] Isolobal substitution of B-H group with other groups having more diffuse orbitals such as $^+$SiH, Fe(Cp), etc., will improve the overlap and may help in the experimental characterization of this skeleton.[7a, 7c]

Insertion of one more ring in a similar way leads to *closo*-$B_{22}H_{22}{}^{2-}$. The argument for the 2- magic electron count is similar to the one given above. The radial BMOs of this species are given in Figure 11. As in the case of $B_{17}H_{17}{}^{2-}$, some of these orbitals will be stabilized by the MOs comprised of the perpendicular p_z orbitals of appropriate symmetry. The optimized geometry at the B3LYP/6-31G* level indicates that in this molecule the B-B bonds of the central ring (1.985 A) is significantly reduced compared to $B_{17}H_{17}{}^{2-}$ (2.127A). One might expect that the B-H bonds of the central rings should be bent towards the terminal ring to avoid steric interactions. But in the optimized geometry

132

they are bent in the opposite direction, i.e., towards each other. This is in accord with the earlier hypothesis that **the** p_z orbitals of the **central rings are** also splayed out a little to maximize the overlap with the terminal rings (Figure 13). To maximize overlap with the B_6H_6 groups, the central ring B-B distance is now reduced.

The next member of the series, $B27H27^{2-}$ **is** also found to have reduced ring elongation (in comparison with $B_{17}H_{17}^{2-}$) at the same level of theory. Here the B-B bonds of the central five-membered ring shrink to 1.854A, since the p_z orbitals of its adjacent rings are splayed 'in' towards the center of the molecule (Figure 13). Frequency calculations are consistent with the bond length trends. These mini-nanotubes were alternatively fat and thin along the tube axis.

It follows by induction that insertion of every additional ring between a ring and cap also will generate similar interactions and lead to a -2 charge. Effectively there arc just three such MOs that are bonding between the rings, irrespective of the number of rings in the system. But the optimized geometry has reasonably short B-B distances along the mini-tube (Figure 1). Obviously there must be more than six electrons contributing to the bonding along the mini-tubes. These must come from orbitals other than these three tangential p_z BMOs. Indeed some locally radial orbitals contribute to bonding along the mini-tube, by the second-order mixing mechanism described earlier for $B_{1.}[_{17}^{2-}$.

4.2.2. An Infinite Extension

The borane nanotubes have hydrogen atoms, which extend radially outward from each boron atom. Though nanotubes with bare boron atoms may also be possible with a similar geometry, the electronic requirements associated with **them** will be totally

different from borane based nanotubes. Here density functional calculations on the possible 1-dimensionally extended borane (B5H5) nanotubes are presented to inquire its properties.

Extended Hückel calculations are carried out using YaEHMOP[20] on a one-dimensional array of B5H5 rings, arranged successively in a staggered form at an ideal B-B distance of 1.75 A to determine its electronic requirements. Geometrical optimization of the five membered borane columns in a three dimensional network is done by embedding these nanotubes in orthorhombic lattice using a set of plane wave calculations using the CASTEP 5.2 simulation code.[21, 22] A generalized gradient approximation (GGA)[23] was used for the exchange and correlation potential and an energy cutoff of 270eV generated a basis set that allowed the total energy of the system to converge to 5.0e-6 eV atom^{-1}. For the Crystal lattice, integration over the symmetrized Brillouin zone were performed using k-points generated via the Monkhost-Pack scheme.[24] Simultaneous optimization of crystal lattice parameters and atomic relaxation were performed under the space group symmetry constraints. Ultra-soft pseudo potentials were used throughout for boron (s, p) and hydrogen (s).
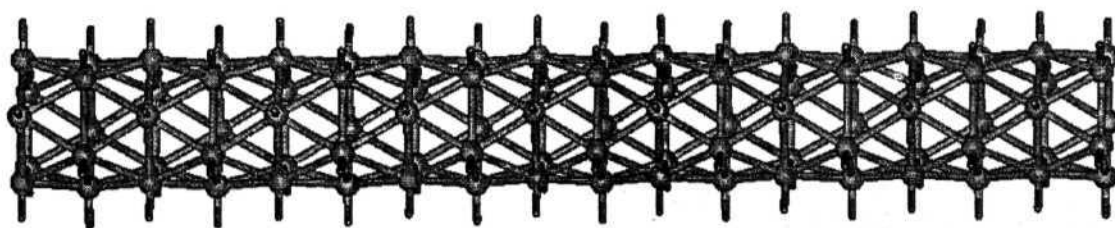

Figure 14

A 1-D extended stacking of planar B_5H_5 rings

Yaehmop calculation on a hypothetical 1-D system gives the Fermi energy at -7.5 eV with an effective direct band gap of approximately 2 eV between the bands at the

Fermi region. The results show that the extended system is stable with a neutral charge. This is in accordance with our observation in molecular systems of $B_{17}H_{17}^{2-}$ and $B_{22}H_{22}^{2-}$.[3, 4, 25] The constancy of 2- charge with stacking becomes negligible when an infinite stacking of B5H5 rings is considered. The bands obtained from Yaehmop are discussed below as it gives a comprehensible insight into the inter-ring bonding wherein the bands can be easily correlated with the fragment orbitals of the unit cell which are already well established.

Below the Fermi level, 20 bands are filled out of which eight are doubly degenerate throughout the brillouin zone. The lower 10 bands which correspond to the *exo* B-H bonds are not shown in Figure 15; the bottommost two lines running down which are excluded from numbering correspond to this set. The bands numbered 1 to 6 originates from cluster molecular orbitals; out of which 2, 4, 5 and 6 are doubly degenerate ones. The bands can be easily correlated with the individual associated MOs of the $B_{10}H_{10}$ unit given in the sides. 1 corresponds to bonding combination of the radial orbtials of the rings ($1a_{1g}$) and 3 correspond to its antibonding combination ($1a_{1u}$). As expected 1 is running upwards when moving from Gamma to X while 3 runs down. 2 and 4 originates from the bonding and anitbonding combinations respectively of the degenerate radial MOs $1e_{2u}$ and $1e_{1g}$. While 2 is running coherently upwards, 4 has a slight dip in the middle reflecting the mixing of the perpendicular p_z MOs that belongs to the same symmetry. The mixing is more pronounced in the antibonding combination resulting in the visible dip of the band 4. 2 and 4 is found to be affected by the e_{1u} MOs shown in Figure 16. 5 and 6 has its major contribution from $1e_{2g}$ and $2e_{2u}$. Like 2 and 4,

135

these tangential MOs also are stabilized by the mixing of perpendicular p_z MOs of appropriate symmetry (e_{1g} in Figure 16).
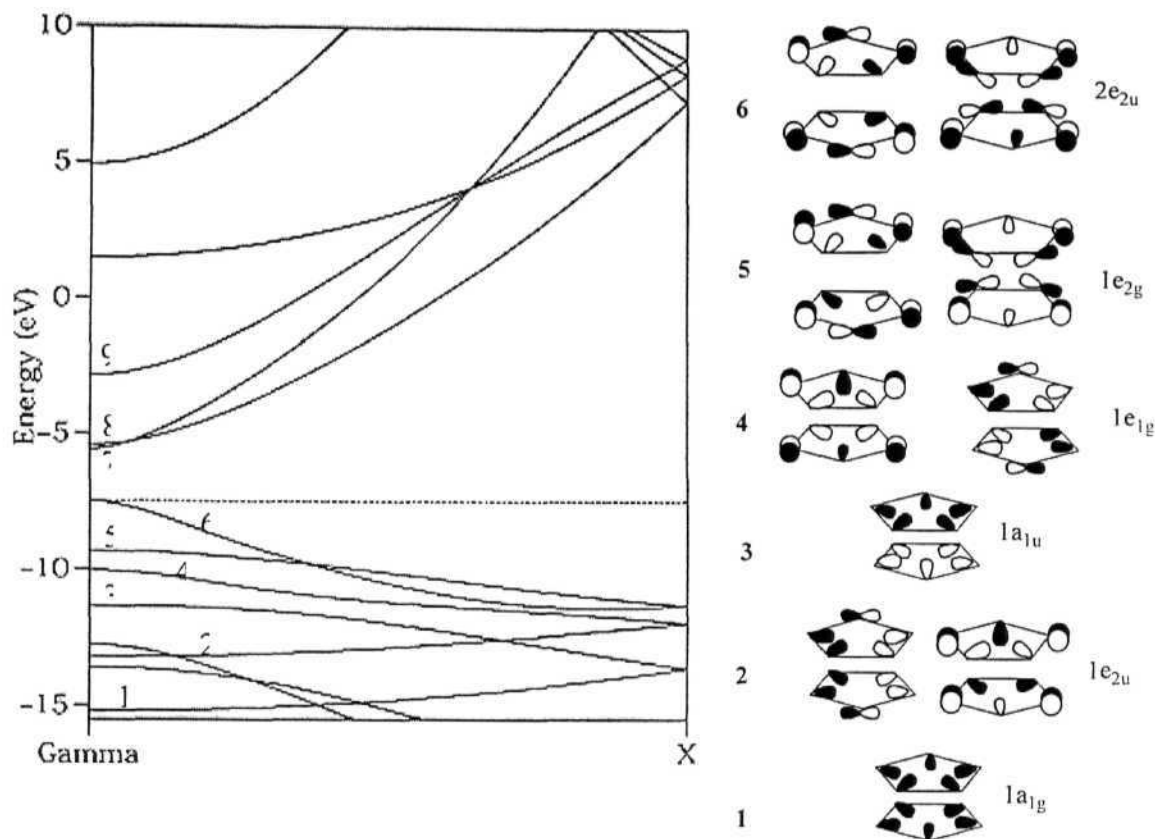

Figure 15

The band structure of a 1-D chain of B_5H_5 rings in a staggered form. The orbitals corresponding to bands 1 to 6 at the gamma point are shown on the R.H.S.

It is interesting to note that the remaining three skeletal molecular orbitals that mainly comprise of perpendicular p_z orbitals that are bonding between the ring (a_{1g} and e_{1u} in Figure 16) are above the Fermi level at the gamma point. These along with e_{1g} of $B_{10}H_{10}$ (Figure 16) affects the energy of the bands characteristic of the radial and in plane tangential MOs. At the gamma point, the bands originating from the MOs involving p_z orbitals of $B_{10}H_{10}$ (a_{1g}, e_{1u} and e_{1g} shown in Figure 16) can be characterized as 9, 8 and 7

136

respectively in Figure 15. The avoided crossing is not visibly observed since the mixing starts at Gamma itself. This is because the unit cell has two interacting B5H5 rings. Hence these mixing of the empty bands with the filled bands results in pronounced stabilization of the system.
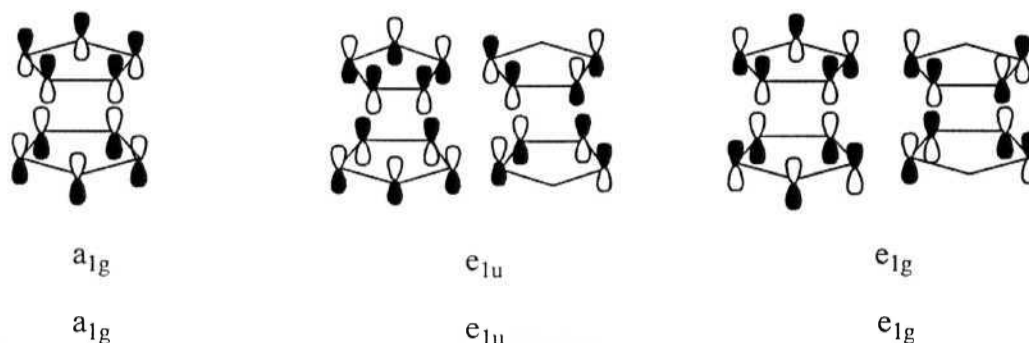

a_{1g} e_{1u} e_{1g}

a_{1g} e_{1u} e_{1g}

Figure 16

The MOs of the unit cell involving perpendicular p orbitals which affect the energetics of the radial and in plane tangential (1-6) MOs.

The projection of the perpendicular p_z orbitals shows high contribution of DOS below the Fermi level (Figure 17a). The Crystal Orbital Overlap Population (COOP)[26] across the rings also (Figure 17b) reveals that p_z orbitals which are bonding between the rings are mainly responsible for the inter ring bonding. Without mixing, band 5, that arise from the bonding combination of tangential orbitals is supposed to run up. The fact that they are running down from gamma shows the effective mixing of p_z molecular orbitals of same symmetry. Band 6, though runs down as expected shows a profound dip near to the X point which again illustrates the p_z mixing. The bonding character between the p_z orbitals even above the Fermi level (Figure 17b) can be attributed to its trivial presence at the gamma point. This is a further support of our observation in molecular systems of $B_{17}H_{17}^{-''}$ and $B_{22}H_{22}^{--}$ that the number of such orbitals remains as three irrespective of the number of rings which are stacked. The COOP curve shown in Figure

4b is between two rings in the same unit cell. The nature of the curve will be similar when the rings from two unit cells are considered as the distance between them are always the same.
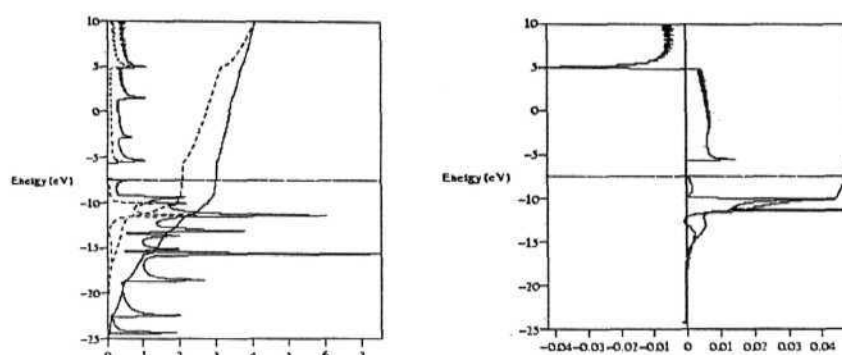

Figure 17

(a) The projected DOS of p_z orbitals on the boron atoms of B_5H_5 ring and (b) COOP between them with another in the same unit cell.

The 3-D network of B5H5 columns is optimized in an orthorhombic unit cell with a space group *of Pmma.* The lattice vectors of the optimized unit cell are a = 3.014071, b = 9.688956, c = 9.823213 There is a net expansion of the B-B bond lengths with B-B bond distance within the ring as 1.910 A and between rings is 1.811 A. The band and DOS of the optimized 3-D borane tubes are given in Figure 18.

A finite gap al the Fermi shows that the infinite stacking of borane rings is favorable. The band gap is found to be around 0.5 eV indicating semi conducting properties for the material.
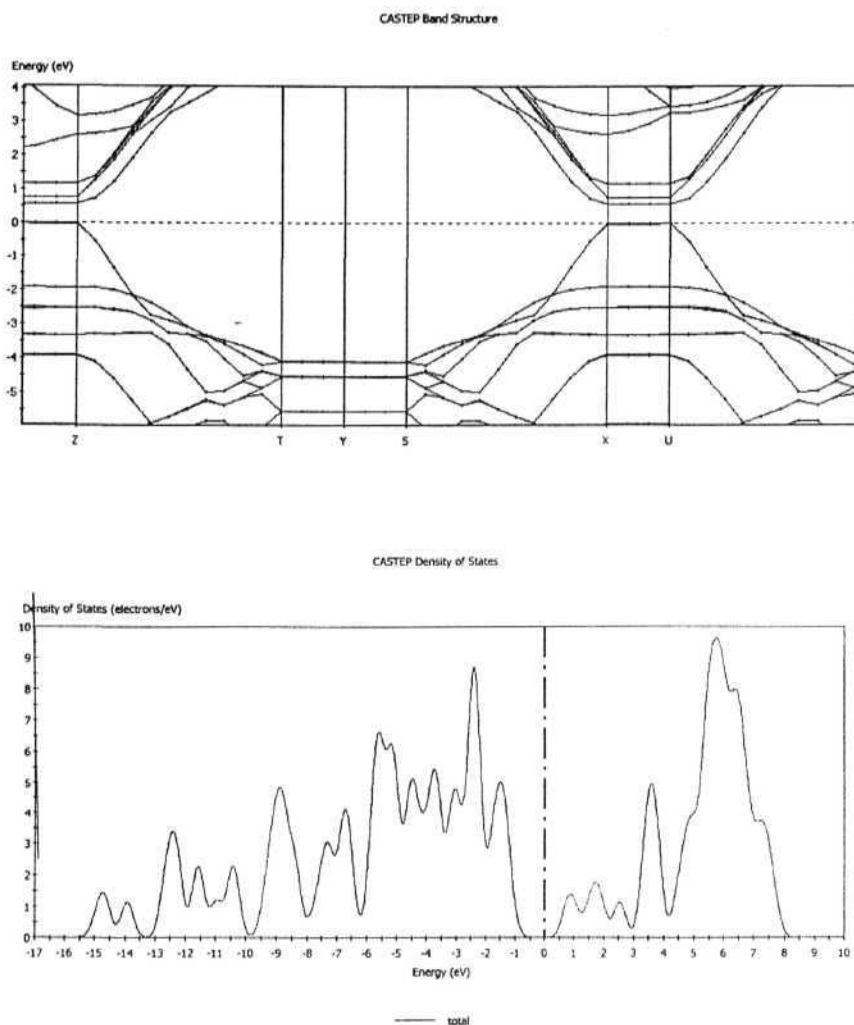
138

Energy (eV)

Density of States (electrons/eV)

Energy (eV)

—— total

Figure 18

The band structure (above) and DOS (below) of the optimized 3-D network of B5H5 columns.

4.3. CONCLUSIONS

The effect of staggered stacking of boron rings that leads to a deltahedral skeleton for tubular $B_nH_n^{2-}$ is studied. Apart from giving an argument for the abundance of icosahedral and octahedral structures in boron-rich borides, these perturbation theory based studies also point out that five-membered ring stacking intrinsically involves more pronounced stabilization than four-membered rings. With the increase in the number of rings, second-order interactions are increasingly responsible for ring-ring bonding. The

139

widely believed explanation that the *closo* boranes have one radial orbital and n tangential orbitals is found to be misleading, even for well known $B_{10}H_{10}^{2-}$ and $B_{12}H_{12}^{2-}$. Nevertheless, Wade's n+1 rule, as a formula, is found to be applicable even for extended borane nanotubes, although it is claimed to be inapplicable in higher spherical systems such as $B_{32}H_{32}$ (/h). In Wade's rule we have a case of a beautiful regularity, remarkably productive in rationalizing and predicting real chemistry. That the reasons for its applicability (the radial/tangential partitioning) fail to be met for some cases - the tubular boranes from $B_{10}H_{10}^{2-}$ on, does not at all detract from the value of this rule.

The bonding in an infinite stacking of B5H5 rings in a staggered form is also explored. The inter-ring bonding is attributed to the mixing of the p_z orbitals perpendicular to the ring with the tangential molecular orbitals. Their projected DOS reveals the mixing of such bands with the radial bands. Its stability has been confirmed by a GGA optimization of a 3-D network of five membered borane columns in an orthorhombic unit cell. A direct band gap of 0.5 eV at the Fermi level predicts semiconducting properties for the material.

REFERENCES

1. (a) Wade, K; *Chem. Commun.,* **1971,** 792. (b) Wade, K; *Adv. Inorg. Chem. Radiochem. 1976,18,* 1.

2. Hoffmann, R.; Lipscomb, W. N. *J. Chem. Phys.,* **1962,** *36,* 2179.

3. (a) Schleyer, P. v. R.; Najafian, K.; Mebel, A. M. *Inorg. Chem.,* **1998,** *37,* 6765. (b) McKee, M. L.; Wang, Z.; Schleyer, P. v. R. *J. Am. Chem. Soc,* **2000,** *122,* 4781.

4. Schleyer, P. v. R.; Najafian, K. in *The Borane, Carborane, Carbocation Continuum* Casanova, J., Ed.; John Wiley & Sons Inc, New York, **1998.** p. 169.

5. (a) Jemmis, E. D.; Balakrishnarajan, M. M.; Pancharatna, P. D.; *Chem. Rev.* **2002,** *102,* 93. (b) Balakrishnarajan, M. M.; Jemmis, E. D.; *J. Am. Chem. Soc.* **2000,** 722, 4516. (c) Jemmis, E. D.; Balakrishnarajan, M. M.; Pancharatna, P. D. *J. Am. Chem. Soc,* **2000,** *123,* 4313.

6. Hoffmann, R. *J. Chem. Phys..* **1963,** *39,* 1397.

7. (a) Jemmis, E. D. *J. Am Chem. Soc.* **1982,** *104,* 7017. (b) Jemmis, E. D., Schleyer, P. v. R. *J. Am. Chem. Soc,* **1982,** *104,* 4781. (c) Jemmis, E. D., Pavankumar, P. N. V. *Proc. Ind. Acad. Sci. (Chem. Sci.)* **1984,** *93,* 479. (d) Jemmis, E. D., Balakrishnarajan, M. M. *Bull. Mater. Sci.,* 1999, *22,* 101.

8. Frisch, M. J.; Trucks, G. W.; Schelegel, H. B.; Gill, P. M. W.; Johnson, B. G.; Robb, M. A.; Cheeseman, J. R.; Keith, T.; Peterson, G. A.; Montgomery, J. A.; Raghavachari, K.; Al-Laham, ML A.; Zakrzewski, V. G.; Oritz, J. V.; Foresman, J. B.; Cioslowsky, J.; Stefenov, B. B.; Nanayakkara, A.; Callacombe, M.; Peng, C. Y.; Ayala, P. Y.; Chen, W.; Wong, M. W.; Andres, J. L.; Replogle, E. S.; Gomberts, R.; Martin, R. L.; Fox, D. J.; Binkley, J. S.; Defrees, D. J.; Baker, J.; Stewart, J. P.; Head-

Gordon, M.; Gonzalez, C.; Pople, J. A. *Gaussian 94, Revision D.I, Gaussian Inc.*, Pittsburg PA, 1995.

9. B3LYP is Becke's three parameter hybrid method with LYP con-elation functional: (a) Becke, A. D. *J. Chem Phys* 1993, *98,* 5648; (b) Lee, C; Yang, W.; Parr, R. G. *Phys Rev B* 1988, *37,* 785; (c) Vosko, S. H.; Wilk, L.; Nusair, M. *Can J Phys* 1980, *58,* 1200; (d) Stephens, P. J.; Delvin, F. J.; Chabalowski, C. F.; Frisch, M. J. *J Phys Chem* 1994,95,11623.

10. (a) Brown, L. D.; Lipscomb, W. N. *Inorg. Chem.,* 1977, *16,* 2989. (b) Gindulyte, A.; Lipscomb, W. N.; Massa, L. *Inorg. Chem.,* 1998, *37,* 6544. (c) Sabra, M. K; Boustani, I. *Europhys. Lett.,* 1998, 42, 611.

11. Albright, T. A.; Burdett, J. K.; Whangbo, M. *Orbital Interactions in Chemistry,* John Wiley & Sons, Inc, 1985, Chap. 22.

12. (a) Underwood, D. J.; Hoffmann, R.; Tatsumi, K.; Nakamura, A.; Yamamato, Y.;./. *Am. Chem. Soc,* 1985, *107,* 5968. (b) Clark, H.C., Jain, V. K. *Coord Chem. Rev.* 1984,55, 151.

13. Derecskei-Kovacs, A.; Dunlap, B. I.; Lipscomb, W. N.; Lowrey, A.; Marynick, D. S.; Massa, L. *Inorg. Chem,* 1994, *33,* 5617. (b) Quong, Andrew A.; Pederson, Mark, R.; Broughton, Jeremy, Q.; *Phys.l Rev. B,* 1994, 50, 4787. (c) Tang, Au; Li, Qian; Liu, Chun; Li, Jun. *Chem.l Phys. Lett.,* 1993, *201,* 465. (d) Fowler, P. W.; Lazzeretti, P.; Zanasi, R. *Inorg. Chem.,* 1988, *27,* 1298.

14. Boustani, I.; Quandt A.; Rubio, A. *J. Solid State Chem.* **2000,** *154,* 269.

15. Dresselhaus, M. S.; Dresselhaus, G.; Eklund, P. C. *Science ofFullerenes and Carbon Nanotube*s; Academic: San Diego, 1996.

16. Mintmire, J. W.; Dunlap, B. I.; White, C. T. *Phys. Rev. Lett.* **1992,** *68,* 631.

17. Bethune, D. S.; Kiang, C.-H.; de Vries, M. S.; Gorman, G.; Savoy, R.; Vazquez, J.; Beyers, R. *Nature* **1993,** *363,* 605.

18. Iijima, S.; Ichihashi, T. *Nature* **1993,** *363,* 603.

19. Stone, A. J. *Mol. Phys.,* **1980,** *41,* 1339.

20. Landrum, G. A.; Glassy, W. V., YAeHMOP (Version 3.01). (Freely available at http://yaehmop.sourceforge.net

21. Accelrys Inc., Materials Studio CASTEP, San Diego: Accelrys Inc., **2001.**

22. Milman, V.; Winkler, B.; White, J.A.; Pickard, C.J.; Payne, M.C.; Akhmatskaya, E.V.; Nobes R.H., *Int. J. Quant. Chem.* 2000, *77,* 895.

23. Payne, M. C; Teter, M. P.; Allan, D. C; Arias, T. A.; Joannopoulos, J. D., *Rev. Mod. Phys.,* 1992, *64,* 1045.

24. Monkhost, H. J.; Pack, J. F., *Phys. Rev. B,* **1976,** *13,* 5188.

25. Schleyer, P. v. R.; Najafian, K. in *The Borane, Car borane, Carbocation Continuum* Casanova, J., Ed.; John Wiley & Sons Inc, New York, 1998. p. 169.

26. (a) Hoffmann, R. *Solids and Surfaces: A Chemist's View of Bonding in Extended Structures,* VCH Publishers Inc, New York, **1988.** (b) Hughbanks, R.; Hoffmann, R., *J. Am. Chem. Soc,* **1983,** *105,* 3528. (c) Wijeyesekera, S. D.; Hoffmann, R., *Organometal.,* **1984,** *3,* 949. (d) Kertesz, M.; Hoffmann, R., *J. Am. Chem. Soc,* **1984,** *106,* 3453.

CHAPTER 5

BONDING IN EXTENDED SYSTEMS

5.0. INTRODUCTION

Computational material science has advanced itself in characterizing new materials with the desired properties providing rational approach to their synthesis[1] thereby rapidly replacing explorative synthesis involving ad-hoc procedures. Polyhedral boranes, despite their very complicated three dimensional networks, is ideal for such design as their skeleton can be systematically perceived as a network of some comprehensible molecular fragments whose bonding requirements are known.[2] An extended fusion of pentagonal pyramids through an edge has been selected for an elaborate study to verify the applicability of the generalized *mno* rule to extended systems.

Though, many borides have B_{12} and B_6 units as primary building blocks,[3] condensed structures where individual units share one or more vertices in common are also ubiquitous.[3] The superconducting MgB_2, in which adjacent B_6 rings share a common edge, serves as an ideal example.[4] Here, a novel and promising extended boride structure is proposed which is constructed from edge sharing molecular skeletons observed in macropolyhedral boranes and its bonding is explored through first-principle calculations. The model structure is isomorphic to the MgB_4 structure observed earlier[5] but has sigma-pi characteristics of the MgB_2 structure and shows remarkable rigidity with various cations. Though both MgB_2 and MgB_4 shows adherence to the electron counting rules only the former exhibits superconductivity. However the minimal requirement for the existence of a boride phase seems to be its adherence to electron counting rules though there are notable exceptions.

5.1. EDGE-SHARING PENTAGONAL PYRAMIDS IN EXTENDED STRUCTURE: A THEORETICAL BORIDE NETWORK

The recent discovery of superconductivity[6] in MgB_2 at a relatively high transition temperature of $39K$ renewed interest in the electronic properties of intermetallic borides. There had been several attempts to synthesize borides of light metals in the hopes of achieving a higher superconducting transition temperature. Standard BCS theory of superconductivity[7] predicts enhanced transition temperatures for materials containing lighter elements due to their higher phonon frequencies.

Among various modes of condensation in polyhedral fragments, edge sharing is found to be dominant for polyhedral networks.[2c] This is evident from the observation that the majority of macropolyhedral boranes characterized experimentally have edge-sharing skeleton. Hence the choice of edge sharing network is ideal for extended networks. Besides, edge sharing offers structural similarity to the MgB_2 structure that holds great promise for superconducting electronics due to its characteristic double gap.[8] Though such edge shared polyhedral networks are known in MgB_4, the 2c-2e bond between a ring and a cap atom of two adjacent chains disturbs the distinct o and *n* framework which is observed in MgB_2. In order to maintain that framework of MgB_2, we choose the edge sharing pentagonal network forming linear chains. However, unlike hexagonal rings in MgB_2, pentagonal rings prefer capping by a boron atom due to ring-cap matching.[9] With these considerations, we chose pentagonal pyramids as building blocks for the extended structure.

5.1.1. Description of the Structure

Condensation of pentagonal pyramids by sharing an edge between adjacent B_6 units can be made to form a linear chain. Capping of the adjacent rings can be done either on the same side or at the opposite sides. However, the *trans* form in which adjacent caps are at the opposite side are favorable over the *cis* form (Figure 1) since proximate cap-cap interactions in *cis* form are only weakly bonding.[10] These linear chains can be extended in two dimensions by placing them parallel so that their unshared ring boron atoms are connected to each other by a two-centered two electron (2c-2e) bond. This can lead to two isomeric forms depending on whether the caps on the adjacent chains are *trans* or *cis* as illustrated in Figure 2.
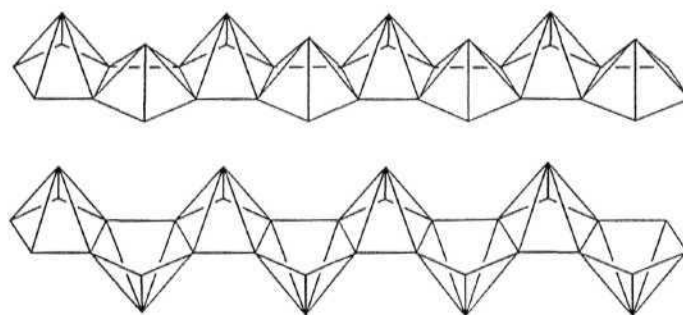
Figure 1

A linear Chain of edge-sharing pentagonal pyramids in *cis* and *trans* forms.

To extend the structure in three dimensions, we can place the layers of these two dimensional skeletons, one over the other by connecting the capping boron atoms through a 2c-2e bond. Similar to the 2-D network, the 3-D network also exists in two isomeric forms with respect to the position of capping atoms across the one-dimensional chain. For the 3D network, the two types a and b which have *trans* and *cis* orientations with respect to the link across 1D chains are shown in Figure 3. The unit cell of this structure

146

is orthorhombic and falls in the space group *Cmcm* for the *trans* orientation and *Immm* for the *cis* orientation (Figure 3).
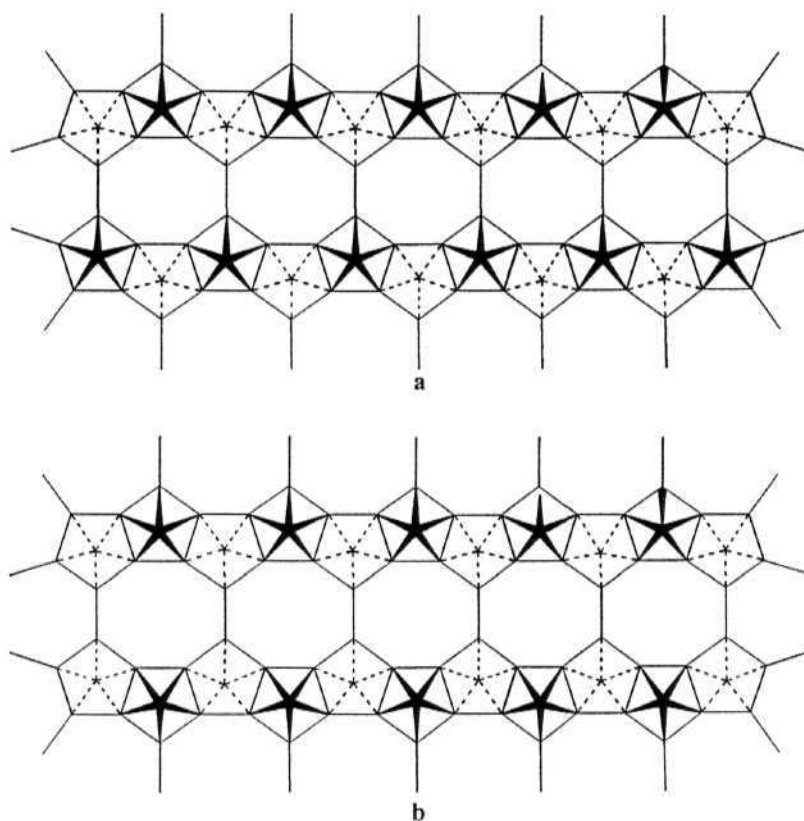

Figure 2

Connection of the capping boron aroms of edge-sharing *trans* pentagonal pyramids by 2c-e bonds to form a 2-dimensional network. (a) and (b) represent the resulting *trans* and *cis* forms respectively.
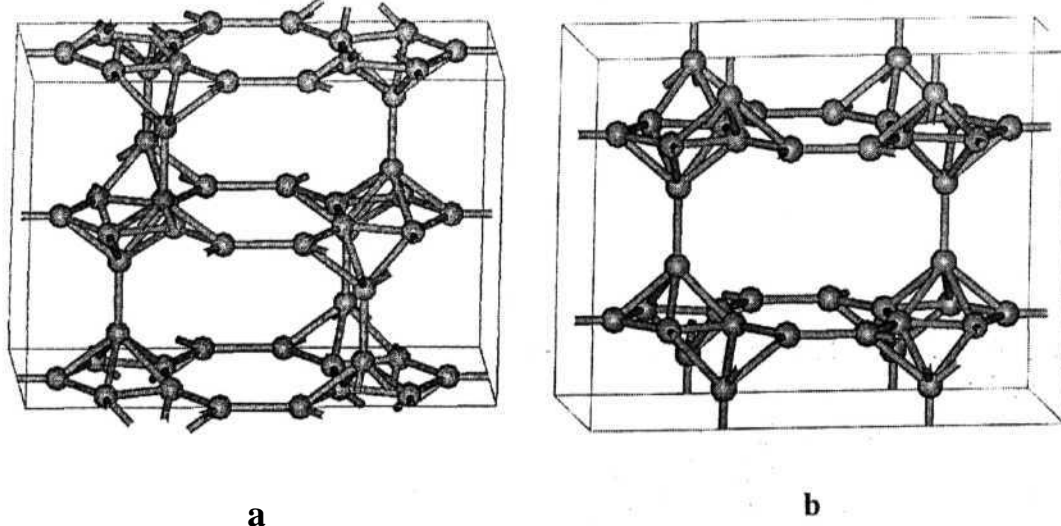

a   b

Figure 3

The orthorhombic unit cell of edge sharing trigonal-pyramidal network. (a) gives the unit cell due to the *trans* orientation of the caps in the adjacent chains and (b) is the unit cell due to the *cis* orientation.

147

Both the structures have twelve vacancies in a unit cell where cations can be occupied which can be categorized into three distinct types. Four of them lie exactly opposite side of the capping boron atom in the pentagonal ring and originates from the 1-D network itself. These are termed as capping voids and are denoted as CAP. The next group of four vacancies originates from the 2-D network due to the 2c-2e linkage between the ring boron atoms on adjacent chains and connects the four capping voids. These form octagonal channels (Channel-1) when a 3-D network is formed. The third type of four voids again forms channels (Channel-2) and is characteristic of the 3-D network that is formed due to the 2c-2e bonds between the caps of the adjacent 2-D networks. They are of different sizes depending on the boride skeleton. Channel-2 in a form is connected with one adjacent capping void, whereas in the b form either it is connected with both the capping voids on its sides or it will be isolated by the cap-cap 2c-2e bonds in which case it will be octagonal. Two such channel-2 voids will be alternating in the b form. These voids and channels can accommodate cations to satisfy its electronic requirements. It is related to the boride network found in MgB_4 that also has edge sharing of pentagonal pyramids, but unlike the known MgB_4, the present skeleton forms a linear array resembling MgB_2.

5.1.2. Determination of Electronic Requirements for Bonding

The electronic requirements of this hypothetical skeleton can be evaluated using our recent electron counting paradigm.[2] According to the rule, a macropolyhedral skeleton that has n vertices and m cages will require n+m electron pairs for its skeletal bonding. Absence of one or more vertices will require additional electron pairs. Hence, an edge-shared condensation of two *closo* pentagonal bipyramids $B_{12}H_{10}$ will require

(n=12, m=2) 14 electron pairs for its skeletal bonding. If two of its vertices are removed from the *trans* position to give the edge-sharing pentagonal pyramid $B_{10}H_8$, the number of electron pairs remains the same i.e., 14 since extra electron pairs have to be added for the missing vertices. Since only ten electron pairs are available, this molecule will exist with 6- charge or will have six bridging hydrogen atoms ($B_{10}H_{14}$). To verify the electronic requirements, $B_{10}H_{14}$ is optimized (Figure 4) at B3LYP/6-31G* level[11, 12] of theory and found that it is a minimum on the potential energy surface, confirming our electron count.
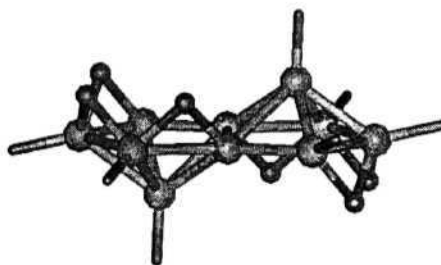
Figure 4
The geometry of $B_{10}H_{14}$ optimised at B3LYP/6-31g* level of theory.

Likewise, the electron counting can be extended to the infinite chains. Edge-sharing *closo* network will require a -2 charge irrespective of the number of units in the chain and can be ignored for an infinite chain. However removal of a vertex from the *closo* skeleton to form the edge sharing pentagonal pyramids (Figure 1) will require one electron pair per individual units. In the orthorhombic unit cell discussed above, there are eight such pentagonal pyramids effectively. Hence the unit cell requires 16 electrons. These electrons can be made available to the network by sufficient cations of appropriate size in the available voids. Though all the twelve voids in the network can accommodate cations, only eight of the voids are chosen for Mg, to arrive at different isomeric MgB_4

structures. This enables a verification of the rigidity of different isomorphic boride networks, and also provides a means to compare their energetics with the known MgB_4 structure. However, to get a compact network, all the twelve voids have to be filled. Hence these networks allow room for substituting Mg^{2+} with monovalent cations. We chose the a form for the ternary phase, replacing some Mg^{2+} ions by Li^+ and adding one more Li^+ in the extra void which results in the stoichiometry of Li_2MgB_8.

Extended structure calculations on the three-dimensional network of edge-sharing pentagonal pyramids are done using extended Hückel based band structure program Yaehmop.[13] The advantage of this simplistic method is that it gives valuable chemical insight of the structure and can be done for highly charged unit cells with ease. The structure was computed with 64 kpoints set in the orthorhombic space group keeping the B-B distances of the optimized $B7H7^{2"}$ molecule. Thus while the ring B-B distance is 1.657 A, the cap to ring B-B distance is 1.830 A. Geometrical optimization of the metal borides; Li_2MgB_8 and MgB_4 structures were done by a set of plane wave calculations using the CASTEP 5.2 simulation code.[14, 15] A generalized gradient approximation $(GGA)^{[16]}$ was used for the exchange and correlation potential. An energy cutoff of 310 eV generated a basis set that allowed the total energy of the system to converge to 2.0e~5 eV atom$^{"1}$. For the Crystal lattice, integration over the symmetrized Brillouin zone were performed using k-points generated via the Monkhurst-Pack scheme.[17] Simultaneous optimization of crystal lattice parameters and atomic relaxation were performed under the space group symmetry constraints. For comparison, the experimentally reported MgB_4 structure is also computed at the same level. Ultra-soft pseudo potentials were used throughout for boron (s, p) and cations (s, p, d).

5.1.3. Results and Discussion

i. Li₂MgB₈

The stability of the *trans* boride (Figure 3, a) based extended systems is tested by optimizing the unit cell with appropriate cations in the vacancies. A possible way of achieving the electronic requirement by filling all the available vacancies in a unit cell is by considering bimetallic systems involving alkali metals and alkaline earth metals.

The *trans* form of the boride corresponding to the structure in Figure 3 **a** with a space group of *Cmcm* is optimized using Li and Mg ions; resulting in a stoichiometry of Li_2MgB_8. Here Mg is placed at the four capping voids and the Li ions occupy both the channels. With such an arrangement, the boride skeleton is found to be very stable with reasonable B-B bond lengths. The different types of B-B bonds present are Bs-Bu (between a shared and a non-shared atom in a pentagonal ring), Bs-Bs (between two shared atoms within a ring), Bs-Bc (between the shared atom and a cap atom within a pentagonal pyramid), Bu-Bc (between the non-shared atom and a cap atom within the pyramid), Bu-Bu (2c-2e bond between two ring atoms of two adjacent chains), Bc-Bc (2c-2e bond between two cap atoms of adjacent chains). The various bond distances in the optimized boride skeleton of Li_2MgB_8 are 1.713 A (Bs-Bu), 1.767 A (Bs-Bs), 1.843 A (Bu-Bc), 1.853 A (Bs-Bc), 1.800 A (Bu-Bu) and 1.842 A (Bc-Bc) respectively. Each chain of a fragmented 2-D network is inclined to the adjacent one by an angle of 171.5°; inverse stacking of these make the complete 3-D network. The geometry of the optimized system with a view along the ac plane is given in Figure 5. The direction of the tilt at both the sides of the chain of pentagonal rings is opposite to each other, giving a ladder like appearance along the c-axis.
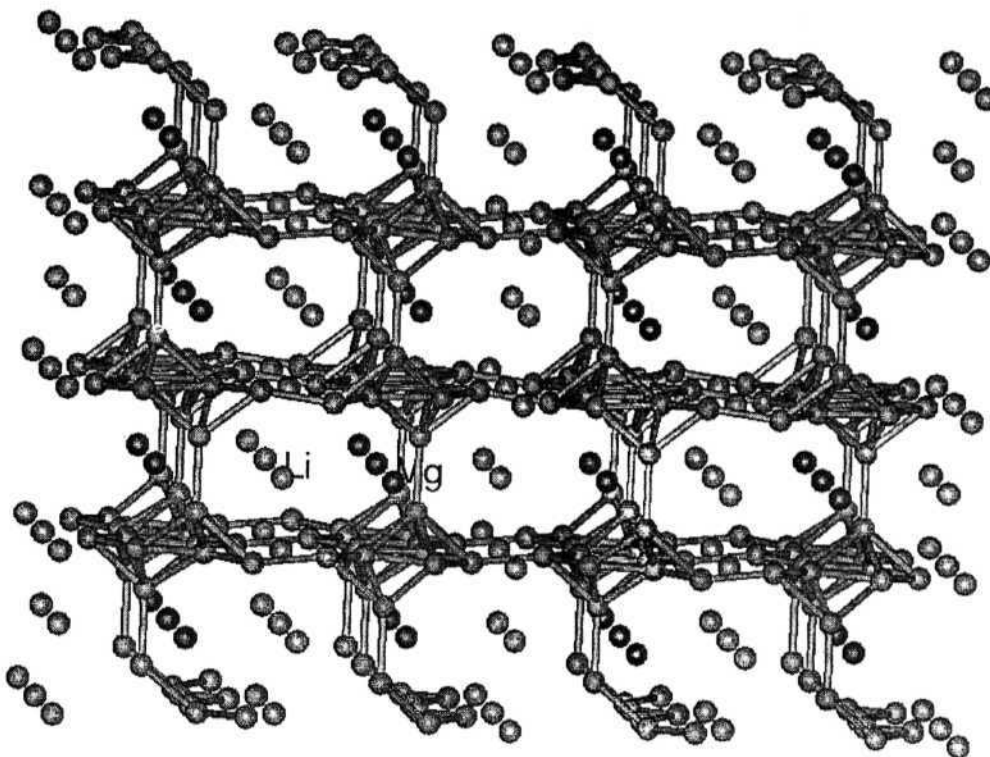
Figure 5

The extended view of the optimized geometry of Li_2MgB_8 along the ac plane.

The *exo* bonds of each pentagonal ring which consists of the 2c-2e bond with the ring atom on the adjacent chain is found to be bend by $10.5°$ with respect to the plane of the ring. This bending helps in an effective ring-cap overlap for both boron and magnesium with the B_5 ring.[9] This indicates that there is considerable covalent interaction between Mg and the pentagonal open face as in the case of MgB_2. The bending is towards the boron cap and away from the Mg because this bending of the *exo* B-B bond towards the boron cap helps in a better overlap between them. This indirectly benefits the overlap between the pentagonal ring and the Mg atom as well which occupies the opposite cap position. Due to the difference in the size of the two caps, both of them have overlap advantage on bending. The channels in between are large enough to

accommodate the Li^+ ions. The band structure and DOS (Figure 6) of the optimized Li_2MgB_8 shows the material to be a finite gap semiconductor with an indirect band gap of around 0.5 eV in the Y-G region.
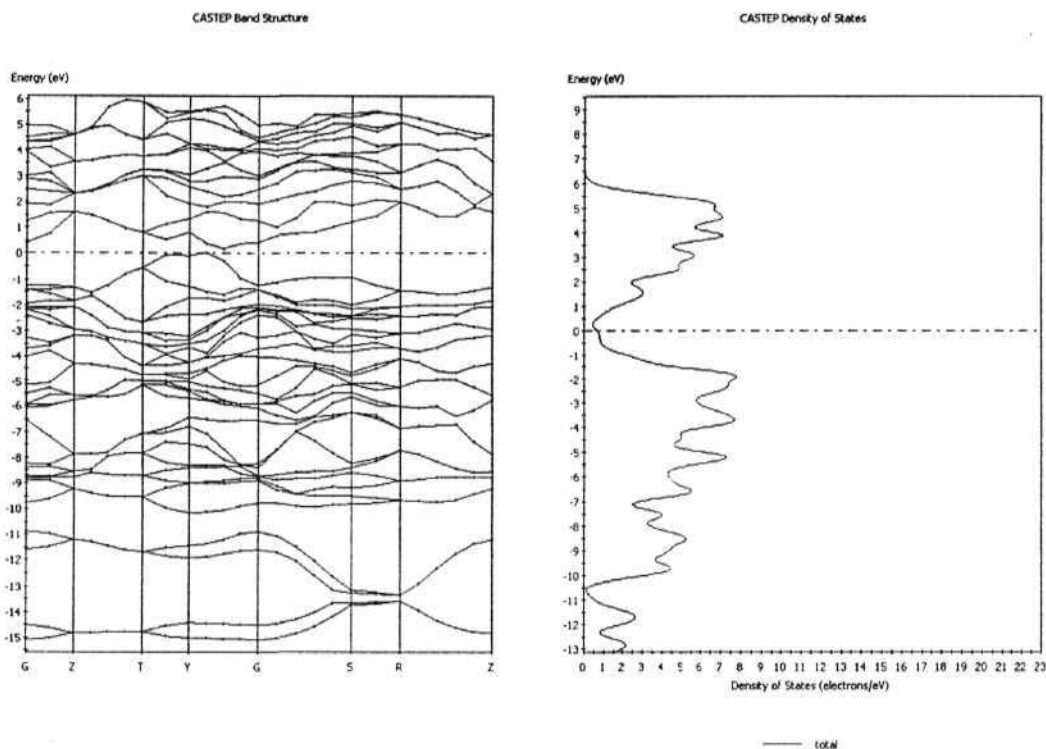

Figure 6

The band structure and DOS of Li_2MgB_8 of an orthorhombic unit cell belonging to *Cmcm* space group

The major difference between MgB_2 network and the present boride network is the existence of capping boron atoms. This capping stabilizes the perpendicular p_z orbitals of the pentagonal rings and may remove the bands arising from them away from the frontier region. Hence an extended structure calculation is performed on the optimized structure to analyze the nature of bands around the Fermi level. The projected DOS of the perpendicular p_z orbitals of the ring atoms calculated using yaehmop is given in Figure 7.
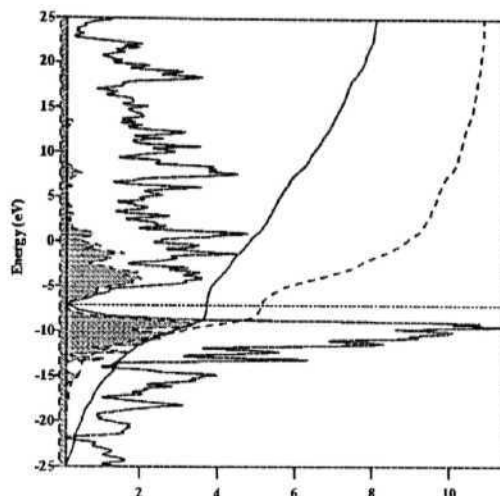
153

Figure 7

The projected DOS of the p_z orbitals of the ring boron atoms in Li_2MgB_8

The DOS is almost zero exactly at the Fermi level as observed in Figure 6. However, the density of states is found to be relatively high around the Fermi region, with major contribution from the p_z orbitals of ring boron atoms, making a striking similarity to the superconducting MgB_2 band structure.

A similar stoichiometry of Li_2MgB_8 in the *cis* form corresponding to Figure 3b, fails to converge. This is presumably because of the absence of bending of the *exo* 2c-2e bonds in the *cis* orientation as both the rings joined by a 2c-2e bond has its caps in the same side. To substantiate this conjecture, the energetic stability of various isomorphic forms of this boride network discussed earlier, are analyzed using pure Mg^{2+} doping.

ii. MgB_4

The electronic requirement of the boride network can also be achieved by replacing the two Li ions in Li_2MgB_8 by Mg^{2+} ion, resulting in MgB_4. Here only eight vacancies **per** unit **cell are filled.** MgB_4 phase is already known where a similar network of edge shared pentagonal pyramids connects to another by forming 2c-2e bonds between

154

a ring atom and a cap atom. In addition changing the positions of the Mg^{+T} ions will generate three isomeric forms in the *trans* form itself. But one of them converged to another form and the *trans*-boride MgB$_4$ isomers are reduced to two. Hence we have four isomers of MgB$_4$ to compare which includes one *cis* boride network and the experimental MgB$_4$ as well. The relative energies (R.E. in kcalmol^{-1}) of the various isomers of MgB$_4$ with respect to the experimental one, with their space groups (G), cell parameters and volume of the primitive cell (V in A^3) are given in Table 1 for comparison. In general, the hypothetical isomers are more spacious presumably due to the availability of additional unfilled voids.

Table 1. The relative energies (R.E.), space group (G), cell parameters and volume of the unit cell of various isomers of MgB$_4$.

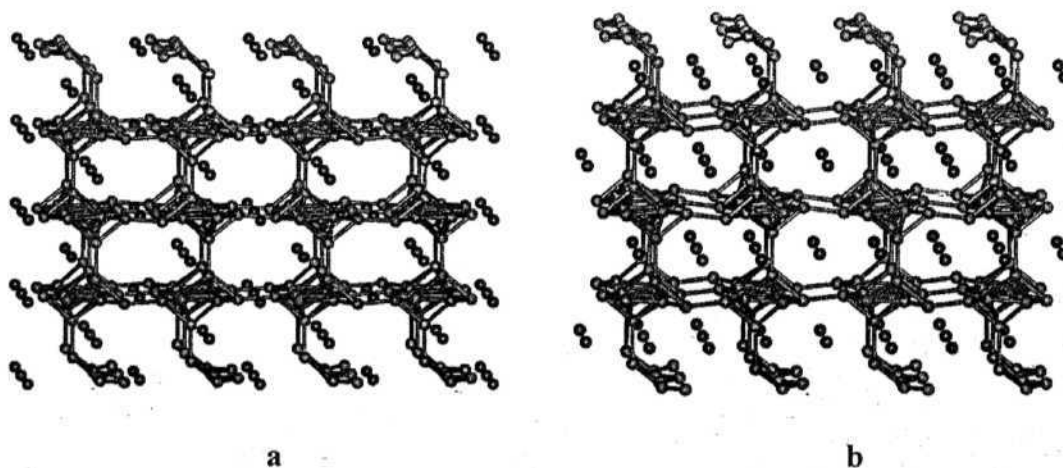| MgB$_4$	R.E.	G	Cell Parameters						V A^3
			a (Å)	b (Å)	c (Å)	α	β	γ	
Expt.	0.0	*Pnma*	5.464000	4.428000	7.472000	90.0	90.0	90.0	180.78
I	13.9	*Cmcm*	6.064608	6.064608	8.037695	90.0	90.0	42.1	198.02
II	19.1	*Cmcm*	5.965752	5.965752	7.972395	90.0	90.0	43.4	194.96
III	33.5	*Immm*	7.264452	7.264452	7.264452	79.0	112.1	144.6	200.90

a   b

Figure 8
The optimized geometries for the isomers of MgB$_4$ in the *trans* form.

155

An isomer of the *trans* boride (Figure 3a) where only the channels are filled leaving the capping voids empty is not found to be stable. The optimized structure converged to the geometry where the Mg ions are migrated from channel-2 to CAP. Such an isomer {I, Figure 8a) where channel-1 and the capping voids are occupied by Mg ions is found to be the most stable among the hypothetical structures and is less stable than the known one by 13.9 kcalmol^{-1} per formula unit. The next isomer that is energetically closer is the one where the channel-2 and the capping voids are occupied by Mg ions (II, Figure 8b) and is less stable than the known form by 19.1 kcalmol^{-1}. Thus the capping void is found to be the most preferable position for Mg in the *trans* boride network. But the reverse is found to be true in the *cis* boride skeleton corresponding to that in Figure 3b.
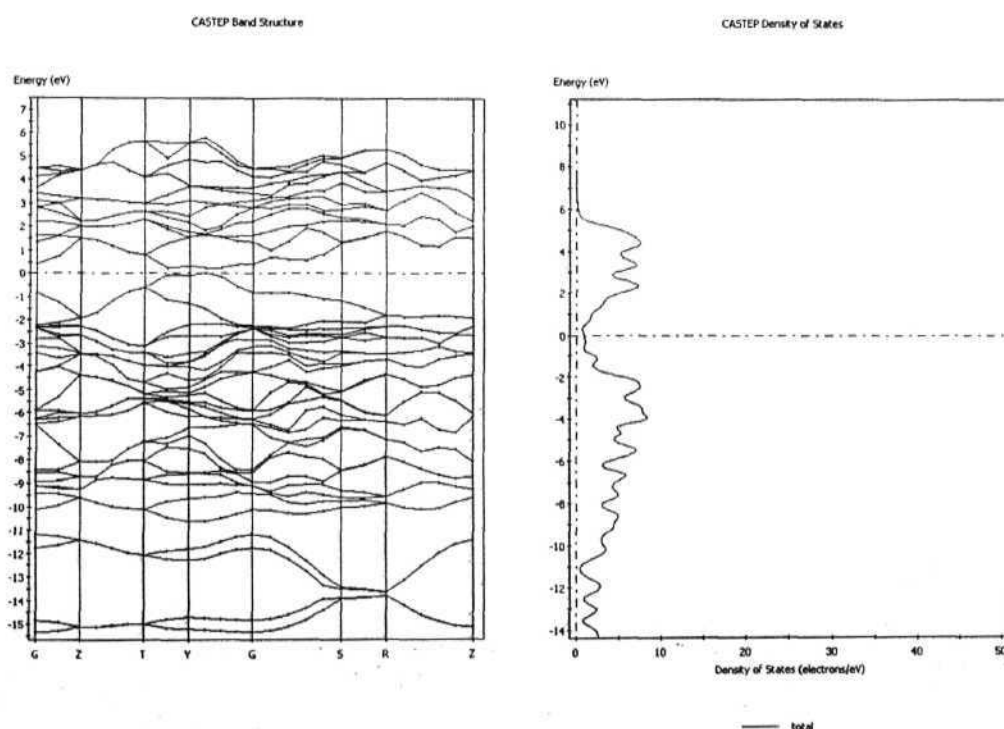

Figure 9
The band and DOS of isomer I of MgB_4

The angle of bending of the *exo* bonds of the pentagonal ring boron atom in isomer I is 6.5° which is less when compared to Li_2MgB_8. The ring has a uniform B-B distance of 1.723 A for both Bs-Bs and Bs-Bu, and the cap to ring distance within the pyramidal unit has expanded slightly to 1.893 A. Between the chains, Bu-Bu distance is expanded to 1.845 A and the Bc-Bc is bond shortened to 1.807 A. The net result is an expansion of channel-1 compared to that in Li_2MgB_8 that suggests that Mg ions are slightly larger for this void than the Li ions. In isomer II, The angle of bending of the *exo* bonds of the pentagonal ring boron atom is 10.8° almost identical to that observed in Li_2MgB_8. This shows that the presence of the Mg ions in channel-2 has an additive effect for the bending. Channel-1 gets compressed while channel-2 gets expanded with the B-B distances as 1.696 A (Bu-Bs) and 1.824 A (Bs-Bs), 1.816 A (Bu-Bc), 1.795 A (Bs-Bc), 1.842 A (Bu-Bu), and 1.939 A (Bc-Bc). In short, the channels where the Mg ions are present are expanded. Thus while I has Mg in channel-1, the ring Bu-Bs distances are longer compared to II and in II where the Mg occupies channel-2, the B-B distances pertaining to the caps are longer. The Bu-Bu distances between the chains that are shared by both the channels are almost the same. The optimized geometries of I and II, with a view along the bc planes is shown in Figure 8. Figure 9 and 10 gives the band and DOS of I and II respectively.

The band gap of the material in both the isomeric forms is around 0.5 eV lying in T-G region. The nature of the DOS is similar to that observed in Li_2MgB_8. The band structure and DOS for the known MgB_4 is given in Figure 11 for comparison. While the DOS looks similar, the band gap in the known MgB_4 is an indirect one. Thus the

157

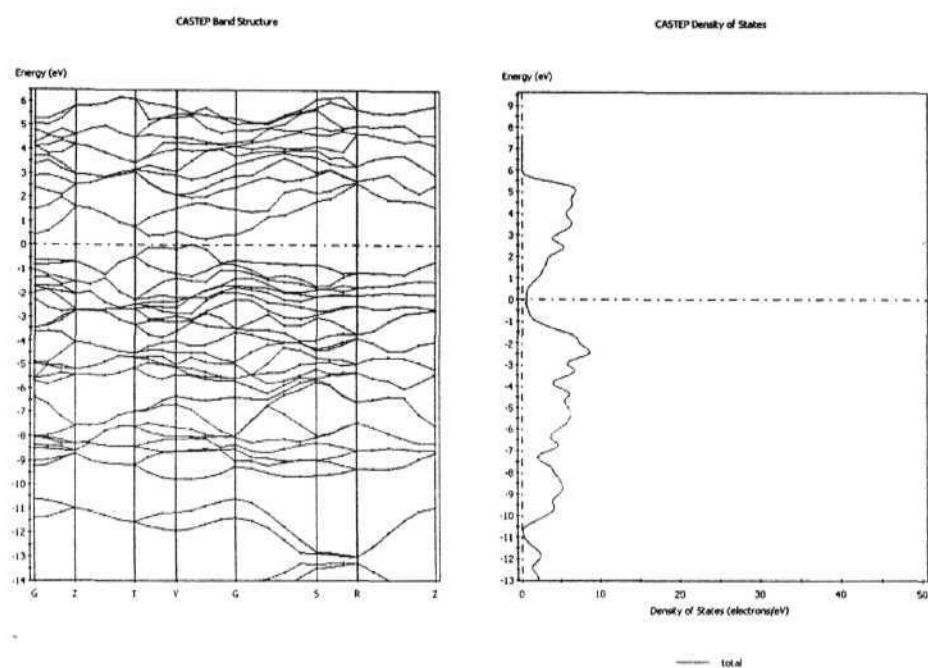theoretical system presented here is likely to possess better conductivity than the isolated

one.

CASTEP Band Structure

CASTEP Density of States

Figure 10

The band and DOS of isomer II of MgB_4

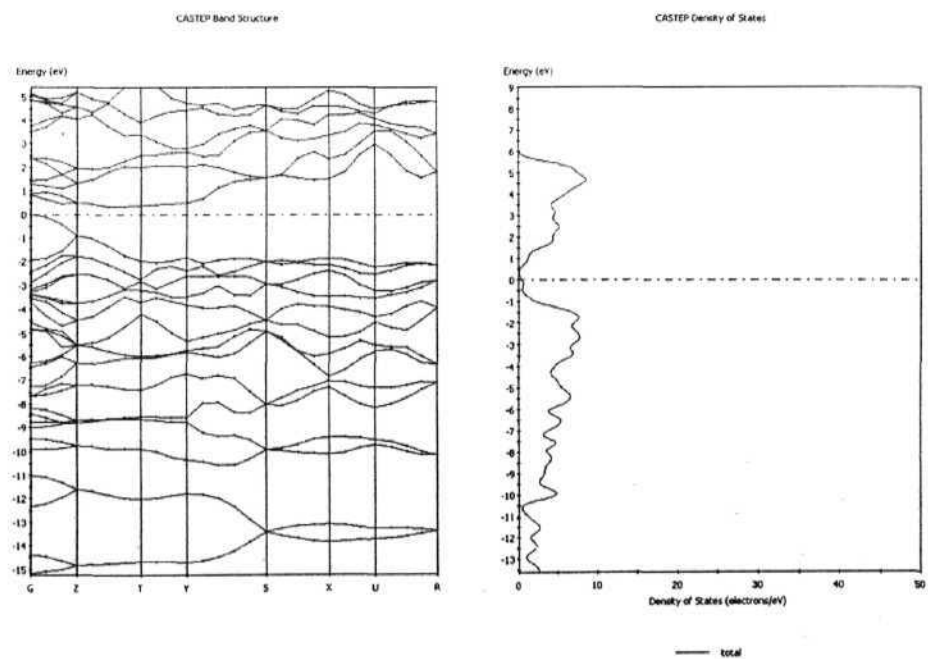CASTEP Band Structure

CASTEP Density of States

Figure **11**

The band and DOS of the known form of MgB_4

Since the *cis* boride in Li_2MgB_8 where Mg occupied the capping voids did not converge, an isomer where they are left vacant is tried for MgB_4. Thus MgB_4 in the *cis* geometry where the CAP are left vacant and the Mg atoms occupy channel-1 & 2 is found to be possible theoretically. The CAP in *cis*-boride is found to be inappropriate for metals. The optimised geometry of MgB_4 (isomer III) along the ab plane belonging to the space group *Immm* of the orthorhombic unit cell is shown in Figure 12. The pentagonal rings of the various chains lie on the same plane. The Bs-Bs distance of 1.674 A is shorter than that compared to Li_2MgB_8. The ring to cap distance within the pentagonal ring (1.837 A) is comparable with Li_2MgB_8. While the Bu-Bu distance between the chains (1.923 A) is little longer than that observed in Li_2MgB_8, the Bc-Bc distance (1.809 A) is shortened. The lengthening of the Bu-Bu distance is presumably to compensate for the shortening of the B-B distance within the ring so as to maintain the size of channel-1 to accommodate the Mg^{2+} ions. Similarly channel-2 need to be smaller as there is only one Mg^{2+} ion in contrast to Li_2MgB_8, where channel-2 is fully connected with the capping void and both are filled.
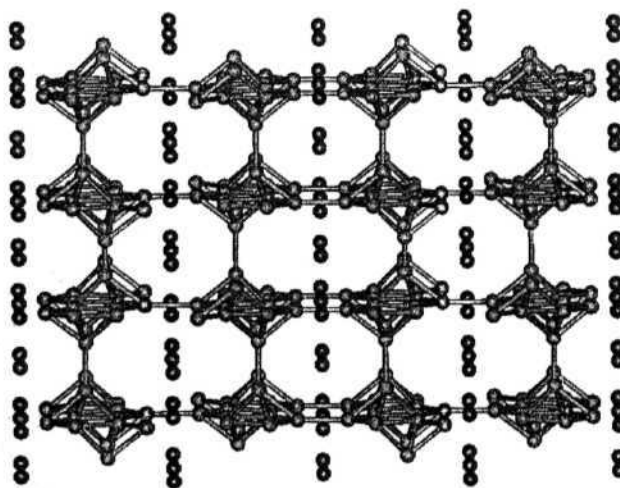

Figure 12

An extended view of the optimized geometry of *cis*-MgB_4 along the ab plane.

159

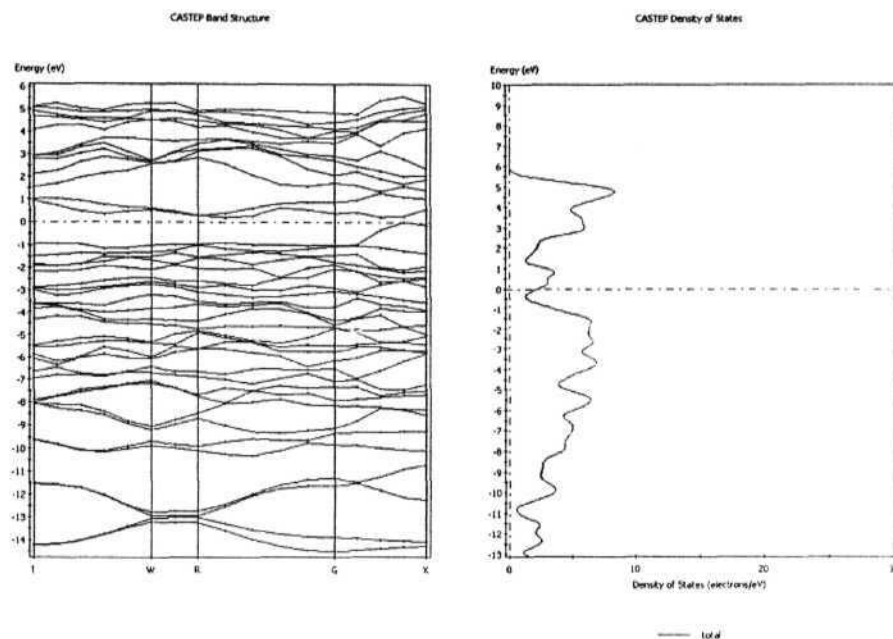CASTEP Band Structure   CASTEP Density of States

Figure 13

The band and DOS of isomer III of MgB_4.

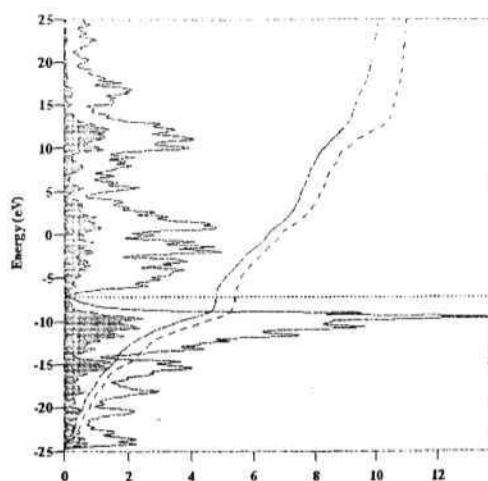

Figure 14

The projection of the pz orbitals of ring boron atoms in the cis boride skeleton of MgB_4.

The band structure on the resulting optimized MgB_4 (isomer III) is shown in Figure 13. Isomer III of MgB_4 is found to be less stable than the known one by 33.5 $kcalmol^{-1}$. However the results show that the borane framework is rigid. This isomer of MgB_4 seems to possess the smallest Fermi gap of 0.1 eV.

The total DOS shows small amount of density at the Fermi energy. This may be due to the insufficient k-sampling. A projection of the p_z orbitals of the ring boron atoms from extended Hückel calculations are shown in Figure 14. As in the case of Li_2MgB_8, the p_z orbitals of the ring boron atoms are concentrated along the Fermi region. The DOS is higher at the Fermi region, which is considered to be one of the factors responsible for superconductivity. A proper tuning of the skeleton with different types of isoelectronic atoms may result in very interesting electrical properties.

5.2. CONCLUSIONS

The stability of borides based on an edge shared pentagonal pyramid framework has been explored. The charge requirement in their 3-D network is compensated by cations in the various types of holes present. The two isomeric forms of the 3-D network - *cis* and *trans* - are stabilized by ions like Li and Mg. The *trans* boride is found to be stable as Li_2MgB_8 where all the possible vacancies are filled and also with MgB_4. MgB_4 have one type of vacancies left empty resulting in different isomers. It is observed that Mg always prefers the CAP void in the *trans*-boride skeleton. Thus one with two channels filled is unstable. The reverse is found to be true in the *cis*-boride skeleton of MgB_4. An isomer where Mg occupies the two channels is found to be more favorable. The different isomers of MgB_4 are compared with the known form. The band structure shows that the designed materials have smaller band-gaps than the experimental one. The greater DOS at the Fermi region also promises superconducting properties, and can be achieved by better tuning of the nature of the cations. The presence of p_z orbitals at the Fermi region shows that the conductivity will be primarily due to the π-type orbitals.

REFERENCES

1. Jansen, M., *Angew.Chem. Int. Ed. Engl.*, **2002**, *41*, 3746.

2. (a) Balakrishnarajan, M. M.; Jemmis, E. D.; *J. Am. Chem. Soc.* 2000, *122*, 4516. (b) Jemmis, E. D.; Balakrishnarajan, M. M.; Pancharatna, P. D. *J. Am. Chem. Soc,* 2001, *123*, 4313. (c) Jemmis, E. D.; Balakrishnarajan, M. M.; Pancharatna, P. D.; *Chem. Rev.* 2002,702,93.

3. Matkovich, V. I. (Ed.), *Boron and Refractory Borides,* Springer Verleg, New York, 1977.

4. Jones, M. E.; Marsh, R. E., *J. Am. Chem. Soc,* 1954, *76*, 1434.

5. Vegas, A.; Martinez-Cruz, L. A.; Ramos-Gallardo, A.; Romero, A.; Z. *Kristallogr.*, 1995,270,575.

6. Nagamalsu, J.; Nakagawa, N.; Muranaka, T.; Zenitani, Y.; Akimitsu, J., *Nature (London)* **2001,** *410*, 63.

7. Ashcroft, N. W.; Mermin, N. D. (Ed.), *Solid State Physics,* Holt, Rinehart and Winston, New York, 1976.

8. Chol, H. J.; Roundy, D.; Sun, H.; Cohen, M. L.; Louie, S. G., *Nature (London),* 2002, *418*, 758.

9. (a) Jemmis, E. D. *J. Am Chem. Soc.* **1982**, *104*, 7017. (b) Jemmis, E. D., Schleyer, P. v. R. *J. Am. Chem. Soc,* **1982**, *104*, 4781.

10. Jemmis, E. D.; Pancharatna, P. D. *Appl. Organomet. Chem.,* Accepted for Publication.

11. B3LYP is Becke's three parameter hybrid method with LYP correlation functional: (a) Becke, A. D. *J. Chem Phys* 1993, *98*, 5648. (b) Lee, C.; Yang, W.; Parr, R. G.

Phys Rev B **1988,** *37,* 785. (c) **Vosko,** S. H.; **Wilk,** L.; Nusair, M. *Can J Phys,* **1980,** *58,* 1200. (d) Stephens, P. J.; Delvin, F. J.; Chabalowski, C. F.; Frisch, M. J. *J Phys Chem* **1994,** *98,* 11623.

12. Frisch, M. J.; Trucks, G. W.; Schelegel, H. B.; Gill, P. M. W.; Johnson, B. G.; Robb, M. A.; Cheeseman, J. R.; Keith, T.; Peterson, G. A.; Montgomery, J. A.; Raghavachari, K.; Al-Laham, M. A.; Zakrzewski, V. G.; Oritz, J. V.; Foresman, J. B.; Cioslowsky, J.; Stefenov, B. B.; Nanayakkara, A.; Callacombe, M.; Peng, C. Y.; Ayala, P. Y.; Chen, W.; Wong, M. W.; Andres, J. L.; Replogle, E. S.; Gomberts, R.; Martin, R. L.; Fox, D. J.; Binkley, J. S.; Defrees, D. J.; Baker, J.; Stewart, J. P.; Head-Gordon, M.; Gonzalez, C; Pople, J. A. *Gaussian 94, Revision D.I, Gaussian Inc.,* Pittsburg PA, **1995.**

13. Landrum, G. A.; Glassy, W. V., YAeHMOP (Version 3.01). (Freely available at http://yaehmop.sourceforge.net

14. Accelrys Inc., Materials Studio CASTEP, San Diego: Accelrys Inc., 2001.

15. Milman, V.; Winkler, B.; White, J. A.; Pickard, C. J.; Payne, M. C; Akhmatskaya, E. V.; Nobes R. H., *Int. J. Quant. Chem.* **2000,** *77,* 895.

16. Payne, M. C; Teter, M. P.; Allan, D. C; Arias, T. A.; Joannopoulos, J. D., *Rev. Mod. Phys.,* **1992,** *64,* 1045.

17. Monkhost, H. J.; Pack, J. F., *Phys. Rev. B,* **1976,** *13,* 5188

18. Ravindran, P.; Vajeeston, P.; Vidya, R.; Kjekshus, A.; Fjellvag, H. Phys. Rev. B, **2001,** *64,* 224509.

Curriculum Vitae

Ms. Pattath D. Pancharatna was born on 6th Sep, 1975 at VileParle, Mumbai. She did her schooling at Mumbai and Trichur after which she joined St. Joseph's College, Irinjalakuda for her Bachelor's, choosing Chemistry as the major subject. She passed her M.Sc. from University of Calicut securing the third rank. After qualifying CSIR-JRF she joined the group of Prof. E. D. Jemmis at University of Hyderabad for pursuing research.

List of Publications

1. "A Unifying Electron-Counting Rule for Macropolyhedral Boranes, Metallaboranes and Metallocenes", Jemmis, E. D; Balakrishnarajan, M. M.; **Pancharatna,** P. D. *J. Am. Chem. Soc,* **2001,** 123, 4313.

2. "Missing Hydrogens in $B_{19}H_{20}^{-}$? Application of Electron Counting Rule for Edge-Shared Macropolyhedral Boranes" Jemmis, E. D.; Balakrishnarajan, M. M.; **Pancharatna,** P. D. *Inorg. Chem.,* **2001,** *40,* 1730.

3. "Electronic Requirements for Macropolyhedral Boranes" Jemmis, E. D; Balakrishnarajan, M. M.; **Pancharatna,** P. D. *Chem. Rev.,* **2002,***102,* 93.

4. "Condensed Polyhedral Boranes and Analogous Organometallic Clusters - A Molecular Orbital and DFT Study on the Cap-Cap Interactions" Jemmis, E. D.; **Pancharatna,** P. D. *Appl. Organomet. Chem.,* **2003,***17,* 480.

5. "Magic Electron Counts and Bonding in Tubular Boranes" Balakrishnarajan, M. M.; Hoffmann, **R.; Pancharatna, P. D.;** Jemmis, E. D. *Inorg. Chem.,* in press.

6. "Theoretical Studies on Nanotubes based on Boron Hydrides" Jemmis, E. D.; **Pancharatna, P. D.** Manuscript under Preparation.

7. "Edge Sharing Pentagonal Pyramids in Extended Structure - A Theoretical Boride Network" Jemmis, E. D.; **Pancharatna, P. D.** Manuscript under Preparation.

8. * "A Theoretical Study on the Positional Preferences of Bridging Hydrogen Atoms in Open Caged Macropolyhedral Boranes" Jemmis, E. D.; **Pancharatna, P. D.** Manuscript under Preparation.

9. * "Design of Novel Open Caged Macropolyhedral Boranes - An Ab initio Study" Jemmis, E. D.; **Pancharatna, P. D.** Manuscript under Preparation.

---

* Not included in the thesis